



Gupta Kheskani, Niyati (2024) *Biochemical characterization of the Parkinson's disease-associated deubiquitylase USP30 using its physiological substrates*. MSc(R) thesis.

<https://theses.gla.ac.uk/84471/>

Copyright and moral rights for this work are retained by the author

A copy can be downloaded for personal non-commercial research or study, without prior permission or charge

This work cannot be reproduced or quoted extensively from without first obtaining permission in writing from the author

The content must not be changed in any way or sold commercially in any format or medium without the formal permission of the author

When referring to this work, full bibliographic details including the author, title, awarding institution and date of the thesis must be given

Enlighten: Theses

<https://theses.gla.ac.uk/>
research-enlighten@glasgow.ac.uk



University of Glasgow

Biochemical characterization of the Parkinson's disease-associated deubiquitylase USP30 using its physiological substrates.

Niyati Gupta Kheskani

Bsc (Hons)

A thesis submitted to the University of Glasgow in fulfilment
of the requirements for the degree of MSc (Research)
in Biochemistry and Biotechnology

School of Molecular Biosciences
College of Medical, Veterinary and Life Sciences
University of Glasgow

JULY 2024

Abstract

Mitochondria are essential for eukaryotic life, existing under tightly regulated control mechanisms. Clearance of damaged mitochondria (mitophagy) is a crucial part of mitochondrial homeostasis and relies on the ubiquitination of proteins on damaged mitochondria, which leads to degradation and removal of the damaged organelle. Crucially, dysregulation of mitophagy is among the leading causes of diverse neurodegenerative disorders, including Parkinson's Disease (PD).

Several deubiquitinating enzymes (DUBs) have gained attention due to their ability to counteract ubiquitination-dependent mitophagy. USP30 is a DUB that emerged as a potential therapeutic target for PD due to its unique position within a mitophagy signalling cascade, whereby USP30 antagonises the heightened mitophagic flux that is common in hereditary forms of PD. Hence, considerable effort has been invested in developing USP30 inhibitors. However, this has been challenging because USP30 substrate recognition is generally poorly understood and there is a dearth of published USP30-inhibitor complex structures available.

By producing a physiologically relevant USP30 substrate, this project aims to develop an *in vitro* enzyme assay to understand USP30 substrate recognition, as well as examine the inhibition of USP30 by the new sulphonamide derivative inhibitors: MF-094 and Compound 39. This information can also be used to guide future structural analysis of USP30 in complex with one of its physiologically relevant substrates in the presence or absence of available inhibitors for the development of a crystal system from which to develop and design new inhibitors.

Table of Contents

Coverpage	1
Copyright	1
Abstract	2
Table of Contents	3
List of Figures	7
List of Tables	9
Acknowledgements	10
Author's Declaration	11
List of Abbreviations	12
Chapter 1: Introduction	14
1.1. An Introduction To Parkinson's Disease (PD)	14
1.2. Ubiquitin Signalling in Mitochondrial Regulation and its Dysfunction As A Hallmark Of PD	15
1.3. Mitophagy Is Regulated By PINK1/PARKIN	22
1.4. Miro1 and its role in the PINK1/Parkin pathway	18
1.5. DUBs Act As A Break On Mitophagy	20
1.6. Known Structural Features Of USP30.....	27
1.6.1. Structural Features Of USP30	27
1.6.2. USP30 Has A Proximal Binding Domain And A K6 DiUB Linkage Specificity	30
1.6.3. USP30 Has A Unique Catalytic Triad	33
1.7. USP30 Inhibitors	38
1.8. Aims Of The Project	43
Chapter 2: Methods and Materials	45
2.1. Reagents	45

2.1.1. Bacterial Strains.....	45
2.1.2. Media.....	45
2.2. DNA Manipulation Methods.....	46
2.2.1. Agarose Gel Preparation.....	46
2.2.2. USP30 Plasmid Design.....	46
2.2.3. Primers.....	47
2.2.4. Vector Amplification and USP30 Insert Ligation.....	48
2.3. Protein Handling Methods.....	49
2.3.1. Protein Production.....	49
2.3.1.1. Transformation and Glycerol Stocks.....	49
2.3.1.2. Expression Cultures.....	50
2.3.2. Protein Purification.....	51
2.3.2.1. HRV3C.....	52
2.3.2.2. UBE2L3.....	53
2.3.2.3. UBIQUITIN.....	54
2.3.2.4. MIRO1.....	54
2.3.2.5. USP30.....	54
2.3.3. SDS-PAGE gels and samples.....	54
2.4. Enzyme Assays.....	56
2.4.1. <i>In Vitro</i> Ubiquitination assays.....	56
2.4.1.1. MIRO1 Ubiquitination Assay.....	56
2.4.2. Profiling USP30 deubiquitinating activity.....	56
2.4.2.1. USP30 MIRO1-UB Deubiquitination Assay.....	56
2.4.2.2. USP30 MIRO1-polyUB Deubiquitination Assay.....	56

2.4.3. Inhibition Assays.....	57
2.4.3.1. USP30 Activity Assay In The Presence And Absence Of The Selected Inhibitors MF-094 and Compound 39.	57
i. Using Mono-Ubiquitinated MIRO1 As The Substrate	57
ii. Using Poly-Ubiquitinated MIRO1 As The Substrate	57
2.4.3.2. Investigating The Potency And Specificity Of Known USP30 Inhibitors	57
i. DUBprofiler™: MF-094 and Compound 39 Selectivity and Potency Against A Panel Of 48 DUBs.	58
ii. DUBprofiler-Cell™: MF-094 and Compound 39 Mediated Inhibition Of Endogenous-USP30 UB-Probe Binding.	58
Chapter 3: Results.....	59
3.1. Protein Expression and Purification	59
3.1.1. Purification of HRV3C, UBE2L3, UB	59
3.1.2. Purification of MIRO1	63
3.1.3. Purification of The USP30 Truncated Protein	65
3.2. Producing The Physiological Substrates For USP30.	68
3.2.1. Production of Mono-UB And Poly-UB MIRO1.	68
3.2.2. Production of K6-linked Di-UB MIRO1.	69
3.3. Profiling USP30 Deubiquitinating Activity.....	70
3.3.1. Investigating USP30 Deubiquitinating Activity Against MonoUB-MIRO1	70
3.3.2. Investigating USP30 Deubiquitinating Activity Against PolyUB-MIRO1	71
3.4. Investigating Potency And Specificity Of Known USP30 Inhibitors	72

3.4.1. DUB <i>profiler</i> [™] Screening Of MF094 Against A Panel Of DUBs.	72
3.4.2. DUB <i>profiler</i> [™] Screening Of Compound 39 Against A Panel Of DUBS.	75
3.4.3. DUB <i>profiler</i> -Cell [™] Of Endogenous USP30 UB-Probe Binding Inhibition Against MF-094.	78
3.4.4. DUB <i>profiler</i> -Cell [™] Of Endogenous USP30 UB-Probe Binding Inhibition Against Compound 39.	82
3.4.5. Investigating USP30 Inhibition Against MonoUB-MIRO1.....	85
3.4.6. Investigating USP30 Inhibition Against PolyUB-MIRO1.....	87
Chapter 4: Discussion.....	90
4.1. Previous Biochemical Characterisation of USP30.....	90
4.2. Producing the Physiological Substrate.....	91
4.3. Re-evaluating USP30 Inhibition Using Physiological Substrate Turnover	96
4.4. Future Prospects Using The Physiological Substrate	97
Chapter 5: References.....	100
Chapter 6: Appendix.....	106
6.1 USP30 Plasmid Design and Cloning.....	106
6.2 Protein Production Optimisation.....	108
6.2.1 MIRO1 Optimisation.....	108
6.2.2 USP30 Optimisation.....	109
6.3 Production Of K6-Linked Diubiquitinated MIRO1 using pre-conjugated linkages...112	

List of Figures

Figure 1. A Simplified Schematic of the Ubiquitination Mechanisms	16
Figure 2. Schematic Representation of PINK1/PARKIN regulation of Mitophagy	18
Figure 3. Dendogram Of The Different Types Of DUBs	20
Figure 4. Comparison of the Predicted alphafold USP30 structure against the previously crystallised USP30 construct.	23
Figure 5. USP30 Domains and Subdomains	24
Figure 6. USP30 Has A Ubiquitin Proximal Binding Domain that confers it substrate specificity	27
Figure 7. USP30 catalytic triad and sequence alignment of the 12 closest USP family members	29
Figure 8. USP30 Orthologue Sequence Alignment.....	31
Figure 9. Reported structures of USP30 bound to inhibitors PXW and PKH	34
Figure 10. Purification of HRV3C	53
Figure 11. Purification of UBE2L3.....	54
Figure 12. Purification of Ubiquitin	55
Figure 13. Purification of MIRO1	57
Figure 14. Purification of USP30 5OHK construct	60
Figure 15. MIRO1-Ubiquitination Assay Shows The Production Of Different Ubiquitinated-MIRO1 Species.	62
Figure 16. USP30 Deubiquitination Activity Against Monoubiquitinated-MIRO1.....	70
Figure 17. USP30 Deubiquitinating Activity Against Poly-Ubiquitinated MIRO1.....	71
Figure 18. MF-094 Against A Panel Of DUBs Including USP30	74
Figure 19. CMPD39 Against A Panel Of DUBs Including USP30.....	74
Figure 20. DUBprofiler-Cell™ Of Endogenous USP30 UB-Probe Binding Inhibition By MF-094. 72	
Figure 21. DUBprofiler-Cell™ of Endogenous USP30 UB-Probe Binding Inhibition By Compound 39.....	74
Figure 22. Investigating USP30 Activity Against Mono-Ubiquitinated MIRO1 In The Presence Of Inhibitors	76
Figure 23. Investigating USP30 Activity Against Poly-Ubiquitinated MIRO1 In The Presence Of Inhibitors	78
Figure 24. AlphaFold 3 prediction of USP30 bound to mono- and poly- ubiquitinated MIRO1...94	

APPENDIX FIGURES

Supplementary Figure 1. pET-15b-6b2 Vector Amplification, Purification And USP30 Insert Ligation 93

Supplementary Figure 2. MIRO1 Optimisation 95

Supplementary Figure 3. USP30 Optimisation 96

List of Tables

Table 1. USP30 Inhibitors Summarised.....	33
Table 2. Bacterial Strains Used During This Project.....	38
Table 3. Concentration Of IPTG Used For Different Proteins.....	38
Table 4. Mutations Introduced Into The USP30 Plasmid.....	39
Table 5. Primers And Their Function	40
Table 6. Thermocycling Conditions For The Vector Amplification.....	41
Table 7. Proteins Produced And Their Corresponding Vector And Affinity Tags	43
Table 8. List Of Buffers Summarised	45
Table 9. Proteins Produced During This Project	52

Acknowledgements

Firstly, I would like to take this opportunity to express my sincere gratitude to my primary and secondary supervisors Mehmet Gundogdu and Helen Walden, for their daily guidance and the opportunity to complete this MScR, which has allowed me to start developing as an independent scientist and encouraged me to gain confidence working in the lab. I'd also like to thank my funders, Ubiquigent, and namely Jason Mundin and Sheelagh Frame, without whom this Master wouldn't have been possible.

Secondly, I'd like to thank each member of the Walden Lab, who have helped and advised me throughout my time there, including Aasna Parui, Amir Mahdi Mazloumi Aboukheili, Joanna Koszela, Kimon Lemonidis and Martin Rennie. Since my primary supervisor was based outwith the university during my project, the members of the lab have all taught me skills, shared their expertise, and contributed to my development, for which I am extremely grateful. Additionally, I'd also like to thank the scientists from Ubiquigent who helped me set up experiments, namely Steven Liness, João Oliveira and Kirsten Sinclair.

Finally, I'd like to thank my friends and family for their constant support and enthusiasm.

Author's Declaration:

I declare that this thesis is the result of my own work unless explicit reference is made to the work of others. The work in this thesis has not been submitted for any other degree at the University of Glasgow or any other institution.

Niyati Gupta Kheskani

List of abbreviations

6 Histidine (6xHis)

Activity based probe (ABP)

Amino Acid (aa)

Autosomal Dominant Parkinsons Disease (ADPD)

Autosomal Recessive Parkinsons Disease (ARPD)

Compound 39 (CMPD39)

Deubiquitinating Enzymes (DUBs)

Exo-deubiquitinating enzyme (exo-DUB)

Gel Filtration (GF)

Glutathione-S-transferase (GST)

Human USP30 (hUSP30)

K = lysine

K6-diUB (K6 diubiquitin)

Machado-Josephine domain proteases (MJDs)

Mitofusin 2 (MFN2)

Mitochondrial Intermembrane Domain (MID)

MonoUB-MIRO1

Motif INTERacting with the ubiquitin-containing Novel DUB family (MINDY)

National Health Service (NHS)

Nickel- Nitrioloacetic acid (Ni^{2+} -NTA)

Neighbour to BRCA1 gene1 (NBR1)

Nuclear dot protein 52 (NDP52)

Optineurin (OPTN)

Outer Mitochondrial Membrane (OMM)

Ovarian Tumour Proteases (OTUs)

Parkinsons Disease (PD)

Phosphoubiquitin (pUB)

PTEN-INduced putative Kinase 1 (PINK1)

PolyUB-MIRO1

RING-between-RING (RBR)

Tax1-binding protein (TAX1BP1)

Translocases of the inner mitochondrial membrane complexes (TIM complex)

Translocases of the outer mitochondrial membrane complexes (TOM complex)

Transmembrane Domain (TMD)

JAMM (JAB1/MPN/MOV34)

Ubiquitin (UB)

Ubiquitin-Activating Enzyme (E1)

Ubiquitin Binding Domains (UBD)

Ubiquitin C-Terminal Hydrolases (UCHs)

Ubiquitin-Conjugating Enzyme (E2)

Ubiquitin-Specific Proteases (USPs)

Ubiquitin Ligases (E3)

Voltage-Dependent Anion Channel 1 (VDAC1)

Zinc Finger with the UFM1-Specific Peptidase Domain Protein (ZUFSP/ZUP1)

Chapter 1: Introduction

1.1 An Introduction to Parkinson's Disease (PD)

Affecting 2-3% of the worldwide population aged over 65, Parkinson's Disease (PD) is the second most prevalent neurodegenerative disorder after Alzheimer's Disease (AD) (Poewe, *et al.*, 2017). PD is a chronic disorder characterised by the loss of dopaminergic neurones within the *substantia nigra pars compacta* region of the brain. The long-term effects of the disease also mean that huge costs are incurred – both social and economic - with the National Health Service (NHS) estimating that over £220 million are spent each year on costs related to PD (Ko, *et al.*, 2023).

PD is characterised by a slowness of movements (bradykinesia), limb tremors, muscle rigidity, and other motor skill dysfunctions (Parkinson, 1817), but it is also accompanied by other non-motor symptoms that severely affect patients, such as PD-related dementia, cognitive impairment, or depression. These symptoms decrease the patient's quality of life and thus increase the morbidity of the disease. While the symptoms are not themselves lethal, after the first decade from symptom onset the mortality of the patients is doubled compared to that of the global population (Poewe, *et al.*, 2017). Despite the enormous efforts and progress made towards understanding PD, there are currently no cures, and most of the available treatments to date only focus on relieving the symptoms. Furthermore, these treatments have been reported to become less efficient over time (Poewe, *et al.*, 2017). This makes finding new potential cures for PD a challenging but crucial endeavour.

1.2 Ubiquitin Signalling in Mitochondrial Regulation and its Dysregulation as a hallmark of PD

The malfunction of mitochondria has been identified as a key hallmark for the development of PD in both hereditary and sporadic cases (Belin, et al., 2008). There are thousands of mitochondria in each cell, which are continually renewed whenever one is damaged or becomes too old. This is very important as mitochondria are prominently acknowledged as the powerhouse of cells due to their role in controlling several key cellular functions, ranging from ATP generation to Ca²⁺ homeostasis, cell death regulation and lipid-carbohydrate intracellular signalling (Tsefou, 2022). Hence, dysregulation and defects severely impact the health of the mitochondrial network, including loss of mitochondrial potential, oxidative stress, reactive oxygen species (ROS) production and cell death (Ferrer, 2022). This is particularly crucial in dopaminergic neurones, which are mostly quiescent and have high energy demands to maintain dopamine metabolism. Therefore, dopaminergic neurones are dependent on a tight regulation of mitochondrial homeostasis.

To maintain this homeostasis, mitochondrial dynamics are regulated through ubiquitin (UB) modifications (Rusilowicz-Jones, *et al.*, 2020). UB is an 8.6 kDa protein composed of 76 amino acids (aa) that is found conserved throughout all eukaryotic organisms. It contains a critical glycine residue on its C-terminus that allows it to attach to other proteins to mark them for a post-translational modification process known as ubiquitination (also known as ubiquitylation) (Lecker *et al.*, 2006). This process is composed of three sequential steps as described in **Figure 1**, which involves a ubiquitin-activating enzyme (E1), a ubiquitin-conjugating enzyme (E2) and a ubiquitin ligase (E3). During the first step, the carboxyl end of a ubiquitin monomer binds to the E1 in an ATP-dependent manner. Secondly, the ubiquitin monomer is transferred onto the E2 via a trans-thiolation reaction to form a thioester bond with the ubiquitin sulfhydryl group. Finally, an E3 ligase transfers the ubiquitin monomer to a substrate via the formation of a covalent bond between the Ubiquitin C-terminal glycine and the target protein. (Lecker *et al.*, 2006; Sahtoe *et al.*, 2015). These ubiquitin monomers can then be ubiquitinated in one of its lysine residues to form chains or branches, termed polyubiquitination. The new ubiquitin moieties form attachments in one of eight discrete key residues comprised of seven lysine residues (K6, K11, K27, K29, K33, K48 and K63) and the N-terminal methionine residue (M1) (Hospenthal, *et al.*, 2013; Michel, *et al.*, 2017).

These ubiquitin modifications are therefore used by mitochondria to perform multiple quality control mechanisms (QCM) to ensure that each of their functions are performed correctly. These include several processes which often run simultaneously to maintain cellular

homeostasis, thus ensuring ATP synthesis and calcium buffering processes run correctly to allow the mitochondria to maintain the cell's energy and to regulate the release of neurotransmitters from presynaptic terminals. Such processes include the control of fusion-fission dynamics and mitochondrial-derived vesicles, which control the mitochondrial content being shared throughout the network (Chen *et al.*, 2019). To prevent mitochondria from triggering cell-death upon the failure of these processes another QCM has evolved to specifically target the damaged mitochondrion through a mitochondrial form of autophagy termed mitophagy. This process has recently gained attention as a potential point for therapeutic treatment of degenerative diseases (Kubli *et al.*, 2013).

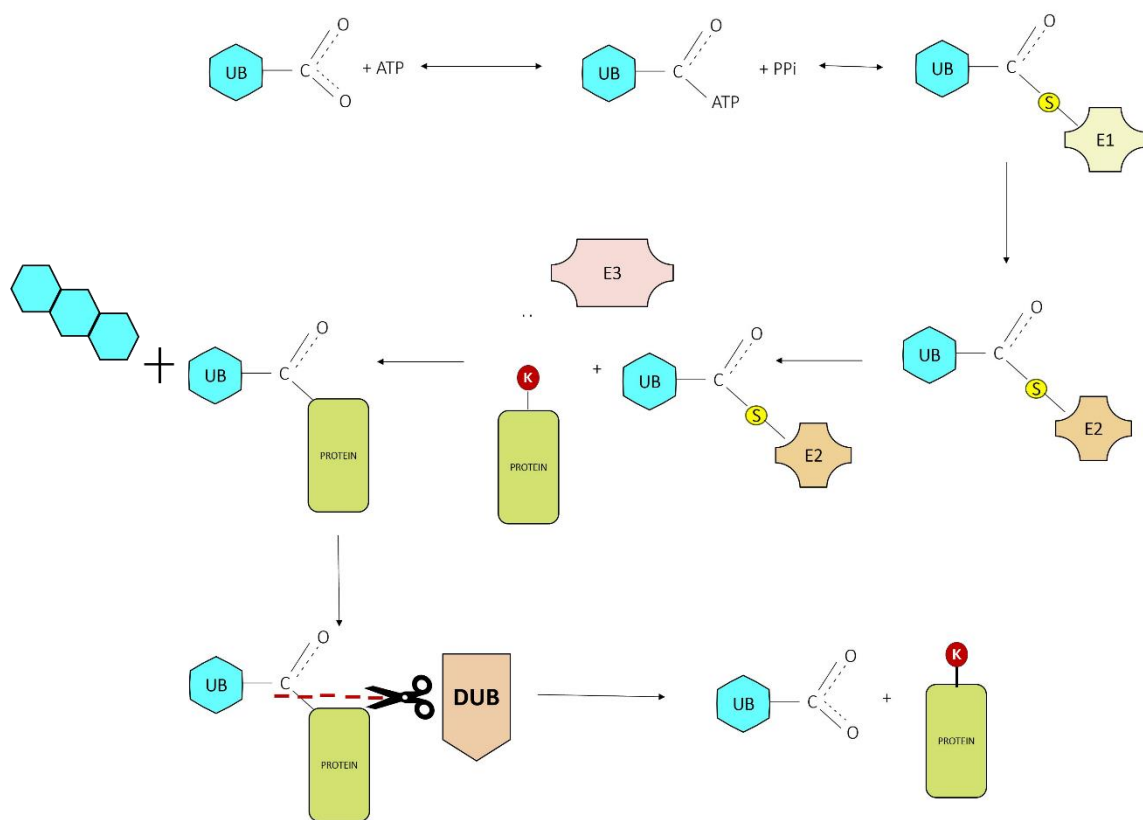


Figure 1. A Simplified Schematic Of The Ubiquitination Mechanism.

When ATP is present, a ubiquitin moiety (UB) is able to bind to a ubiquitin-activating enzyme (E1) through its carboxyl group. This E1 then transfers the UB moiety via a trans-thiolation reaction onto the sulfhydryl group of a ubiquitin-conjugating enzyme (E2). The sulfhydryl group is represented here as an S in a yellow circle. The E2 then recruits a ubiquitin ligase enzyme (E3) which attaches the UB moiety onto a lysine residue on the target protein. In the mitophagy cascade, the main E3 involved in ubiquitinating the mitochondrial proteins to target them for degradation is Parkin. The

UB moieties are then further ubiquitinated on one of seven lysine residues (K6, K11, K27, K29, K33, K48 and K63) or the N-terminal methionine residue (M1) of UB to form chains or branches that target the substrate for a specific purpose (Lecker *et al.*, 2006). In the case of Parkin, K6 and K11 chains are predominantly formed, followed by K48 and K63 linkages. This process can be reversed through the action of a deubiquitinating enzyme (DUB), which can cleave the UB moieties deposited on the target proteins to remove and antagonise the ubiquitination signal (Nijman *et al.*, 2005), such as USP30 which antagonises Parkin ubiquitination of K6 linkages (Bingol *et al.*, 2014).

.....

In mitochondria, a series of E3 enzymes have been described to play a role in the mitophagy cascade, namely Parkin, ARIH1, March5, MULAN, P62-Keap1-Rbx1 axis, and HUWEI (Onishi *et al.*, 2021). Although a certain level of redundancy on the function of the E3s has been postulated, Parkin appears to be the critical E3 ligase involved in the regulation of mitophagy. In dysfunctional mitochondria, the E3 ligase Parkin forms several types of ubiquitin chain linkages (**Figure 1**) that degrade the mitochondrial proteins to maintain mitochondrial homeostasis to signal for different, specific cell fates. Parkin preferentially forms non-canonical K6 and K11 chains and, to a lesser extent, canonical K48 and K63 chains (Bingol *et al.*, 2016). Although the function of K11 chains is not well documented, the K6 chains appear to play a role in the PTEN-induced putative kinase 1 (PINK1) /PARKIN mitophagy clearance pathway (Michel, *et al.*, 2017). Meanwhile K63-linked chains are documented to recruit ubiquitin binding adaptors involved in the early stages of the autophagosome formation cascade, such as HDAC6 and p62, although their relevance in parkin- mitophagy is still unclear (Chan *et al.*, 2011); while K48-linked polyubiquitinated chains play a separate role and appear to recruit the 26S proteasome onto the mitochondria surface causing degradation of the mitochondrial outer membrane proteins (Chan *et al.*, 2011).

Interestingly, the disturbance of the K6 PINK1/Parkin Mitophagy pathway has been observed to be significantly decreased in hereditary forms of parkinsonism. While heritable PD cases are only responsible for 5-10% of all cases, the proteins encoded by the genes involved in heritable PD have also been identified as perturbed in sporadic forms of the disease (Belin, *et al.*, 2008). PD can be inherited in an autosomal dominant (ADPD) or autosomal recessive manner (ARPD); the latter of which is further sub-classified into either complex genetic forms of PD or early-onset PD (Belin, *et al.*, 2008; Poewe, *et al.*, 2017). ARPD accounts for 50% of the clinically

diagnosed cases, and is responsible for early-onset PD, with patients exhibiting symptoms by their 40s, and sometimes even before they're 20 years old (Bonifati, 2012). Mitochondrial dynamics are affected in early-onset PD and certain sporadic cases of PD due to loss of function mutations within *PARK2*, the gene which encodes for the RING-between-RING (RBR) E3 ligase Parkin (**Figure 2**), which ubiquitinates the damaged or old mitochondria to tag them for eventual lysosomal degradation. Early-onset PD cases have also been reported due to mutations within *PARK1* and *PARK7*, as well as in the PTEN-induced putative kinase 1 (PINK1) genes, all of which cause mitophagy dysregulation (Bonifati, 2012).

1.3 Mitophagy is regulated by PINK1/PARKIN

In healthy mitochondria, the serine/threonine kinase PINK1 is imported through the Translocases of the Inner and Outer Mitochondrial membrane complexes (TIM and TOM complex), where it is processed and cleaved, causing PINK1 to become unstable and rapidly degraded in the cytosol (Bingol, *et al.*, 2016). However, when a mitochondrion is damaged in a healthy system, the membrane potential is lost and mitochondrial import is impaired causing PINK1 to be overexpressed. This leads to dimerization and stabilisation that cause PINK1 accumulation on the outer mitochondrial surface, where it auto-phosphorylates. PINK1 accumulates in the TOM complexes with the kinase domain facing the cytosolic side. This subsequently causes the UB moieties present on the mitochondrial proteins at the mitochondrial surface to be phosphorylated on the Ser65 site (Bingol, *et al.*, 2016; Zhang *et al.*, 2016; Miller *et al.*, 2019).

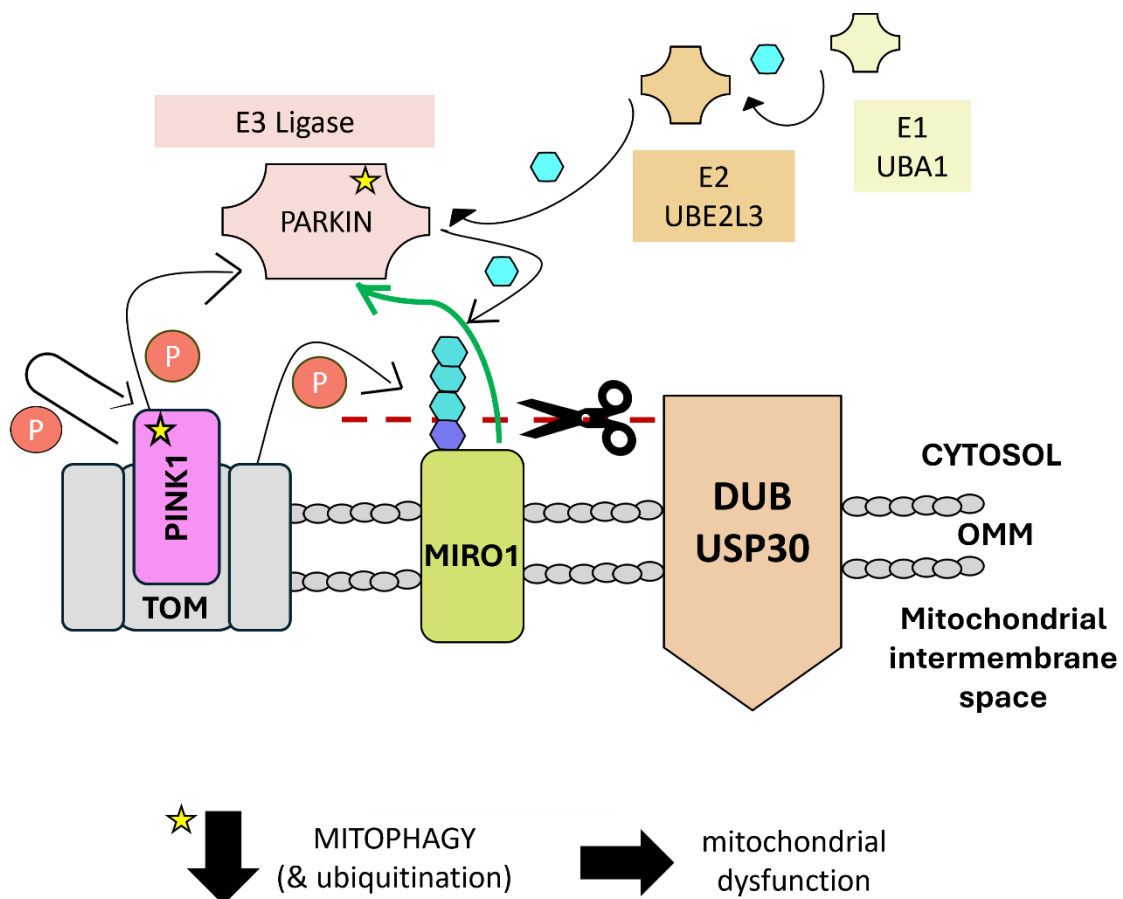


FIGURE 2. Schematic Representation Of PINK1/PARKIN Regulation Of Mitophagy.

Figure 2 depicts PINK1 phosphorylating Ubiquitin (UB) moieties, represented here in blue, at the Ser65 site. This in turn recruits the E3 ligase Parkin, which gets phosphorylated by PINK1 and therefore activated. Parkin then starts recruiting more

UB to the Outer mitochondrial membrane (OMM), thus ubiquitinating the mitochondrial proteins and creating a positive feedback loop that targets the mitochondria for mitophagy.

USP30 can antagonise this ubiquitination by cleaving the UB chains from the mitochondrial proteins such as MIRO1 (coloured green), thus preventing mitophagy from taking place. USP30 is thought to cleave between the proximal (coloured dark blue) and distal (coloured light blue) UB, thus leaving a mono-ubiquitin tag behind. The green arrow depicts the purported ability of MIRO1 to recruit Parkin to the mitochondria.

In early-onset PD cases, mutations in certain components (yellow star) of the system cause a decrease in ubiquitination levels. Hence this causes a decrease in mitophagy leading to mitochondrial dysfunction.

.....

At the same time, PINK1 phosphorylates Parkin (**Figure 2**) on the Ser65 site of its ubiquitin-like (UBL) domain thereby activating it from its auto-inhibited state to expose its active site (Kumar *et al.*, 2017). Activated parkin is then able to recruit more ubiquitin moieties to the target protein, thus triggering a positive feedback loop with PINK1, causing the kinase to act as a signal amplifier (**Figure 2**).

During mitophagy the targeted mitochondrial proteins are further ubiquitinated – typically by K63 chains – to recruit autophagy receptors that contain specific ubiquitin-binding domains (UBDs) that have ubiquitin length and linkage preference (Michel, *et al.*, 2017). During mitophagy the ubiquitin linkages attract one of five autophagy receptors: Optineurin (OPTN), nuclear dot protein 52 (NDP52), p62, neighbour to BRCA1 gene1 (NBR1) or Tax1-binding protein (TAX1BP1). Of these, NDP52 and OPTN are the key autophagy receptors and have been observed to act redundantly to ensure mitochondrial homeostasis is maintained (Zhang, *et al.*, 2016). After recruitment the receptors bind simultaneously to the target protein and the autophagosomal membrane, thus promoting the engulfment of the substrate into contained vesicles. The autophagosome subsequently fuses with the lysosome to degrade the contents of the vesicles, thus completing the process (Nguyen, *et al.*, 2016). However, when there is a loss of function mutation affecting the PINK1/Parkin pathway, the ubiquitination of the target proteins is compromised, thus disrupting the mitophagy signalling cascade and leading to the accumulation of unhealthy mitochondria within the cell (Bingol *et al.*, 2014). This affects the

health of the entire mitochondrial network, causing toxic effects that have been identified as a common feature of PD (Miller, *et al.*, 2019).

1.4 Miro1 and its role in the PINK1/Parkin pathway

In mammals there exists two MIRO GTPases, MIRO1 and MIRO2, which are anchored to the OMM through a transmembrane domain and have been well characterised to play two critical roles in mitochondrial dynamics. Firstly, it regulates trafficking and distribution by anchoring the mitochondria to motor proteins. MIRO1/2 are part of the adaptor complex, along with other motor proteins such as kinesin and dynein. This adaptor complex mediates mitochondria axonal transport and upon ubiquitination by Parkin, MIRO1 detaches from the mitochondrion causing kinesin to also be removed. This has been suggested to aid in the mitophagy cascade by triggering the arrest of mitochondrial mobility, thus isolating the organelle and subsequently facilitating the degradation process of the damaged mitochondrion (Wang *et al.*, 2011; López-Doménech *et al.*, 2021). Secondly, MIRO1 also plays a role in Ca^{2+} homeostasis by binding Ca^{2+} through its EF-hand domains. This binding causes steric hindrance that prevents the kinesin from being able to bind other interacting microtubules while the Ca^{2+} remains bound to the MIRO1, thus arresting mitochondrial mobility in a transient manner (Wang *et al.*, 2011).

Curiously, mutations in the EF-hand of MIRO1 responsible for this Ca^{2+} binding ability have been reported to disrupt Parkin recruitment to the mitochondrion (Safiulina *et al.*, 2018). A baffling finding given its well documented role as a downstream substrate of Parkin ubiquitination (Bingol *et al.*, 2014). Safiulina *et al.*, hence postulated that MIRO1 acts as initial docking site for inactive Parkin, which exists in an inactive pool in the cytosol and is recruited by MIRO1 to the mitochondrial surface (**Figure 2**) before any mitochondrial damage takes place. Eventually a mitochondrial depolarisation event takes place, causing Parkin to be amplified by PINK1 phosphorylation through the PINK1/PARKIN pathway described in **Figure 2**, where it promiscuously ubiquitinates MIRO1 lysine residues (K92, K107, K153, K182, K187, K194, K230, K235, K249, K330, K427, K512, K535, K572) to form different length linkages, although their exact role is still unclear (López-Doménech *et al.*, 2021). However, this mitochondrial depolarisation event is also purportedly triggered by an increased Ca^{2+} influx into mitochondria, further indicating that MIRO1 Ca^{2+} binding is involved in Parkin translocation (Safiulina *et al.*, 2018). This would align with reported perturbations of Parkin recruitment to mitochondria when either MIRO1 is depleted or truncated to remove the Ca^{2+} binding domain (Safiulina *et al.*, 2018). Thus, MIRO1 has gained traction not just as a key player mitochondrial mobility, but also as a potential regulator of Parkin recruitment to the pathway and subsequent stabilisation onto damaged mitochondria (Safiulina *et al.*, 2018,

López-Doménech *et al.*, 2021), making it's role in the PINK1/PARKIN pathway even more critical to elucidate.

1.5 DUBs Act As A Brake On Mitophagy

As with all biological processes, an excess of something is as harmful as a shortage. Since Parkin is an E3 ligase that ubiquitinates mitochondrial proteins, research has focused on deubiquitinating enzymes (DUBs) as the corresponding negative regulator to prevent excess mitophagy from having damaging effects on cellular homeostasis. DUBs are protease enzymes that play a role in the proteasomal and lysosomal degradation machinery by removing the ubiquitin modifications from the substrates. In proteasomal degradation DUBs either prevent the substrate from being targeted to the proteasome, or if it's a proteasome-associated DUB, allow the ubiquitin cleaved from the substrate to be recycled. Meanwhile, in the lysosomal pathway DUBs antagonise the degradation of proteins by preventing the ubiquitin tags from recruiting the cargo receptors required to trigger phagophore formation and subsequent lysosomal degradation, as would be the case for mitophagy (Schauer *et al.*, 2020).

There are approximately 100 human DUBs (**Figure 3**), divided into metalloproteases, which cleave using a JAMM metal-binding motif, and cysteine proteases, which are characterised by the cysteine residue in their catalytic triad. Cysteine proteases make up the bulk of DUBs, with over 87 different cysteine proteases encompassed within six different subclasses: Ubiquitin C-terminal Hydrolases proteases (UCHs); Ovarian Tumour proteases (OTUs); Machado-Josephine Domain proteases (MJDs); Zinc Finger with the UFM1-specific peptidase Domain Protein (ZUFSP/ZUP1); the Motif Interacting with the ubiquitin-containing Novel DUB family (MINDY) and Ubiquitin-Specific Proteases (USP) (Elu *et al.*, 2022; Schauer, *et al.*, 2020). Of these, the majority of cysteine proteases are USPs, with over 58 different USPs identified to date (Nijman *et al.*, 2005; Schauer *et al.*, 2020; Snyder *et al.*, 2021).

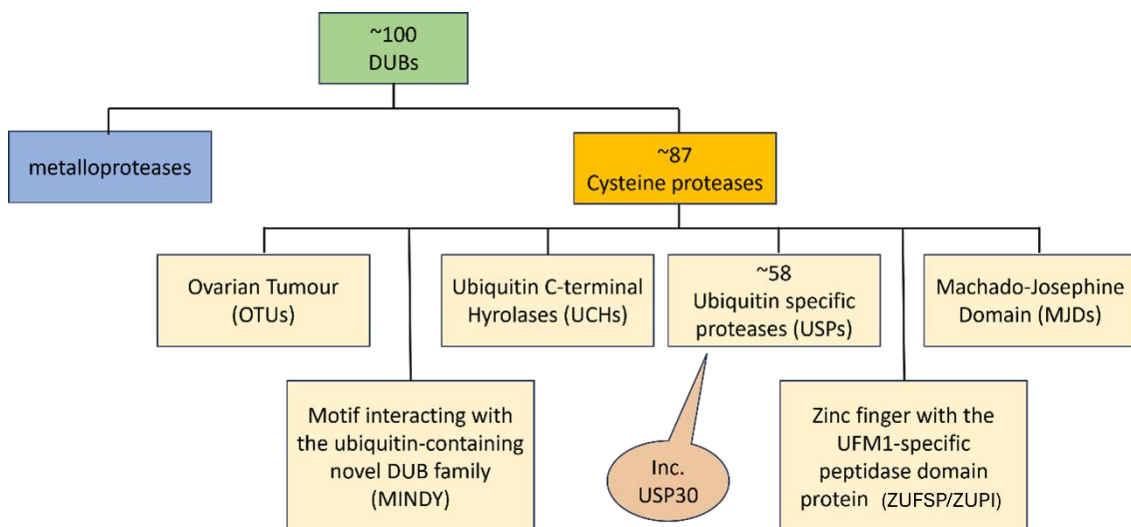


Figure 3. Dendrogram Of The Different Subfamilies Of DUBS.

Dendrogram representation of the different subfamilies of deubiquitinating enzymes (DUBs). DUBs are divided into metalloproteases and cysteine proteases, the latter of which can be further subdivided into 6 different subclasses that include Ovarian TUmour proteases (OTU), Motif Interacting with ubiquitin containing Novel DUB family (MINDY), Ubiquitin C-terminal Hydrolases (UCH), Zinc finger with specific UFM1-specific Peptidase domain protein (ZUFSP/ZUPI), Machado-Josephine Domain (MJD) and Ubiquitin Specific Proteases (USP). USPs make up the bulk of cysteine proteases, with ~56 USPs currently known, including USP30.

.....

USPs can regulate Parkin activity directly, by deubiquitinating Parkin itself as exemplified by USP8, USP13, and USP33 (Liu *et al.*, 2019), or indirectly, by deubiquitinating a Parkin substrate, as is the case for USP15, USP30 and USP35 (Bingol *et al.*, 2014; Cornelissen *et al.*, 2014; Durcan *et al.*, 2014; Wang *et al.*, 2015). From these DUBs, USP30 has attracted a lot of attention due to its well-documented central role in regulating mitophagy (**Figure 2**).

Experiments performed on rat models using shRNA designed to silence USP30 showed an approximately 60% increase in the levels of mitophagy. Normal levels of mitophagy were then restored through the co-transfection of shRNA-resistant human USP30 (hUSP30) cDNA, but not the catalytically dead version, suggesting there were no non-specific effects taking place and that endogenous USP30 regulates mitophagy *in vivo* (Bingol *et al.*, 2014). Furthermore, these results also suggested the possibility that the recovery of physiological mitophagy levels may be attainable via the inhibition of USP30.

Further experimental evidence achieved by mass spectrometry of both USP30 overexpressed and KO cell lines has shown that USP30 impacts mitochondrial turnover in neurons (Bingol *et al.*, 2014). Cell lines overexpressing USP30 show impaired levels of mitophagy, an effect not recapitulated by catalytically dead versions of USP30. Meanwhile, USP30 KO cells showed an increase in mitophagy dependent on functional Parkin and PINK1 (Bingol *et al.*, 2014; Hou *et al.*, 2017). This dependency on Parkin is further emphasised by the fact that USP30 specifically antagonizes the ubiquitination of Parkin substrates.

Further mass spectrometry analysis of the KO cell lines built on the previous findings also identified 41 common substrates of Parkin and USP30, including a multitude involved in mitochondrial signalling, such as MUL1, VDAC1-3, MTX1, MFN1, TOM20 and MIRO1

(Cunningham, *et al.*, 2015), thus further cementing the idea that USP30 is a potential target for stimulating mitochondrial turnover.

Of these, TOM20 and MIRO1 (a.k.a. RHOT1) – two proteins involved in mitophagy – showed particularly strong increases in ubiquitination and thus attracted attention as good substrates to test USP30 deubiquitinating activity, with TOM20 currently being the most commonly used substrate (Bingol *et al.*, 2014; Cunningham, *et al.*, 2015). Meanwhile, MIRO1 remains a known but less well characterised substrate for USP30 – hence experiments based on this substrate could potentially yield an alternative substrate on which to run orthogonal assays and allow greater understanding of USP30 substrate recognition.

1.6 Known Structural features of USP30.

1.6.1. Structural Features Of USP30

Given the central role USP30 plays in modulating mitophagy within cells, understanding the structural features of the protein is required to gain insight into its molecular mechanism and facilitate the development of inhibitors. Previous crystallisation experiments have managed to yield both human (PDB: 5OHK) and zebrafish (PDB: 5GVI) crystals at a resolution of 2.34 Å (Gersch et al., 2017) and 1.86 Å (Sato *et al.*, 2017), respectively.

From the human USP30 (hUSP30) crystal structure, along with HDX-MS experiments (Gersch *et al.*, 2017) it was determined that USP30 is a 517 amino acid protein composed of three different domains which include the mitochondrial intermembrane domain (MID), located at the N-terminus, spanning from residues 1-35, and the transmembrane domain (TMD), spanning residues 36-56, and the catalytic domain. It should be noted that the TMD is a unique domain among DUBs that makes USP30 the only DUB capable of anchoring to the outer mitochondrial membrane (OMM), thus allowing USP30 to localise near Parkin substrates to deubiquitinate them. It has been postulated that the TMD keeps USP30 inactive within the cytosol by shielding the catalytic triad in such a way that it is only when the TMD binds to the OMM that a structural rearrangement exposes the catalytic site for substrate engagement (Qin *et al.*, 2022). However, since the TMD is not involved directly with the USP30 deubiquitinating activity, and due to protein aggregation, solubility and activity issues Gersch *et al.*, removed the TMD and the MID domains, along with a few other disordered regions and key residues (listed on Section 2.2.2.) to be able to synthesize the 5OHK truncated protein and crystalize it. **Figure 4** shows a superposition of the predicted alphafold of the Q70CQ3 structure for full-length USP30 with the PDB: 5OHK catalytic construct (Gersch et al., 2017) that was employed in this project.

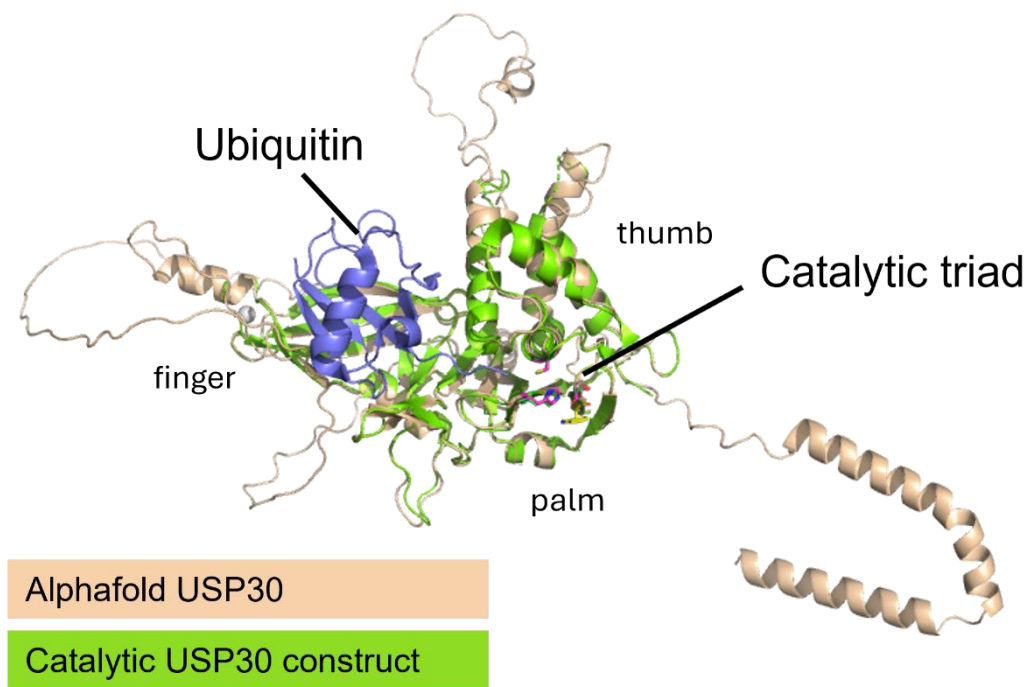


Figure 4. Comparison of the predicted alphaFold USP30 structure against the previously crystallised USP30 construct.

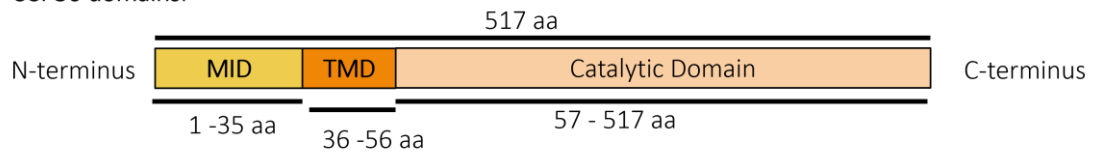
Cartoon representation of PDB: 5OHK (green) crystal structure (Gersch *et al.*, 2017) and Q70CQ3 alphaFold predicted full-length structure (wheat). The 5OHK structure has had the Transmembrane Domain (TMD) and Mitochondrial Intermembrane Domain (MID) removed, along with the long-disordered regions corresponding to residues 1-63, 180-213, and 358-431. The 5OHK structure was crystallised with a proximal ubiquitin bound to it, here depicted in blue while the catalytic triad is highlighted in pink and represented in stick and ball format.

.....

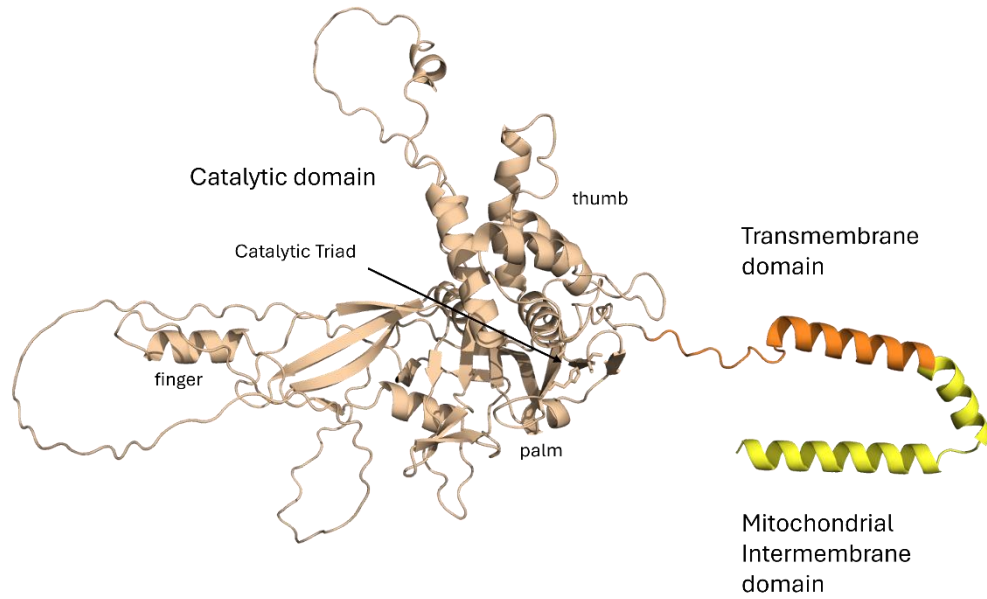
The catalytic domain of USP30 lies at the C-terminus of the protein which spans from residues 57 – 517, and enables the enzyme’s deubiquitinating activity (**Figure 5a, 5b**) (Gersch *et al.*, 2017). This domain can be further divided into three subdomains found in most USPs: the palm, thumb and zinc-binding finger subdomains (**Figure 5C**). These are arranged such that the thumb and fingers form a binding pocket within the protein where the UB C-terminal tail can enter, hence allowing the UB moiety to interact with the USP30 active site, so that the isopeptide bond between the first and second UB moieties, or between the UB moiety and the substrate, can be hydrolysed by the DUB (Miller *et al.*, 2019; Schauer *et al.*, 2020).

a.

USP30 domains:



B



c.

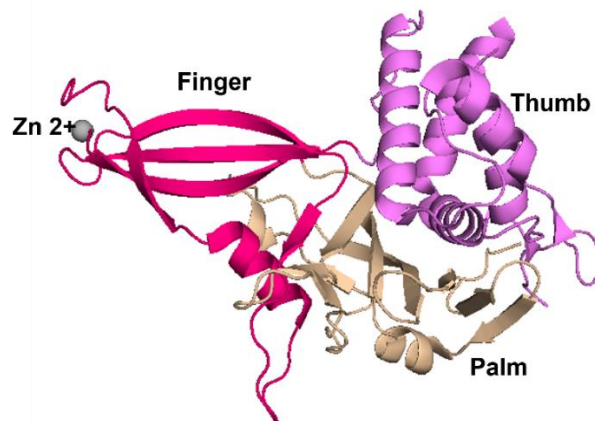


FIGURE 5. USP30 Domains And Subdomains.

Figure 5a Schematic representation of the three USP30 domains: the mitochondrial Inter membrane domain (MID) at the N-terminus coloured in yellow and spanning residues 1-35. The transmembrane domain (TMD) coloured in orange covers residues 36 – 56 and the catalytic domain, responsible for the DUBs catalytic activity covers the bulk of the protein (residues 57 – 517) and is represented in wheat colour (Gersch *et al.*, 2017).

Figure 5b Alphafold prediction of the full-length USP30 structure visualised using Pymol™ (version 1.7.4.5 Edu). The same colour scheme is used for the cartoon representation of the three USP30 domains. The catalytic triad present within the catalytic domain is represented in stick and ball format and coloured in pink.

Figure 5c The USP30 catalytic domain can be further subdivided into three subdomains – the zinc binding fingers; here coloured in hot pink; the thumb domain, here coloured in magenta and the palm subdomain, coloured in wheat. The catalytic triad lies between the thumb and palm subdomains.

.....

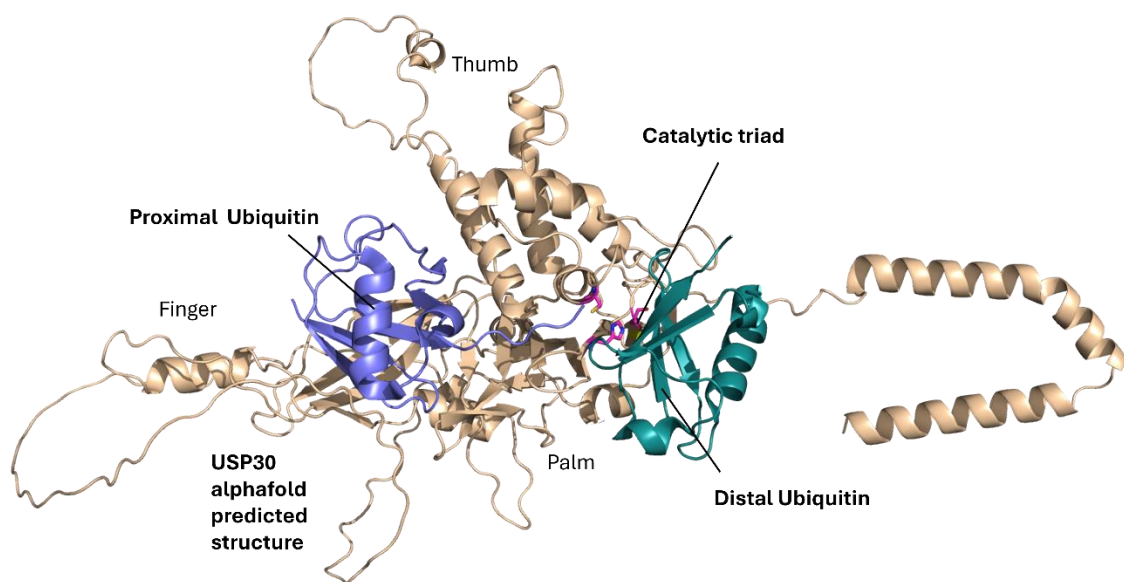
1.6.2. USP30 Has A Proximal Binding Domain That Confers K6 Di-UB Linkage Specificity

Although several DUBs such as OTUD7B and AMSH-LP display chain specificity, most USPs are promiscuous and cleave all linkage types (Hospenthal, *et al.*, 2013; Miller *et al.*, 2019; Lange, *et al.*, 2022; Caba *et al.*, 2022). Yet, USP30 shows a strong preference for K6-diubiquitin chains, and to a lesser degree, also demonstrates some selectivity for K11, K48 and K63 chains (Gersch *et al.*, 2017). Notably, RBR ligases also demonstrate linkage specificity when assembling chains. In Parkin's case it has been shown to have a predilection for assembling K6-linkages (Michel, *et al.*, 2017), thus allowing USP30 to antagonise Parkin activity quite specifically. DUBs that display linkage specificity also tend to be less substrate-specific, hence accounting for the big substrate overlap between Parkin and USP30 (Cunningham, *et al.*, 2015; Mevissen *et al.*, 2020).

This substrate selectivity has been linked to the proximal binding domain (**Figure 6a**). USP30 is one of the few DUBs to display a proximal ubiquitin-binding site, which has been determined to confer linkage preference (Gersch *et al.*, 2017; Mevissen *et al.*, 2020; Lange, *et al.*, 2022). USP30 hence binds two ubiquitin moieties between the palm and thumb subdomains (**Figure 5c**), where the non-canonical catalytic serine and the neighbouring hydrophobic tryptophan residues sit. This interface interacts with the hydrophobic Ile44 ubiquitin patch and causes structural hindrance with the polyubiquitinated linkages such that only the preferred linkages

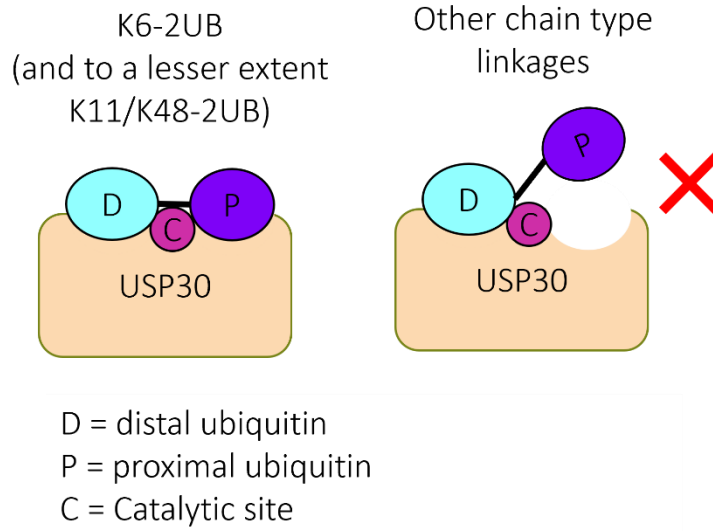
can bind (**Figure 6b, c**) (Gersch *et al.*, 2017; Lange, *et al.*, 2022). USP30 therefore structurally prefers to cleave between the two ubiquitin moieties. This preference for cleaving from the distal end of the ubiquitin chain makes USP30 an exo-deubiquitinating (exo-DUB) enzyme (Gersch *et al.*, 2017), and while exo-deubiquitinating enzymes are capable of cleaving the monoubiquitin tag from the substrate which has been observed with the mono-ubiquitinated TOM20 substrate (Rusilowicz-Jones *et al.*, 2020). However, an extensive study has not been conducted on USP30's ability to cleave the mono-ubiquitinated form of its substrates although it should be noted that other linkage specific DUBs have been observed to leave a monoubiquitin tag behind after cleavage (Mevissen *et al.*, 2020). Implying a need for further characterisation of USP30 cleavage on alternative chain lengths and orthogonal substrates.

a.



b.

USP30 diubiquitin binding



c.

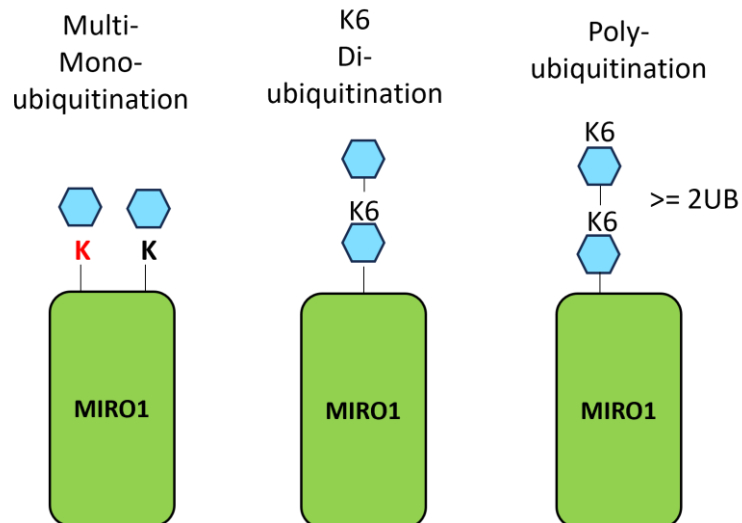


Figure 6. USP30 Has A Ubiquitin Proximal Binding Domain That Confers It Substrate Specificity

Figure 6a. AlphaFold representation of full-length USP30 bound to a proximal (dark blue) and distal (light blue) K6-diubiquitin linkage. The catalytic triad, depicted in pink stick and ball format, sits in the region where the isopeptide bond between the two UB moieties lies, allowing the catalytic cysteine the

perfect position to perform the nucleophilic attack required to cleave the bond.

Figure 6b. Schematic of USP30 distal and proximal ubiquitin (UB) binding sites. Distal UB (light blue) and proximal UB (dark blue) bind to USP30 in such a way that the scissile bond is placed over the catalytic site (pink) to be cleaved. Only K6 diUB linkages, and to a lesser extent K11 and K48 diUB linkages (left) can bind to the DUB, as steric hindrance prevents other polyubiquitinated chains from binding to the proximal UB binding site (right).

Adapted from Lange et al., 2022

Figure 6c. Schematic of the different types of MIRO1 ubiquitination. MIRO1 can be mono-ubiquitinated on different lysine residues (coloured here in black and red) or polyubiquitinated. Further ubiquitination of the ubiquitin moieties causes polyubiquitinated chains to build up, with the favoured substrate linkage for USP30 cleavage being K6-diubiquitinated-MIRO1 (K6-diUB-MIRO1) (Gersch *et al.*, 2017; Sato *et al.*, 2017), although since USP30 reportedly prefers to cleave the bond between the proximal and distal ubiquitin moieties any polyubiquitinated linkage assembled on the K6 site should act as a good substrate (Gersch *et al.*, 2017; Sato *et al.*, 2017).

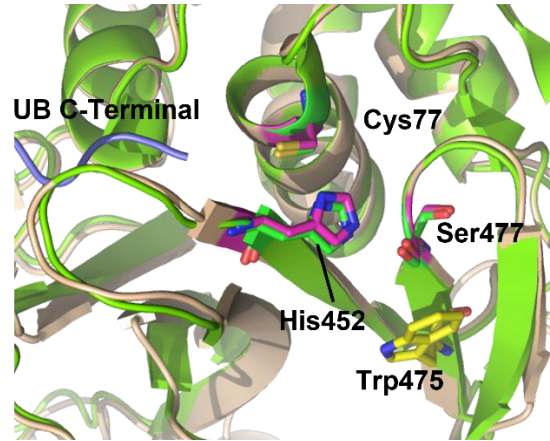
.....

1.6.3. USP30 Has A Distinct Catalytic Triad

Most USPs have a catalytic triad composed of a cysteine, a histidine and an acidic residue – usually an asparagine, aspartate or glutamate residue. Here, during catalysis, the acidic residue polarises the basic histidine, allowing it to lower the pKa of the catalytic cysteine. This primes it to engage in a nucleophilic attack against the carbonyl group within the peptide bond between the ubiquitin tag and the substrate, which makes an oxyanion intermediate before releasing the substrate and free UB. However, USP30 is distinct from the majority of the other members of the USP family because the USP30 catalytic triad is composed of Cys77, His452 and Ser477 (**Figure 7a**), thereby substituting the acidic residue for a serine (**Figure 7b**). This makes USP30 one of the few USPs, along with USP16 and USP45, to have a serine as part of their catalytic triad (Gersch, *et al.*, 2017). In the USP30 non-canonical catalytic triad, the serine residue forms a hydrogen bond with the catalytic histidine, thus presumably allowing for a Ser477-His452-

Cys77 charge relay by causing the His452 side chain to change orientation (Gersch *et al.*, 2017; Sato *et al.*, 2017).

a.



b.



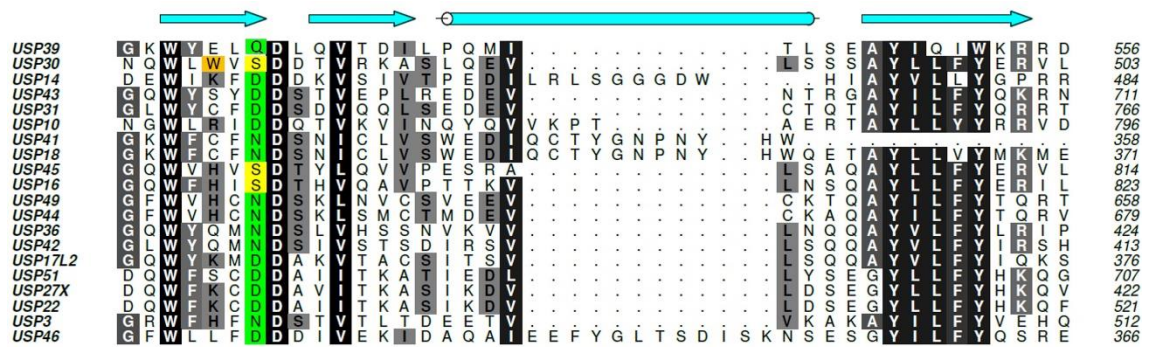


Figure 7. USP30 catalytic triad and sequence alignment of the 19 phylogenetically closest USP family members.

Figure 7a depicts the USP30 catalytic triad of PDB:5OHK (green) (Gersch *et al.*, 2017) and alphaFold: Q70CQ3 (wheat) structure superposed. The catalytic triad is composed of the catalytic cysteine residue 77, histidine 452 and the non-cannonical serine 477 residues (all represented in pink stick diagrams). The conserved tryptophan residue at position 475 (W475) responsible for linkage specificity is depicted in yellow. Once the C-terminal end of the ubiquitin (UB) moiety (blue) enters the binding pocket, the catalytic residues work together to allow the cysteine 77 to perform a nucleophilic attack on the carbonyl end of the UB moiety to cleave it from the target protein. During cleavage an oxyanion intermediate is stabilised by an oxyanion hole formed after the catalytic histidine residue is polarised by the serine residue. This causes the target protein to be released along with the intermediate, which then reacts with a free water molecule to release the UB and free the enzyme (Nijman *et al.*, 2005).

Figure 7b displays the conserved catalytic triad and neighboring residues of the 19 phylogenetically closest USP30 family members as determined by UBIHUB (Liu *et al.*, 2019). The sequence alignment was produced using Clustal Omega and the conserved residues are displayed such that the darker the residue, the more conserved it is. Green residues show the conserved catalytic triad composed of Cys-His- Acidic residue, while the distinct USP30 serine 477 and tryptophan 477 residues are highlighted in yellow and orange respectively. The Uniprot: Q70CQ3 (red) and PDB: 5OHK (blue) files were supplied to the Aline™ software to determine where the residues would localise within the structural features of USP30. Beta sheets are depicted with arrows, alpha helices with cylinders, and loops by long wavy strands.

This unusual catalytic triad is observed to be conserved in other USP30 orthologues (**Figure 8**). Sato et al., speculated that the serine residue may arise due to the conserved hydrophobic tryptophan residue in its proximity (Sato *et al.*, 2017; Gersch *et al.*, 2017; Jiang, *et al.*, 2020). This residue in humans lies only two amino acids apart from the catalytic serine residue, which would potentially cause steric hindrance in the presence of the traditional acidic residue, thereby explaining why USP30 has this unique catalytic triad (Sato *et al.*, 2017). Notably, both of these residues lie within the proximal ubiquitin binding site responsible for substrate selectivity. Hence, experiments focused on characterising the function of the catalytic serine residue have postulated that W475 plays a role in diubiquitin linkage selectivity, likely due to its polar interactions (Jiang, *et al.*, 2020). Sato *et al.*, carried out the experiments using *Danio rerio* (zebrafish) USP30 and showed that USP30 linkage specificity was completely eradicated when the W475 residue was mutated to an alanine, thereby indicating that the residue is critical for selectivity. When the serine residue was swapped for a polar, uncharged residue (asparagine) the DUB showed decreased substrate binding and catalytic activity due to the disturbance of the nucleophilic attack required to cleave the bond between the substrate and its ubiquitin tag. The subsequent mutation of the tryptophan residue for an alanine to make a double mutant was able to regain a higher catalytic activity than the S-to-N mutant only (Sato *et al.*, 2017). Thus, the experiments with the serine and tryptophan double mutants proved that the W475 residue that lies within the proximal binding domain is involved in USP30 linkage selectivity, and that while the serine residue may not play a direct role in substrate specificity, its structure prevents any conformational hindrance from taking place between the W475 and the catalytic triad (Sato *et al.*, 2017).

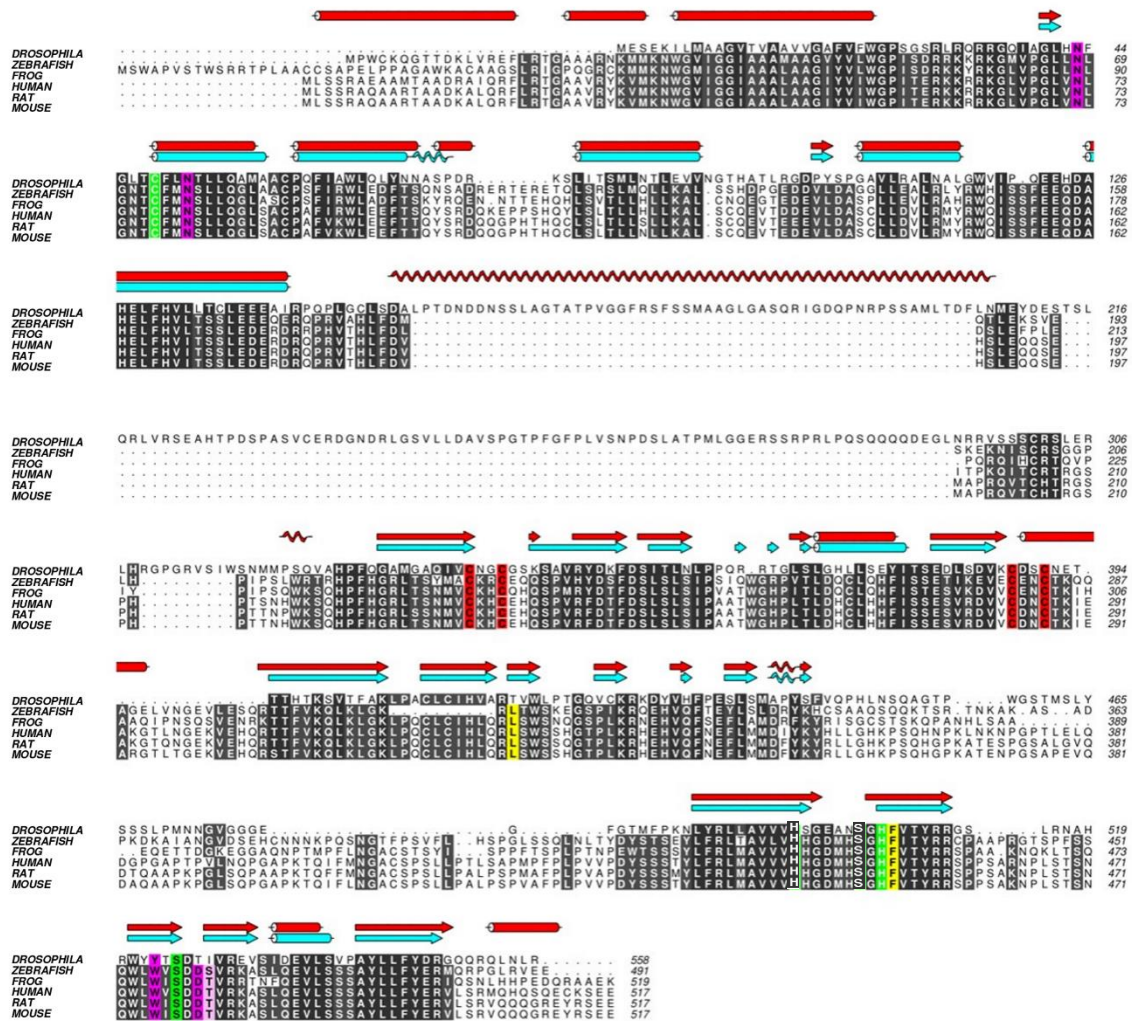


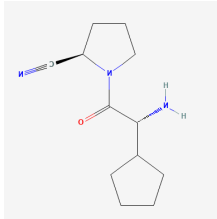
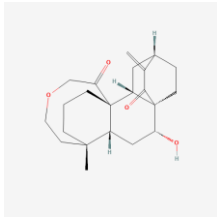
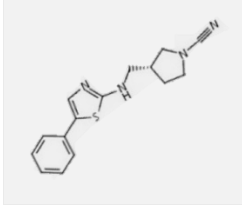
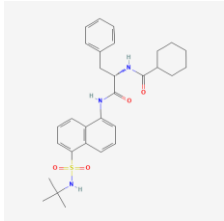
Figure 8. USP30 Orthologue Sequence Alignment.

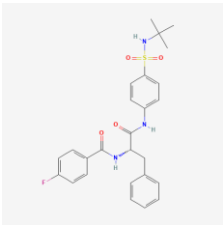
The alignment of USP30 sequences corresponding to six different species was generated using Clustal Omega and visualised using Aline™ Software. The more conserved residues are displayed in darker colours, while certain key residues have been highlighted in colour. The zinc-finger-binding cysteine residues conserved throughout all species are coloured in red and the catalytic triad residues in green – note that the USP30 serine residue is conserved throughout all the reported species. Pink residues represent those present in the interface that interact with the proximal ubiquitin while yellow residues are key hydrophobic residues that were removed from the 50HK construct to allow for better solubility and expression. The Uniprot: Q70CQ3 (red) and PDB: 50HK (blue) files were also used to determine where the residues would localise within the structural features of USP30. Beta sheets are depicted with arrows, alpha helices with cylinders and loops by long wavy strands.

1.7. USP30 inhibitors

USP30 plays an important role in the PINK1/Parkin-mediated mitophagy pathway and as such has become an attractive target for inhibition to treat early-onset PD, along with other related neurodegenerative disorders. USP30 inhibition could also be potentially used to treat other disorders in which mitochondrial dysfunction plays a key role in the aetiology, including other forms of PD, and certain types of Alzheimer's Disease and Amyotrophic Lateral Sclerosis (Bingol *et al.*, 2014; Rusilowicz-Jones *et al.*, 2022). As such, efforts have been focused on the development of small molecule inhibitors capable of interacting with the USP30 binding pocket. To date, the only USP30 inhibitor to have reached phase I clinical trials is MTX652 by Mission Therapeutics, which is being developed to treat chronic kidney disease (CKD). If successful, this proof-of-principle may lead to the development of a brain-penetrating drug based on the same biology (Silvian, 2022). At the same time, there are several potential small molecule drug candidates (**Table 1**) currently in biological evaluation and pre-clinical studies (Kluge *et al.*, 2018; Chen *et al.*, 2021; Tsefou, *et al.*, 2021; Varca *et al.*, 2021; Wang *et al.*, 2022). While the drug discovery efforts are underway, there still remains an important drawback with most of the drug candidates presented: limited potency and off-target effects (Wang *et al.*, 2022). Since the catalytic cysteine is present in all cysteine proteases, off-target effects have been observed in cell lines to occur at higher concentrations when inhibitory compounds work by targeting the catalytic cysteine of USP30, with off-target effects noticed more predominantly with other USP family members (Wang *et al.*, 2022). This is the case for most of the characterised inhibitors, and possibly for PXW (a.k.a. covalent inhibitor 552; PDB:8D0A) and PKH (a.k.a. covalent inhibitor 829; PDB:8D1T), the first two inhibitors to be crystallised with USP30 (**Figure 9a and 9b**) (Song, *et al.*, 2023) which clearly show the formation of a covalent bond with the catalytic cysteine of USP30 and thus may run into similar issues with off-target effects.

Table 1. Summary of USP30 inhibitors.

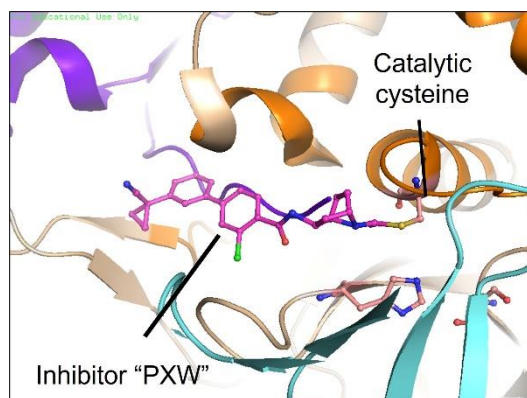
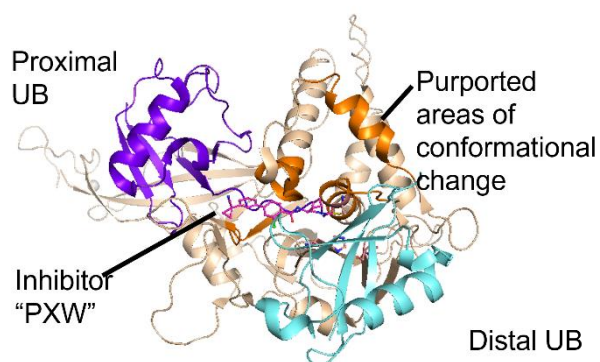
TYPE OF INHIBITOR	INHIBITOR	POTENCY	MODE OF ACTION	COMMENTS	REFERENCES
Cyanopyrrolidines and other N-cyano derivatives.		15 – 30 nM (very potent)	Binds to the catalytic cysteine.	Poor selectivity at high concentrations. Includes inhibitors USP30Inh1-3; FT-385; and new inhibitors PXW and PKH.	Tsefou <i>et al.</i> , 2021
Small natural diterpenoid derivatives	15-oxospiramylactone derivatives 	2.5 μM (not potent)	Binds to the catalytic cysteine.	Not enough information about the compound's selectivity and underlying molecular mechanism.	Yue <i>et al.</i> , 2014; Wang <i>et al.</i> , 2011
Novel compounds	USP30i 	2.45 μM (not potent)	Not known	Poor selectivity	Phu <i>et al.</i> , 2020; Wang <i>et al.</i> , 2022
Racemic phenylalanine derivatives	MF-094 	0.12 μM (potent)	Not known	highly selective	Kluge <i>et al.</i> , 2018

Benzosulphonamide derivatives	<p>Compound 39</p> 	20 nM (very potent)	Not known	Highly selective	Kluge <i>et al.</i> , 2018; Rusilowicz-Jones, <i>et al.</i> , 2020; O'Brien <i>et al.</i> , 2023
-------------------------------	--	---------------------	-----------	------------------	--

Structures from PubChem

a.

For Educational Use Only



b.

For Educational Use Only

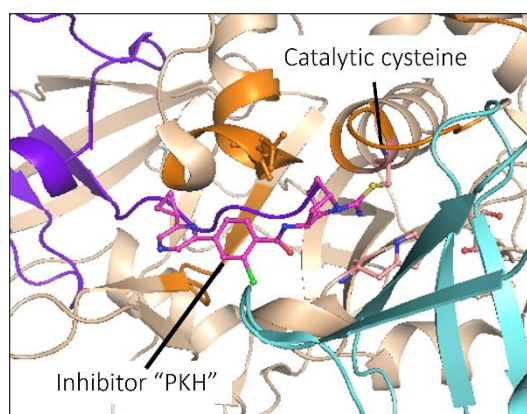
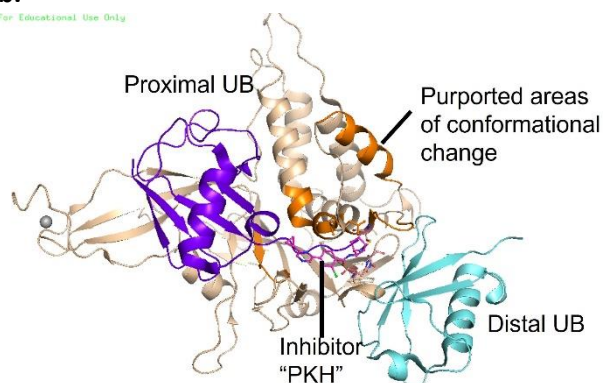


Figure 9. Reported structures of USP30 bound to inhibitors PXW and PKH.

USP30 covalently bound to inhibitors PXW (PDB: 8D0A) and PKH (PDB: 8D1T) (Sato, *et al.*, 2023).

Figure 9a shows the PDB: 8D0A file corresponding to USP30, coloured in wheat, bound to the covalent inhibitor 552, here called PXW (Song, *et al.*, 2013). The inhibitor is

depicted in stick and ball format (pink) and in the figure to the right can be seen bound through a sulfhydryl group (yellow) to the catalytic cysteine (orange-coloured stick representation). The proximal UB (dark blue) and the distal UB (light blue) are shown bound to USP30, and the orange regions demarcate the purported areas of conformational change (O'Brien *et al.*, 2023).

Figure 9b shows the PDB: 8D1T file corresponding to USP30 bound to the covalent inhibitor 829, here called PKH (Song, *et al.*, 2013). The structure is represented using the same colour scheme as described in Figure 9a and the same binding interaction is observed between PKH and USP30 as seen with PXW.

.....

Recent advances have brought sulphonamide derivatives to the forefront of the investigation pipelines, as these types of compounds are able to bind to USP30 with high selectivity. Chief among them are MF-094, a naphthyl-sulphonamide derivative with a reported IC_{50} of 0.12 μM and Compound 39 (CMPD39), a benzosulphonamide derivative with an IC_{50} of 0.02 μM (Kluge *et al.*, 2018; Mandal *et al.*, 2022; Li, *et al.*, 2022; Rusilowicz-Jones, *et al.*, 2022; O'Brien, *et al.*, 2023). This latter small molecule inhibitor, CMPD39, was observed to bind in a slow and tight manner, reminiscent of the formation of a covalent bond through *in vitro* enzyme kinetics and Hydrogen/Deuterium eXchange Mass Spectrometry (HDX-MS), an *in-solution* technique capable of monitoring protein movements (**Figure 9**). These lie in the binding pocket located between the USP30 thumb and palm subdomains that confer substrate specificity (O'Brien *et al.*, 2023), thus suggesting that CMPD39 interrupts the entrance of the UB C-terminus tail into the binding pocket. This is further supported by molecular docking simulations that predict CMPD 39 lies approximately 7.4 Å away from the catalytic Cys77 thiol side chain.

Comparison of the PDB 5OHK crystal structure to the 8D0A and 8D1T structures, which show the ubiquitin-bound truncated USP30 and the PKH/PXW inhibitor-bound USP30 respectively, has brought attention to structural differences found predominantly in the loops (loop1, loop2 and loop residues 150 -162). These regions, highlighted in orange in **Figure 9**, could provide flexibility for substrate recognition. This, along with docked structures, infer that the highlighted areas likely undergo conformational changes when binding the substrate (O'Brien *et al.*, 2023). However, despite the progress made in the last few years, further characterisation of USP30 substrate specificity is required to understand how these inhibitors engage with the enzyme. Hence a crystal structure of USP30 bound to a physiological substrate

would provide insight into USP30 binding mechanisms. This in turn needs to be complemented by structural validation of the new sulphonamide-derivative inhibitors bound to USP30.

1.8. Aims of the project

This project focuses on the biochemical characterisation of USP30 by establishing a methodology to produce its physiological substrate ubiquitinated-MIRO1. The hypothesis is that **the physiological substrate generated here can be used to run *in vitro* enzyme assays to characterise USP30 substrate recognition and inhibition in the presence of the new sulphonamide derivative inhibitors MF-094 and CMPD39.**

This will be achieved through 3 main objectives:

1. Design and generate a USP30 construct that can be used to successfully produce the protein for biochemical and structural studies, alongside other proteins required for probing USP30 deubiquitinating activity (the HRV3C protease required to cleave the affinity tags from the construct; the E2 enzyme UBE2L3; UB and the substrate MIRO1).
2. Establish a way to produce a physiological substrate of USP30 through the use of MIRO1 ubiquitination assays.
3. Conduct enzyme assays focused on USP30 deubiquitinating activity against the generated physiological substrates and in the presence or absence of the inhibitors.

Furthermore, while X-ray crystallography has been able to generate the structures of zebrafish and human USP30, these crystals are both already engaged with ubiquitin moieties. This makes structural probing of the apo-structure or of USP30 bound to one of the promising sulphonamide derivative inhibitors. This work will provide a platform from which to enable structural characterisation of the protein bound to its physiological substrate, either mono- or poly- ubiquitinated MIRO1, in the presence and absence of one of the new specific inhibitors, MF-094 or CMPD39, in the future. Of note, determining whether USP30 can bind monoubiquitinated-MIRO1 could also help establish the minimal substrate for future structural work. The combination of this biochemical and structural characterisation will in turn aid in future drug-discovery efforts by providing a springboard from which more selective inhibitors can be designed, thus streamlining the drug-discovery and production pipeline to treat early-onset forms of PD and other related disorders characterised by mitochondrial dysfunction.

2. Materials and Methods

2.1 Reagents

2.1.1. Bacterial Strains

The bacterial strains used in this project are listed in **Table 2** along with their purpose. The ampicillin (Amp100) and chloramphenicol (CLA02) were sourced from Formedium.

Table 2. Bacterial strains used during this project.

Bacterial Strain	Antibiotic used	Use	Source
NEB DH5- <i>a</i> high efficiency cells	Ampicillin	Plasmid cloning + ligation	NEB; C2987H
One Shot™ BL21 Star™ (DE3) E. coli	Ampicillin	Protein production	Thermo FisherScientific; C601003
Rosetta 2(DE3)pLysS Chemically Competent E. coli	Ampicillin, Chloramphenicol	Protein production	Novagen; 70956

2.1.2. Media

Formedium LB Broth Miller was used to generate the agar plates, while 2YT (Formedium; YDB0102) and auto-induction 2YT media (Formedium; AIM2YT0210) were used for the expression cultures to produce the proteins. For the former, isopropyl- β -D-thiogalactopyranoside (IPTG) (Formedium; IPTG025) had to be used at different concentrations depending on the protein to induce optimal expression of the proteins as listed in **Table 3**.

Table 3. Concentration of IPTG used for different proteins:

Protein	Concentration of IPTG used (μ M)
Ubiquitin	800
UBE2L3	800
MIRO1	300
USP30	500

2.2. DNA manipulation methods

2.2.1. Agarose gel preparation

The agarose gels used to visualise DNA samples contained 0.35g Multi-Purpose Agarose (Formedium; 11 388 991 001), 50 ml TAE buffer (Thermo Fisher Scientific; B49) and 5 μ l SYBRsafe stain (Invitrogen; 2291850). Gels were run at 100 V for approximately 25 minutes.

2.2.2. USP30 Plasmid Design

The USP30 plasmid was designed by using the UniProt Q70CQ3 and PDB: 5OHK files (Gersch *et al.*, 2017) and had an N-terminal 6 Histidine (6xHis) affinity tag, followed by a 3C protease cleavage site, a glutathione-S-transferase (GST) affinity tag, and another 3C cleavage site introduced before the protein sequence, along with the mutations specified in **Table 4**. The 6xHis tag was originally incorporated into the 5OHK construct to be able to separate the free GST out (Gersch *et al.*, 2017), and thus was kept for additional purification purposes should it be required at later stages of the project. The insert was supplied by Integrated DNA Technologies (IDT) and cloned into a pET-15p-16b2 vector. **Figure 4** depicts the superposition of the predicted full-length USP30 against the truncated 5OHK construct utilised here while **Supplementary Figure 1** shows the plasmid map and pertaining cloning experiments.

Table 4. List of mutations introduced into the previously crystallised 5OHK USP30 construct.

MUTATION	REASON
' Δ 1-63 +GP	Removed the N-terminus disordered regions and left the overhang from the GST affinity tag.
Δ 179-216 + GSGS	The disordered loop was removed to allow for better protein stabilisation and the +GSGS motif was added to reintroduce the flexibility needed.
F348D	Removal of hydrophobic residue allowed for improved expression, activity and solubility.
M350S	As above.
I353E	As above.
Δ 358-431 + SNA	Removed a flexible, proline-rich insertion

2.2.3. Primers

Primers were designed using Snapgene Viewer 6.1.1. software and purchased from IDT. The primers were subsequently solubilised in Elution Buffer (EB) from the Mini-prep Kit (Qiagen; 27104) to achieve a concentration of 100 μ M. Subaliquots were taken and further diluted to 10 μ M. All the primer aliquots were then stored at -20° C for future use. **Table 5** lists all the primers used in this project.

Table 5. Primers and their function

PRIMER	PRIMER SEQUENCES (5' \rightarrow 3')	Use
INSERT_F_001	GATATACCATGGGCAGCAGC	Forward Primer for insert amplification.
INSERT_R_002	CTTCCTTTCTGGGCTTTGTTAGC	Reverse Primer for insert amplification.
VECTOR_F_003	GCTAACAAGCCCGAAAGGAAG	Forward Primer for vector amplification.
VECTOR_R_004	CTGCTGCCCATGGTATATC	Reverse Primer for vector amplification.
T7_F_007	TAATACGACTCACTATAGGG	Forward Sequencing primer
T7_R_008	GAAATCTAACAATGCGCTCATC	Reverse Sequencing primer
MUTAGENESIS_F_011	TATGAATAGCCTGCTGCAAGGTTTATCCGCCT	Forward mutagenesis primer for catalytically dead USP30
MUTAGENESIS_R_012	AAGgcAGTATTTCCAAGGTTGACCAGACCAGGA	Reverse mutagenesis primer for catalytically dead USP30

2.2.4. Vector Amplification and USP30 Insert Ligation.

An empty pET-15b-6b2 vector was acquired from the Walden lab. This vector was then amplified using a KOD Hot Start DNA Polymerase Kit (Sigma-Aldrich; 71086) and the thermocycling conditions listed in **Table 6**. A sequential temperature gradient was set up for the annealing step with sequential temperature increases between 58 – 66 °C and allowed to run for 30 cycles.

Table 6. Thermocycling conditions for the vector amplification.

Step	Temperature (°C)	Time (seconds)
Initial denaturation	95	120
1. Denaturation	95	20
2. Annealing	58-66	10
3. Extension	68	180
Hold	4	-

The optimal annealing temperature (61 – 63 °C) was determined by running an agarose gel and the corresponding lanes were further purified using a PCR purification Kit (Qiagen; 28104).

The USP30 insert provided by IDT was then solubilised and ligated using a HiFi DNA Assembly Kit (NEB; M5529AVIAL) following the manufacturer’s protocol (#E5520S). After transformation, random colonies were selected and sent for sequencing to Eurofins. Colonies with no unexpected mutations from the designed plasmids were then purified by Mini-prep (Qiagen; 27104) following the manufacturer’s protocol and stored at -20 °C for protein production.

Ligation of the insert was performed using the NEBioCalculator with an optimised ratio of 1 vector: 3 insert. The quantity of insert required when employing the standard 100ng of vector was determined using the following equation (NEB):

$$\text{Ng of insert} = \frac{\text{ng of vector (100 ng)}}{\text{Vector (kbp)}} * \text{ratio (1: 3)} * \text{insert size (kbp)}$$

2.3. Protein Handling Methods

2.3.1. Protein Production

2.3.1.1 Transformation And Glycerol Stocks

Human Rhinovirus HRV-3C protease containing a 6xHis affinity tag encoded in vector pHisGEX was transformed into One Shot™ BL21 (DE3) *E. Coli* cells by first thawing the cells for 10 minutes and then adding 1 µl of approximately 100 ng/ µl plasmid into an aliquot containing 9-99 µl of cells. These were kept on ice for 25 minutes before being heat-shocked at 42 °C for 30 seconds and allowed to cool for 2 minutes on ice. The reaction was then diluted 10-fold by using room-temperature Super Optimal broth with Catabolite repression (SOC) medium and the cells were allowed to recover for 30 minutes at 37 °C, 180 RPM using the eppendorf thermomixer comfort shaker. Afterward, 100 µl of the transformation mix was added into either an ampicillin-only or an ampicillin and chloramphenicol selection plate and left to incubate overnight at 37 °C.

The exact same transformation methodology was followed for the production of the remaining proteins listed in **Table 7**, except Rosetta cells were employed for MIRO1 and USP30 for higher expression yields.

Glycerol stocks were then made by setting up a starter culture with one of the colonies in 2YT media containing antibiotic (Ampicillin at 10 mg/ml and if required Chloramphenicol at 3.5 mg/ml) and incubating overnight at 30 °C while shaking at 180 RPM. Then 0.5 ml of this starter culture was mixed with 0.5 ml of 50 % glycerol and stored at -80 °C to initiate future cultures.

Table 7. Proteins produced and their corresponding vector and affinity tags.

PROTEIN	VECTOR	CELL TYPE	AFFINITY TAG	ANTIBODY USED
HRV3C	pHisGEX	One Shot™ BL21 Star™ (DE3) E. coli	6xHis	Ampicillin
UBE2L3	pET-15b-6b2	One Shot™ BL21 Star™ (DE3) E. coli	6xHis	Ampicillin
UBIQUITIN	pET-15b-6b2	One Shot™ BL21 Star™ (DE3) E. coli	6xHis	Ampicillin
MIRO1	pET-15b-6b2	Rosetta 2(DE3)pLysS E. coli	GST	Ampicillin, Chloramphenicol
USP30	pET-15b-6b2	Rosetta 2(DE3)pLysS E. coli	6XHis/ <u>GST</u>	Ampicillin, Chloramphenicol
USP30_C77A	pET-15b-6b2	Rosetta 2(DE3)pLysS E. coli	6XHis/ <u>GST</u>	Ampicillin, Chloramphenicol

2.3.1.2. Expression Cultures

Starter cultures were set up by scraping glycerol stock into 15 ml of media in the same conditions used in Section 2.3.1.1. From here 15 ml of the starter culture was inoculated into each liter of media to scale up the protein production for expression cultures. Each liter of media was also supplied with Ampicillin at 10 mg/ml and if required Chloramphenicol at 3.5 mg/ml antibiotic(s), along with 3 drops of Antifoam 204. These expression cultures were then allowed to grow at 37 °C, 180 RPM until the cultures reached an OD A_{600nm} of 0.8 – 1.0.

Protein expression for cultures using regular 2YT media (but not for auto-induction 2YT media), was then induced by incubating 1.30 hrs at 16 °C, 180 RPM before adding IPTG to the concentration stated in **Table 3**. Autoinduction media was directly cooled to 16 °C after the OD reached A_{600nm} of 0.8 – 1.0 levels.

The expression culture was then left to incubate with the same conditions overnight regardless of the type of media used. The cells were then harvested by centrifugation using a Beckman JS-4.2 Swinging-Bucket Rotor (4000 RPM, 4 °C, 30 min, 1L centrifuged vials) and subsequently resuspended with 1 ml of ice cold Harvest buffer (50 mM Tris-HCl pH 7.5 + 150 mM NaCl + 20

mM imidazole + 5% glycerol + 250 μ M TCEP) for every 1 g of pellet and stored at -80°C until ready to continue with the purification.

Once ready to proceed with the purification, the harvested cells were thawed and treated with 1 ml of ice cold lysis buffer (50 mM Tris-HCl pH 7.5 + 150 mM NaCl + 20 mM imidazole + 5% glycerol + 250 μ M TCEP + 1: 5,000 DNase + 8 mM MgCl_2 + 4 mg/ml Lysosyme + a large protease tablet (Thermo Fisher; #A32955) per 50 ml of buffer) for every 1 g of cell pellet. The cells were subsequently sonicated using a VCX 130 sonicator with a 13 mm probe for 2 minutes using 10-second pulses with 50 seconds off between each pulse at an amplitude of 60 %. The lysate was then clarified using a Beckman Allegra 64R, fixed-angle rotor and spun at 4°C , 31,000 RPM (50 ml vials) for 40 minutes before the supernatant was filtered through a 22 μ m syringe and purified.

2.3.2. Protein Purification

As listed in **Table 7**, protein lysate was incubated in gravity columns using either His-Pur™ Nickel-NTA beads for 6xHis-tagged proteins or glutathione-sepharose (GSH) beads for GST-tagged proteins, including USP30. The proteins were then purified by first washing thoroughly with high salt buffer to remove any impurities, followed by low salt buffer to remove unbound proteins. The proteins were then eventually eluted using either the High Imidazole Buffer or the Low Salt Buffer. All the buffers utilised for protein purification are listed in **Table 8**.

Table 8. List of Protein purification buffers.

PROTEIN	BUFFER	COMPONENTS
HRV3C, UBE2L3, UBIQUITIN, USP30	High salt buffer	50 mM Tris-HCl pH 7.5 + 500 mM NaCl + 20 mM imidazole + 5% glycerol + 250 μ M TCEP
	Low salt Buffer	50 mM Tris-HCl pH 7.5 + 150 mM NaCl + 20 mM imidazole + 5% glycerol + 250 μ M TCEP
HRV3C	High Imidazole Buffer	50 mM Tris-HCl pH 7.5 + 150 mM NaCl + 250 mM imidazole + 5% glycerol + 250 μ M TCEP
MIRO1	MIRO1 High salt buffer	PBS pH 7.3 + 350 mM NaCl + 800 μ M TCEP + 5% glycerol
	MIRO1 Low salt Buffer	50 mM Tris-HCl pH 7.5 + 150 mM NaCl + 5% glycerol + 250 μ M TCEP
USP30	Pre-anion exchange buffer	50 mM Tris-HCl pH 7.5 + 20 mM imidazole + 5% glycerol + 250 μ M TCEP
	Anion exchange high salt buffer	25 mM Tris pH 8.5 + 500 mM NaCl + 5 mM DTT +5 % glycerol
	Anion exchange Low salt buffer	25 mM Tris pH 8.5 + 50 mM NaCl + 5 mM DTT + 5 % glycerol
UBE2L3, UBIQUITIN, MIRO1 AND USP30	Gel filtration Buffer	40 mM HEPES-NaOH pH 7.6 + 80 mM NaCl + 0.5 mM TCEP + 5 % glycerol

2.3.2.1. HRV3C

For HRV3C protein, columns containing 4 ml of 50 % Ni-NTA bead slurry was used for 6 L of expression culture. The beads were first washed with 20 resin volumes (RV) of high salt buffer, followed with 20 RV of low salt buffer before being eluted using the High Imidazole Buffer. The eluted protein was concentrated to 2.5 ml using a spin-concentrator with a molecular weight cut off of 10,000 Da at 4 °C, 4000 RCF. The sample was then buffer exchanged into 25 ml of storage buffer (made up of low salt buffer supplemented with an equal amount of 50% glycerol) using a PD-10 column. An SDS-PAGE gel was run to confirm sample purity and an

absorbance (280 nM) reading was measured to determine the sample concentration – in this case, 6.6 mg/ml. The protein was then snap-frozen in liquid nitrogen and stored at -80 °C.

2.3.2.2. UBE2L3

For UBE2L3 protein 8 ml of 50 % Ni-NTA bead slurry was used for 3 L of expression culture. The beads were washed with 20 RV of high salt buffer, followed with 20 RV of low salt buffer. The beads were then incubated for 16-18 hours with 100 µg of HRV3C protease at 4 °C before eluting the protein using 4 RV of the low salt buffer. Samples were observed in SDS-PAGE and the protein elution was spin concentrated down to 1 ml using a spin-concentrator with a molecular weight cut off of 3,000 Da at 4 °C, 4000 RCF.

The sample was then further purified via size-exclusion chromatography using the gel filtration buffer and an ÄKTApure system. The sample was loaded onto a pre-equilibrated Superdex 75 Increase 10/300 GL column and 0.5 ml fractions were collected – peak fractions were analysed under SDS-PAGE and the pure samples (fractions 10 -12) were pooled together and further spin concentrated using the same conditions as stated above. The absorbance (280 nM) reading for the sample suggested a concentration of 8.6 mg/ml, when normalised to the calculated extinction coefficient. The protein was then snap-frozen in liquid nitrogen and stored at -80 °C.

2.3.2.3. UBIQUITIN

The purification of the C-terminal 6xHis-Ubiquitin was carried out using the exact same procedure described above in Section 2.3.2.2. for UBE2L3. Absorbance (280 nM) reading for the ubiquitin produced suggested a concentration of 18.8 mg/ml, when normalised to the calculated extinction coefficient and the protein was subsequently stored at -20 °C.

2.3.2.4. MIRO1

For MIRO1 20 ml of 50 % GSH bead slurry was used for 6 L of expression culture. The binding was performed by allowing the beads and lysate to rotate for 2 hrs at 4 °C. The beads were then washed with 20 RV of the MIRO1 high salt buffer, followed by 20 RV of the MIRO1 low salt buffer. The beads were then incubated 16-18 hours with 100 µg of HRV3C protease at 4 °C before eluting the protein using the MIRO1 Low Salt Buffer. Samples were observed in SDS-

PAGE and the protein elution was spin concentrated down to 1 ml using a spin-concentrator at 4 °C, 4000 RCF.

The sample was then further purified via size-exclusion chromatography in the same manner as described above for UBE2L3. The concentration was determined to be 8.7 mg/ml based on the absorbance (280 nM) and the protein was then snap-frozen in liquid nitrogen and stored at -80 °C.

2.3.2.5. USP30

For USP30, 3 ml of 50 % GSH bead slurry was used for each Liter of expression culture. The binding was performed by allowing the beads and lysate to rotate for 2 hrs at 4 °C. The beads were washed with 20 RV of high salt buffer followed with 20 RV of low salt buffer before being incubated for 16-18 hours with 200 µg of HRV3C protease at 4 °C and subsequently eluting the protein with 5 RV of Low Salt Buffer. Samples were observed by SDS-PAGE and the protein elution was spin concentrated at 4 °C, 4000 RCF.

The sample was then diluted 3-fold using a pre-anion exchange buffer and purified in the ÄKTA via anion exchange using a pre-equilibrated 1 ml resource Q (ResQ) column or a 1 ml HiTrapQ column. Fractions of 0.5 ml corresponding to the peak were collected and analysed via SDS-PAGE.

The pure samples were then spin-concentrated down to 500 µl and further purified via size-exclusion chromatography using a Superdex 75 Increase 10/300 GL column or a Superdex 75 HiLoad 16/600 column in the same way as described previously for UBE2L3. Absorbance (280 nM) readings were then taken of the final sample and the protein was snap-frozen in liquid nitrogen and stored at -80 °C.

2.3.3. SDS-PAGE Gels And Samples

SDS-PAGE samples were prepared by adding 4x dye containing 8% β- mercaptoethanol (BME) as a reducing agent and heated to 95 °C for 5 minutes before loading. These samples were then run on a 4-12 % Bis-Tis SDS-PAGE commercial gel (NuPAGE; NP0321BOX) and visualised via Instant Blue Coomassie staining (Abcam; ISB1L) while rocking gently. The stain was then removed, and the gel was rinsed and incubated while rocking with MQ H₂O. Afterwards, the

gels were scanned – and if quantification was required a LICOR Odyssey CLx scanner was further employed along with the Image Lite™ Software to process the data.

2.4. Designing and Performing Enzyme Assay

2.4.1. In Vitro Ubiquitination Assays

2.4.1.1. MIRO1 Ubiquitination Assay

Ubiquitination assays were carried out to generate the physiological substrate of USP30, ubiquitinated-MIRO1. Time and UB concentration were varied according to specific parameters to generate different lengths of ubiquitin linkages on MIRO1, which were later used as substrates to compare USP30 substrate recognition. This method produced both monoubiquitinated MIRO1 (monoUB-MIRO1) and different length linkages of polyubiquitinated MIRO1 (polyUB-MIRO1). From the latter, the longest time point and highest UB concentration was selected to proceed to ensure maximal polyubiquitination. Ubiquitin was incubated at different concentrations (7.5, 15, 30, 60 μ M) along with 15 μ M MIRO1, 0.1 μ M UBA1 (E1), 1.0 μ M UBE2L3 (E2), 0.2 μ M of *C. elegans* Parkin (PDR-1) (E3), 0.4 μ M pUB (with a 6xHis tag on C-terminus) and 2.5 mM ATP to a final volume of 22 μ l (reaction schematic available in **Figure 2**). The reaction was performed in a buffer containing 50 mM HEPES, 150 mM NaCl, 5 mM MgCl₂, 5 % glycerol and 250 μ M TCEP. All reactions were performed at room temperature and stopped with the addition of LDS loading buffer at different time points (0, 15, 45, 60 min).

2.4.2. Profiling USP30 Deubiquitinating Activity

2.4.2.1. USP30 MIRO1-UB Deubiquitination Assay.

MIRO1 was ubiquitinated as outlined in section 2.4.1 but the reaction was stopped by the addition of 5 U/ml of apyrase. The concentration of the reagents used was kept the same, except MIRO1 (5 μ M) and ubiquitin (2.5 μ M), which were nevertheless kept at the same ratio employed in the previous experiments (2 MIRO1: 1 UB). USP30 was subsequently added at different concentrations (0, 0.5, 1 μ M) to start the deubiquitination reaction, which was run for either 0, 10 or 30 minutes before being stopped by the addition of LDS loading buffer. Note that for the 0-minute time-point, the USP30 was added directly to the LDS buffer before adding the other reagents into the tube to ensure that no residual activity was observed.

2.4.2.2. USP30 polyUB -MIRO1 Deubiquitination Assay.

MIRO1 ubiquitination was carried out as outlined above in section 2.4.1 but the reaction was incubated for 1 hour at 30°C before being stopped by the addition of aprotinase (5 U/ml) and the use of different concentrations for MIRO1 (5 µM) and Ubiquitin (20 µM).

USP30 (1 µM) was then added and the deubiquitination reaction was run for 0, 10 and 30 minutes at 30°C before stopping the reaction by adding LDS loading buffer.

2.4.3. Inhibition Assays

2.4.3.1. USP30 Activity Assay In The Presence And Absence Of The Inhibitors MF-094 and CMPD 39.

i. Using MonoUB-MIRO1 As The Substrate

This experiment was run with the same set-up used for the reactions described in Section 2.4.2.1., with the conditions optimised for monoUB-MIRO1 production (5 µM of MIRO1 and 2.5 µM UB). The inhibitors were pre-incubated with USP30 (0.5 µM) for 15 minutes before the DUB: Inhibitor mix was added to the stopped ubiquitination reaction mix. The deubiquitination reaction was then allowed to run for 30 minutes at 30°C before the LDS loading buffer was added to stop the reaction.

ii. Using PolyUB-MIRO1 As The Substrate.

The poly-UB-MIRO1 substrate was produced by following the experiment outlined in Section 2.4.2.2. (with a 1 MIRO1: 4 UB concentration ratio), before the deubiquitination reaction was performed in the same manner described in Section 2.4.3.1.i.

2.4.3.2. Investigating The Potency And Specificity Of Known USP30 Inhibitors.

Preparation for these experiments was kindly undertaken by the team at Ubiquigent (Steven Liness, Kirsten Sinclair, and João Oliveira), who then allowed me to shadow them and take part in the experiments.

i. DUBprofiler™: MF-094 and Compound 39 Selectivity and Potency Against A Panel Of 48

DUBs

DUBprofiler™ is an *in vitro* ubiquitin cleavage assay that uses ubiquitin bound to the fluorescent probe rhodamine (110)-glycine. A fluorescent signal is produced when the ubiquitin is cleaved from the probe, indicating that the DUB is active. In this project, a panel of 48 DUBs, including USP30 was measured in triplicate against the two new sulphonamide derivatives: MF-094 and CMPD39, to investigate the specificity and potency of the inhibitors (Experiment performed by Steven Liness).

ii. DUBprofiler-Cell™: MF-094 And Compound 39 mediated Inhibition Of Endogenous-USP30

UB-Probe Binding.

DUBprofiler-Cell™ is an assay performed within cell lysates or cell cultures to test DUB target engagement by the sulphonamide derivative compounds. For the live cell assay, SH-SY5Y neuronal cells were seeded and treated with either MF-094 or CMPD39 at different concentrations (0, 0.01, 0.03, 0.1, 0.3, 1, 3 and 10 μ M) to test the effect on USP30 activity in live cells. The cell pellets were collected, and lysates were prepared from the samples before being incubated with the proprietary Ubiquigent ubiquitin Activity-Based Probes (ABP) and finally analysed by western blotting. Meanwhile, for the lysate assay, the SH-SY5Y cell lysates were pre-incubated with the same range of inhibitor concentrations followed by incubation with the ABP before western blot analysis.

Note that the required cell work was performed by João Oliveira and Kirsten Sinclair (Ubiquigent), allowing me to lyse the cells, introduce the inhibitor and perform the subsequent SDS-PAGE and Western Blot. João Oliveira and Kirsten Sinclair (Ubiquigent) then scanned the gels and processed the data to produce the EC₅₀ graphs.

CHAPTER 3. Results

3.1 Protein Expression and Purification

Purification of the proteins required for setting up the enzyme assays (listed in **Table 9**) was carried out via affinity chromatography and, when required, anion exchange and gel filtration as specified in the methods section 2.3.2. before analysis via SDS-PAGE gels. Three additional proteins were kindly supplied for the project: phospho-UB (pUB) with a 6xHis tag on its C-terminus (~9.5 kDa) supplied by Joanna Koszela, K6-diubiquitin supplied by Ubiquigent and the E3 ligase PDR-1 (i.e. *C. elegans* Parkin) supplied by Mehmet Gundogdu, who had previously run experiments (unpublished) that concluded that the PDR-1 protein behaved exactly the same as its human counterpart Parkin.

Table 9. Proteins produced during this project.

PROTEIN	CONCENTRATION (mg/ml)	VOLUME (μ l)
HRV3C	6.6	3500
UBE2L3	8.6	120
UBIQUITIN	18.8	1850
MIRO1	8.7	110
USP30	2.0	50
	1.0	400

3.1.1 Purification Of HRV3C, UBE2L3 And UB

Affinity chromatography and subsequent purification stages carried out in the ÄKTA pure were analysed via SDS-PAGE gels. **Figure 10** showed the purification of HRV3C protease via affinity chromatography.

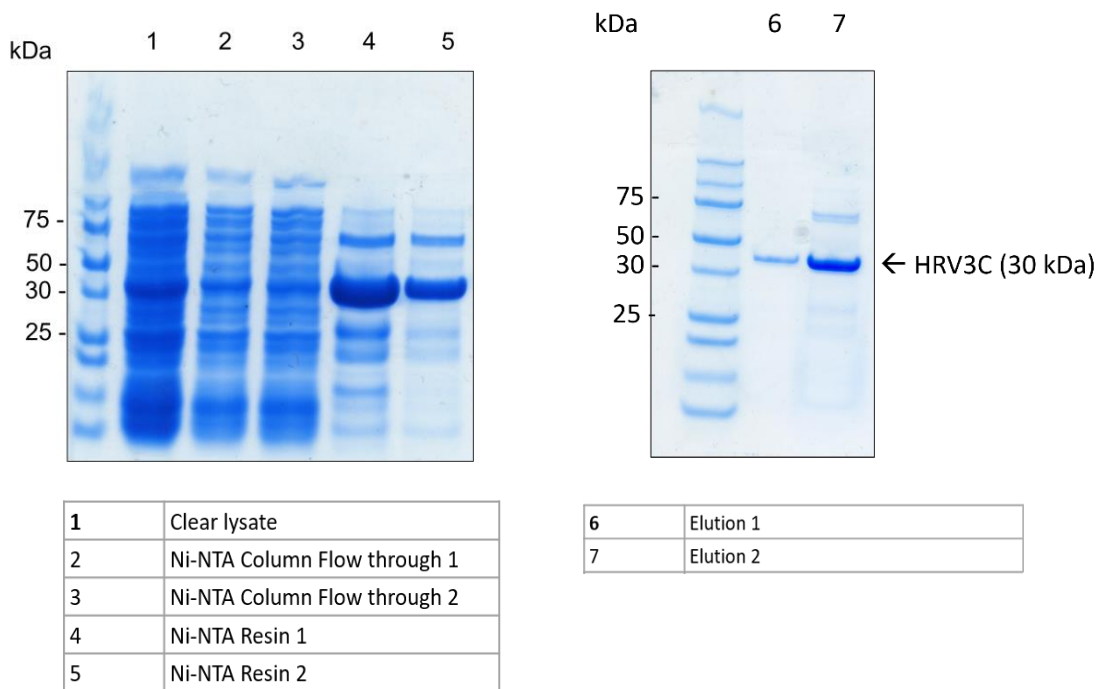


Figure 10. Purification of HRV3C

Affinity chromatography purification of HRV3C protease using His-Pur™ Nickel-NTA beads. Lane 1 shows the protein lysate before being passed through the column. The lysate flowthrough (FT) is visible in lanes 2 and 3, where the band corresponding to HRV3C (30 kDa) is no longer as intense as in the clear lysate. Lanes 4 and 5 show the protein bound to the resin, which was subsequently eluted with a High Imidazole buffer (lanes 6 and 7).

.....

Figure 11a shows UBE2L3 affinity chromatography was carried out successfully, as a single, thick band was present at roughly the UBE2L3 molecular weight (18 kDa) in the elution lane (lane 6). Gel filtration of the spin-concentrated elution (lane 8) was then performed (**Figure 11b**) and a single, sharp peak was produced, characteristic of an intact and pure protein. Fractions corresponding to the peak were analysed via another SDS-PAGE gel and fractions 10-13 were observed to produce a single clean band at ~18 kDa. However, since the intensity of the band present at lane 13 was very poor, only fractions 10 – 12 were spin-concentrated for future use.

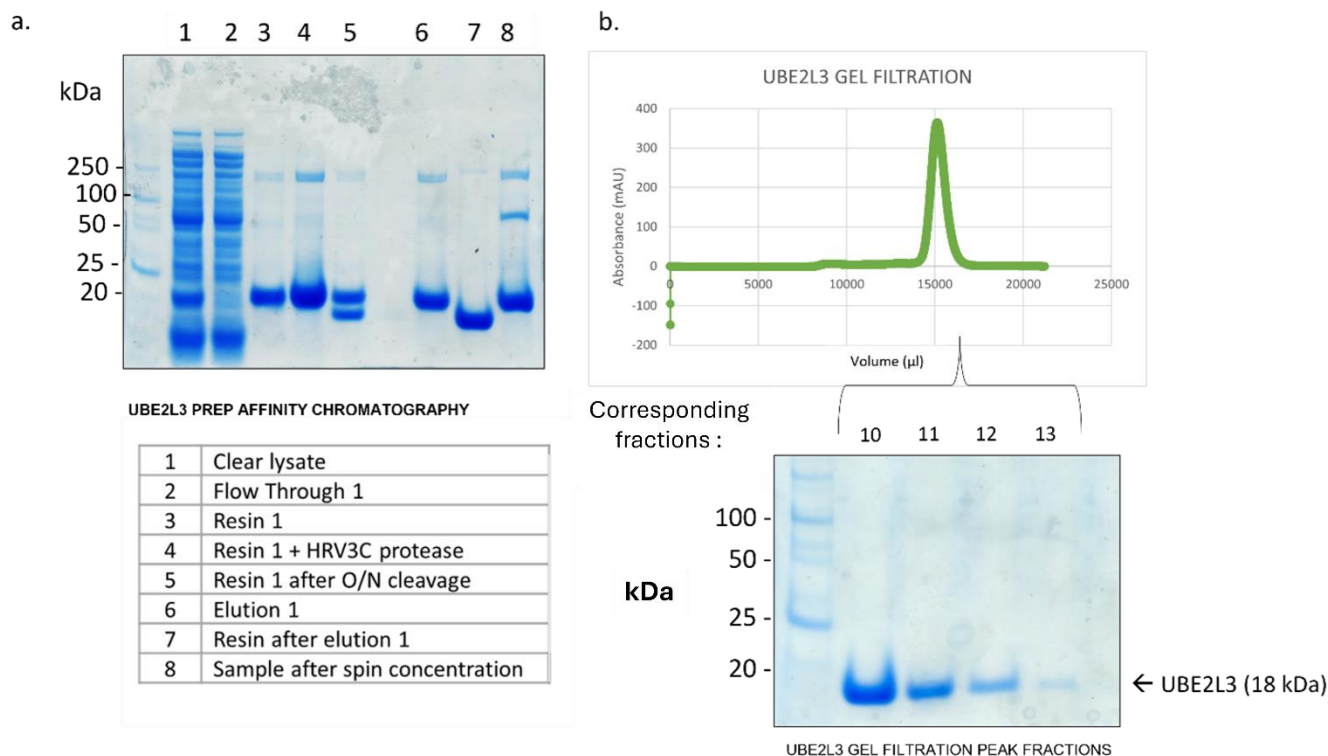


Figure 11. Purification of UBE2L3

Figure 11a. Affinity chromatography of UBE2L3. The clear lysate was loaded into lane 1, and the flow through from the Ni²⁺ column– now missing the 18 kDa band corresponding to UBE2L3 – into lane 2. Lane 3 shows the resin has a single clear band corresponding to the UBE2L3 molecular weight bound to it. Lane 4 shows the resin once the previously produced HRV3C protease was added and lane 5 shows the protein after overnight incubation was completed, were two bands are visible - UBE2L3 with the affinity tags still attached and UBE2L3 after cleavage. Lane 6 shows UBE2L3 after elution with the low salt buffer while Lane 7 shows the resin after the elution. UBE2L3 was then spin-concentrated (Lane 8) before being further purified.

Figure 11b. Gel filtration of UBE2L3 in the ÄKTApure using a Superdex 75 Increase 10/300 GL column shows a single clear chromatogram peak. Fractions corresponding to the peak were analysed via SDS-PAGE gel and fractions 10-12, which showed a clear band at the expected molecular weight of 18 kDa, were spin-concentrated and stored at -80°C for future use.

.....

Figure 12a shows the SDS-PAGE analysis of the affinity chromatography of UB with a 6xHis tag on the C-terminus (hereafter referred to simply as UB). Lane 4 showed a thick band at approximately 10 kDa, where UB was expected to elute. However, other bands were present at higher molecular weights (>20 kDa). This became more apparent at the gel filtration (GF) stage, (**Figure 12b**) where the UB ÄKTA chromatogram showed multiple peaks. Fractions corresponding to all the peaks were analysed via SDS-PAGE and the cleanest lanes, 15 and 16 (**Figure 12b**), were pooled, spin-concentrated and stored.

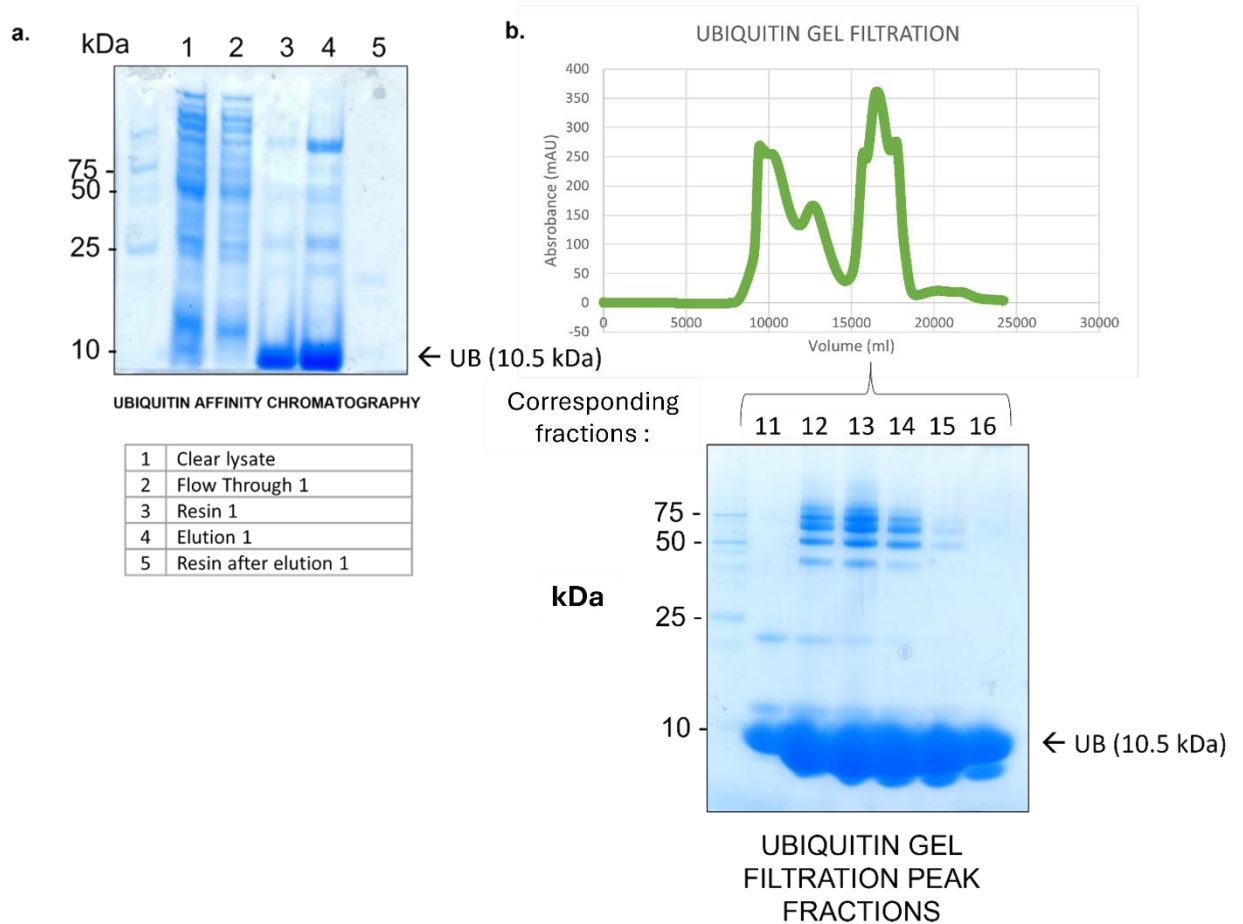


Figure 12. Purification of Ubiquitin

Figure 12a. Affinity chromatography of C-terminal His-tagged UB. The clear lysate was loaded into lane 1, and the flow through from the Ni^{2+} column– now with a less intense 10.5 kDa band corresponding to UB – into lane 2. Lane 3 shows the resin has the protein bound to it. The protein was then incubated overnight with the previously produced HRV3C protease and lane 4 shows the protein after elution with the low salt buffer. Meanwhile, Lane 5 shows the resin after the elution, which no longer contains any traces of the protein left behind.

Figure 12b. Gel filtration of UB in the ÄKTApure using a Superdex 75 Increase 10/300 GL column. A chromatogram with multiple peaks was generated, hence fractions corresponding to all the peaks were collected and analysed via SDS-PAGE. From here lanes 15 and 16 were selected to be further spin concentrated and stored at – 20 °C for future use.

.....

3.1.2. Purification Of MIRO1

Protein production for MIRO1 and USP30 was optimised by using different cell types (BL21 OneShot and Rosetta cells) as well as different media (2YT and auto-induction 2YT). Here the results for the optimised preps are displayed, but the results from the other conditions tested within the optimisation trials are available in the Appendix (**Supplementary Figures 1 and 2**).

The first step in purifying MIRO1 involved affinity chromatography. **Figure 13a** showed a strong, thick band at approximately the 47.5 kDa mark corresponding to cleaved MIRO1 after spin-concentrating the elution (lane 8), however, traces of uncleaved MIRO1 (71 kDa) are still apparent after overnight incubation with the protease (lane 8).

Meanwhile, the GF chromatogram showed the formation of at least two distinct peaks (**Figure 13b**). These peaks were run on a gel and the second, higher peak was determined to be purified MIRO1. The corresponding fractions were spin-concentrated to 8.7 mg/ml and stored at -80 °C for later use. The shoulder peak visible on the ÄKTA trace showed a molecular weight fitting of MIRO1 with the affinity tags (71 kDa) and thus was determined to be uncleaved MIRO1. However, since the amount of yield lost to uncleaved MIRO1 was so small no further optimisation is required.

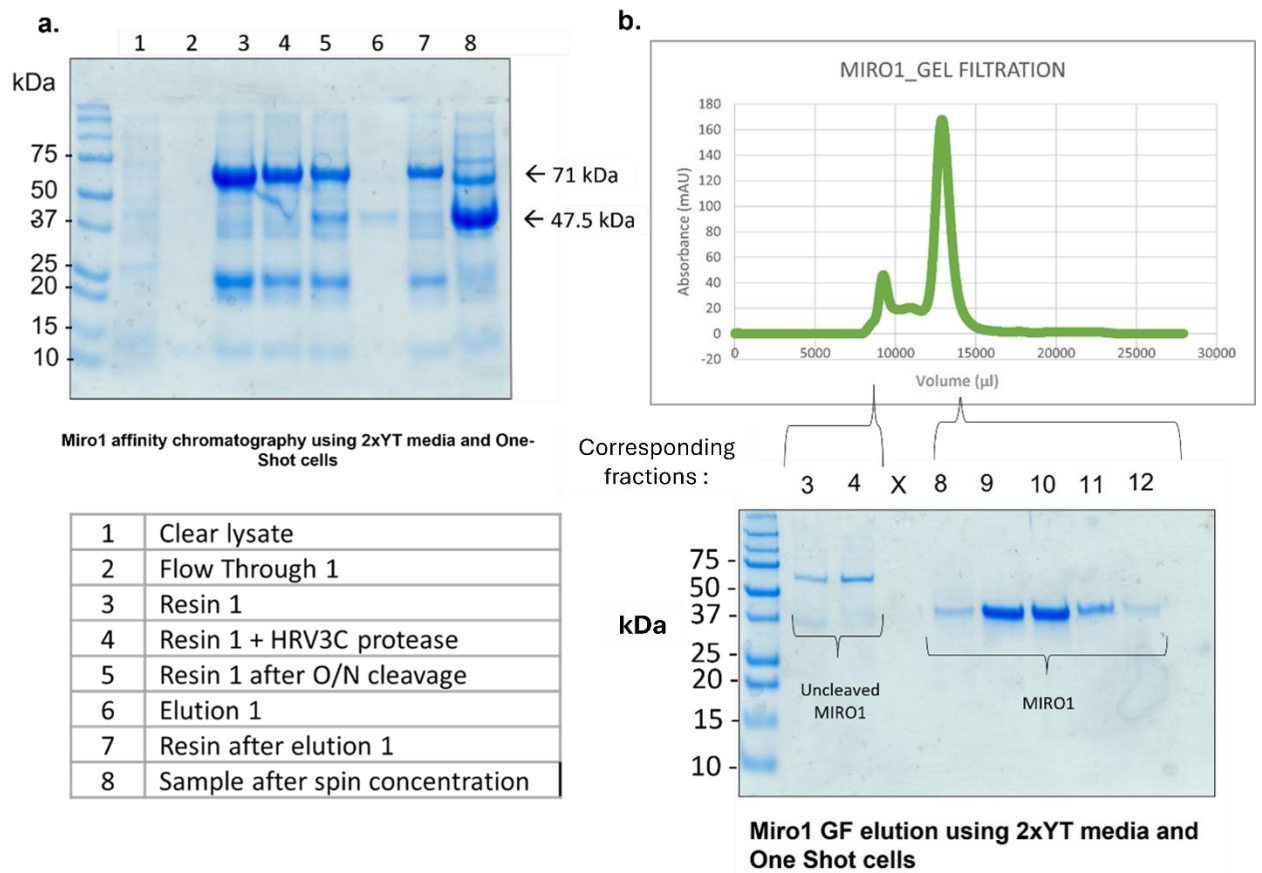


Figure 13. Purification of MIRO1

Figure 13a. MIRO1 affinity chromatography using glutathione-sepharose (GSH) beads. The clear lysate was loaded into lane 1, and the flow through into lane 2, although only faint traces are visible for these two lanes due to pipetting errors. Lane 3 shows the resin has the protein bound to it, which was then incubated with the previously produced HRV3C protease, as visualised in lane 4. Lane 5 shows the protein after overnight incubation was completed, where three bands are visible - cleaved MIRO1 at 47.5 kDa, uncleaved MIRO1 at 71 kDa and HRV3C at approximately 30 kDa. Lane 6 shows a faint band corresponding to MIRO1 after elution with the low salt buffer while Lane 7 shows the resin after the elution, which still contains uncleaved-MIRO1. The eluted MIRO1 was then spin-concentrated (Lane 8) before being further purified.

Figure 13b. MIRO1 was further purified via gel filtration in the ÄKTApure. At least two clear peaks are visible in the trace, which were analysed via SDS-PAGE. The fractions corresponding to the more abundant peak had a molecular weight corresponding to cleaved MIRO1, hence fractions 9-11 from this peak were spin-concentrated and stored

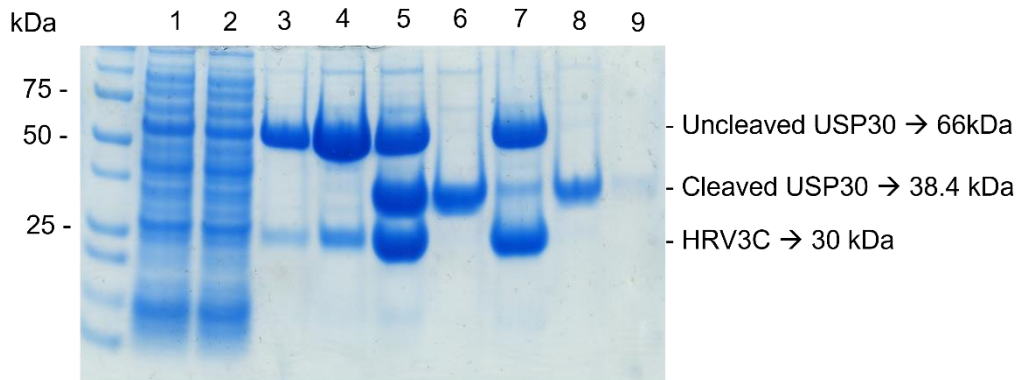
at -80°C for future use. The fractions corresponding to the shoulder peak were analysed and found to have a molecular weight matching that of uncleaved-MIRO1.

.....

3.1.3. Purification Of The USP30 Truncated Protein

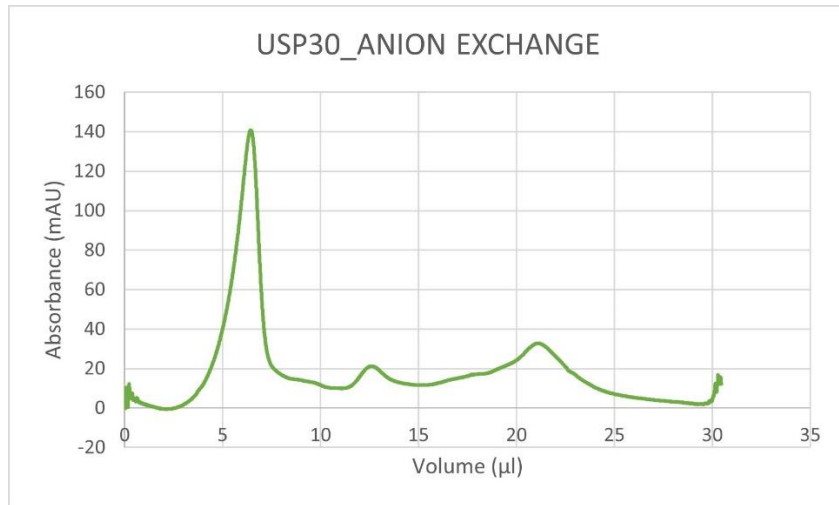
With USP30, at the affinity chromatography stage (**Figure 14a**) a thick band was present at the expected molecular weight of ~38 kDa. However, in lane 7, the resin after elution shows a strong band corresponding to uncleaved USP30 at approximately 66 kDa. Additionally, more than one prep of USP30 was carried out, and when using large expression volumes (12L) USP30 was observed to be prone to aggregation, thus leading to yield losses. During the anion exchange step (**Figure 14b**), further accommodations were made for the USP30 precipitation. An HPQ column was used instead of a ResQ column to allow for a greater pressure tolerance and the system flow was kept well below the maximum levels. USP30 was then further purified via gel filtration (**Figure 14c**), and a clean peak indicative of a pure protein was produced (**Figure 14d**). However, due to aggregation issues, the concentration of the purified USP30 was not very high.

a.

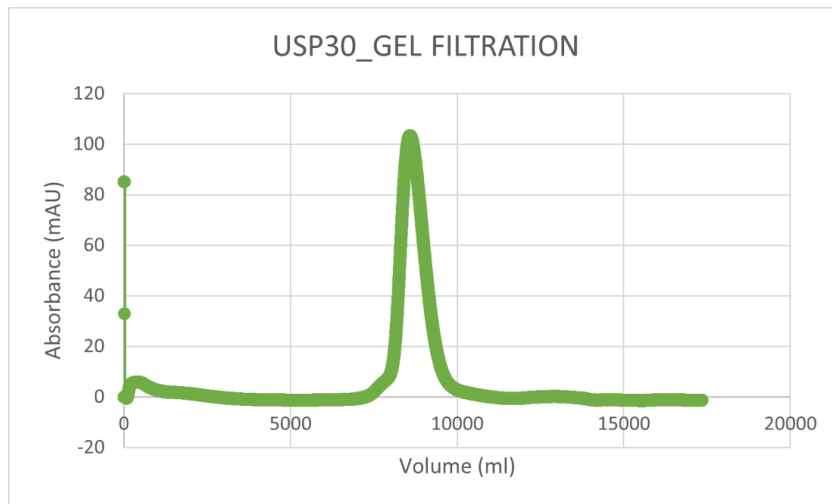


1	Clear lysate
2	GST Flow Through 1
3	Resin 1
4	Resin 1 + HRV3C protease
5	Resin 1 after O/N cleavage
6	Elution 1
7	Resin after elution 1
8	Sample after X3 dilution with pre-anion exchange buffer
9	Sample after ResQ

b.



c.



d.

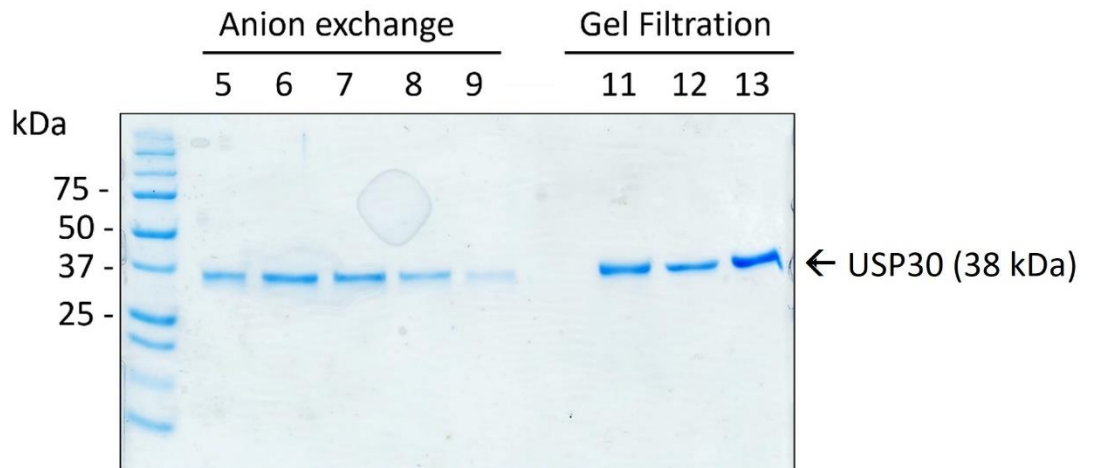


Figure 14. Purification of USP30.

Figure 14a. USP30 was purified via affinity chromatography using glutathione-sepharose (GSH) beads. The clear lysate was then loaded into lane 1, and the flow through into lane 2. Lane 3 shows the resin has the protein bound to it, which was then incubated with the previously produced HRV3C protease, as visualised in lane 4. Lane 5 shows the protein after overnight incubation was completed, where three bands are visible - cleaved USP30 at 38 kDa, uncleaved USP30 at 66.4 kDa and HRV3C at approximately 30 kDa. Lane 6 shows a strong, intense band corresponding to USP30 after elution with the low salt buffer while Lane 7 shows the resin after the elution, which displays a strong band corresponding to uncleaved-USP30. The eluted USP30 was then spin-concentrated (Lane 8) before being further purified.

Figure 14b. Anion exchange ÄKTA trace shows a sharp peak followed by two shoulder peaks. Fractions corresponding to the first peak were collected and further purified by gel filtration. Samples of the peaks were also kept to be analysed by SDS-PAGE.

Figure 14c. Gel filtration trace shows a clear single peak. The corresponding fractions were collected and analysed by SDS-PAGE.

Figure 14d. SDS-PAGE gel analysis of the anion exchange and gel filtration peaks shows bands at the expected molecular weight of USP30 after cleavage (38 kDa). Fractions 11-13 were spin-concentrated and stored for future use at – 80°C.

.....

3.2 Producing the physiological substrate for USP30.

3.2.1 Production Of MonoUB And PolyUB MIRO1.

To biochemically characterize the substrate preference of USP30 *in vitro*, a MIRO1 ubiquitination assay (**Figure 15**) was first set up using the components required for the reaction to be carried out as visualised in **Figure 2**. This reaction constituted of 1.0 μM UBE2L3 (E2), 0.2 μM of *C. elegans* Parkin (PDR-1) (E3), 0.4 μM pUB and 2.5 mM ATP as listed in Section 2.4.1.1. The purpose of this assay was to establish a way to generate a monoubiquitinated substrate using MIRO1, as USP30 is an exoDUB (Gersch *et al.*, 2017) and is therefore predicted to be able to cleave the monoubiquitin tag from the MIRO1 substrate. However, the USP30 activity is also predicted to be lower compared to longer K6 linkages. Hence, polyubiquitinated MIRO1 species were also generated to compare USP30 deubiquitinating activity on the two substrates as USP30 allegedly preferably cleaves the bond between the proximal and distal ubiquitin rather than the bond between the ubiquitin and the substrate (Gersch *et al.*, 2017; Sato *et al.*, 2017). These would then prove useful to biochemically characterise USP30 substrate recognition and inhibition in the presence of the reported inhibitors.

Discrete ubiquitinated species of MIRO1 were generated by controlling key parameters, specifically the ubiquitination reaction time and the UB concentration. The concentration of UB was calculated based on the amount of MIRO1 that was available at the beginning of the ubiquitination reaction, with the MIRO: UB ratios covering the range of 2:1, 1:1, 1:2, and 1:4.

From this assay (**Figure 15**), a combination of the 15-minute time-point and the 2:1 MIRO: UB ratio was observed to yield the optimal conditions for monoUB-MIRO1 production, as indicated by formation of an additional band matching the expected molecular weight of singly-ubiquitinated MIRO1 at approximately 57 kDa as indicated. Meanwhile, the 45- and 60-minute time-points were observed to favour the generation of MIRO1 monoubiquitinated on multiple sites or polyUB-MIRO1 at all MIRO:UB ratio concentrations (**Figure 16**). As such, the time-point and highest MIRO1: UB ratio was selected to allow for maximal polyubiquitination. Notably, the successful ubiquitination of MIRO1 also validates that all the proteins previously produced are fully functional. In contrast, no higher molecular weight bands corresponding to MIRO1 ubiquitination were present in the negative controls for the ubiquitination reaction, in which either no ubiquitin was present in the reaction or where the reaction was immediately stopped.

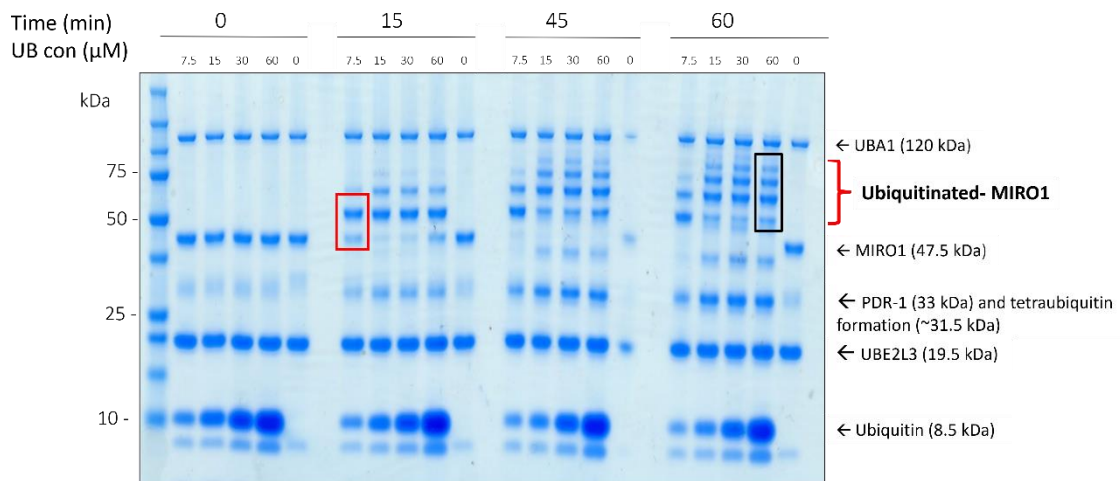


Figure 15. MIRO1-ubiquitination assay shows the production of different ubiquitinated-MIRO1 species.

The MIRO1 ubiquitination assay was performed twice using four separate ubiquitination reaction times (0,15, 30 and 60 min) and five ubiquitin concentrations (0, 7.5, 15, 30, and 60 μ M) to optimise the production of mono-ubiquitinated MIRO1 (monoUB-MIRO1) or poly-ubiquitinated MIRO1 (polyUB-MIRO1).

The combination of the 15-minute time-point and the 2:1 MIRO: UB ratio was observed to yield the optimal conditions for monoUB-MIRO1 production, with the presence of a band at the corresponding molecular weight of 57 kDa confirming this (demarcated here with a red box). For the polyUB-MIRO1 the best set of conditions was determined to be the 60-minute timepoint and the 1:4 MIRO: UB ratio, where multiple high molecular weight bands corresponding to polyUB-MIRO1 are present (demarcated here with a black box). These higher molecular weight bands corresponding to ubiquitinated MIRO are not present in the negative controls, where either no ubiquitin was present in the reaction, or the reaction was stopped immediately, therefore demonstrating that the bands were produced by the formation of the substrate.

.....

3.3 Profiling USP30 deubiquitinating activity

3.3.1. Investigating USP30 Deubiquitinating Activity Against MonoUB-MIRO1

To investigate USP30 deubiquitination activity the DUB was incubated at three different concentrations (0, 0.5, 1 μ M) with the previously generated monoUB-MIRO1 and analysed using an SDS-PAGE gel (**Figure 16**). Bands corresponding to monoUB-MIRO1 are visible in the control lanes, where either no USP30 was added or the deubiquitination reaction was not allowed to start (0 min time points). The strongest deubiquitinating activity was observed with the maximum USP30 concentration (1 μ M) and maximum reaction time (30 minutes) as there was more free ubiquitin available, although the difference in the monoUB-MIRO1 band intensity between different deubiquitinating conditions was not very pronounced. Note that there is a band present between MIRO1 and monoUB-MIRO1 of unknown origin on the gel, which doesn't correspond to any of the expected molecular weights of the proteins used in this assay.

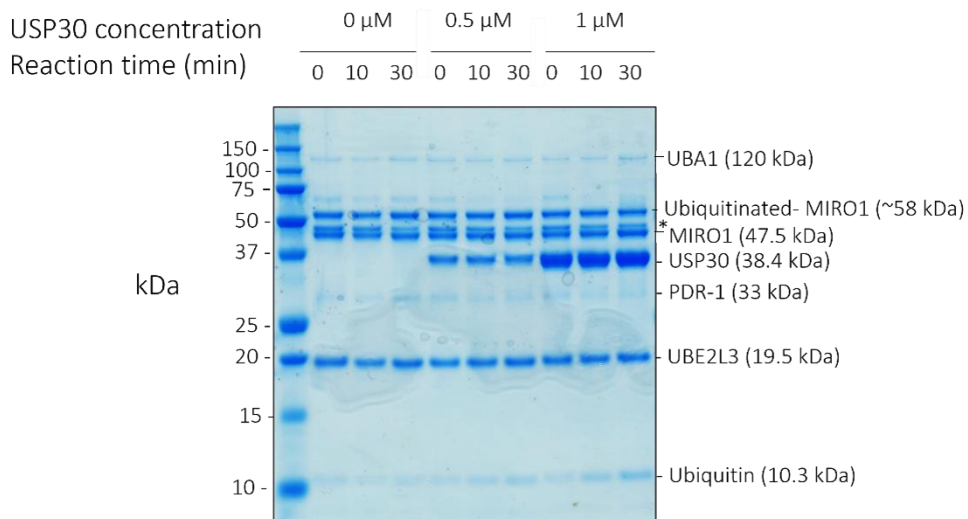


Figure 16. USP30 deubiquitination activity against monoubiquitinated-MIRO1

USP30 deubiquitinating activity was analysed via SDS-PAGE using the previously generated monoubiquitinated-MIRO1 as the substrate, while testing three different USP30 concentrations (0, 0.5, 1 μ M) and three different reaction times (0, 10, 30 minutes). The experiment was conducted once and the zero-minute time-point and the zero μ M USP30 acted as negative controls with no substrate deubiquitination.

.....

3.3.2. Investigating USP30 Deubiquitinating Activity Against Polyubiquitinated-MIRO1

To test the USP30 deubiquitinating activity against polyUB-MIRO1 (**Figure 17**) the optimal ubiquitin concentration (60 μ M) established during the first ubiquitination assay (**Figure 15**) was used. The reaction was run using the same conditions utilised to investigate the USP30 deubiquitinating activity of the monoUB-substrate (**Figure 16**), including three USP30 concentrations (0, 0.5, 1 μ M) and the three different deubiquitination reaction time points (0, 10, 30 minutes).

USP30 showed a stronger deubiquitinating activity against the polyubiquitinated substrate (**Figure 17**) than the monoUB-MIRO1 counterpart (**Figure 16**). The maximum concentration of USP30 (1 μ M) and reaction time (30 minutes) once again displayed the strongest deubiquitinating activity (**Figure 17**), concordant with the previous deubiquitination assay, leaving no high molecular weight bands beyond the monoUB-MIRO1 band (i.e. no bands above 58 kDa). The effect of USP30 on polyUB-MIRO1 was concentration and time dependent, with the lower concentration and reaction time showing less deubiquitination taking place (**Figure 17**). Meanwhile, the negative controls run using 0 μ M USP30 or with zero minutes of reaction time still clearly show the presence of bands corresponding to polyUB-MIRO1 (**Figure 17**).

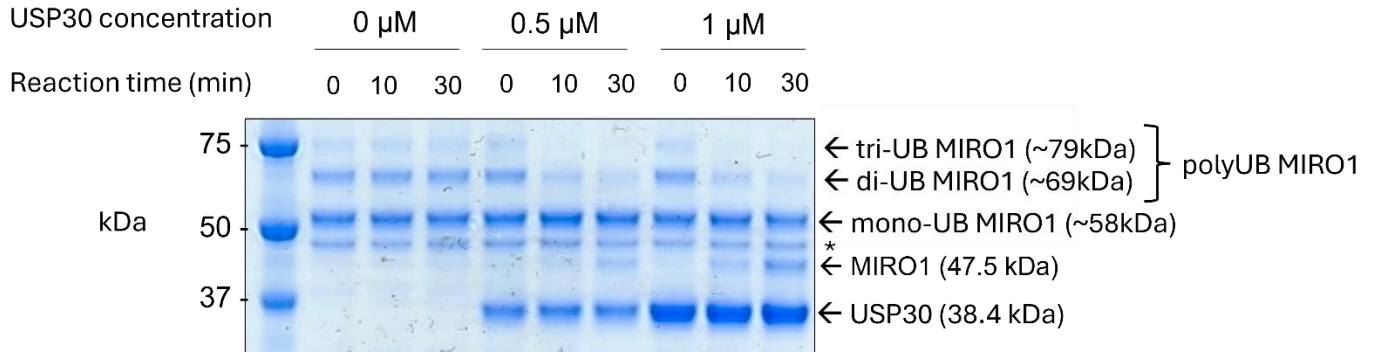


Figure 17. USP30 deubiquitinating activity against poly-ubiquitinated MIRO1.

USP30 cleavage was analysed via SDS-PAGE using the previously generated polyubiquitinated-MIRO1 as the substrate, while testing three different USP30 concentrations (0, 0.5, 1 μ M) and three different reaction times (0, 10, 30 minutes). The experiment was conducted once and the zero-minute time-point and the zero μ M USP30 acted as negative controls with no substrate deubiquitination taking place.

.....

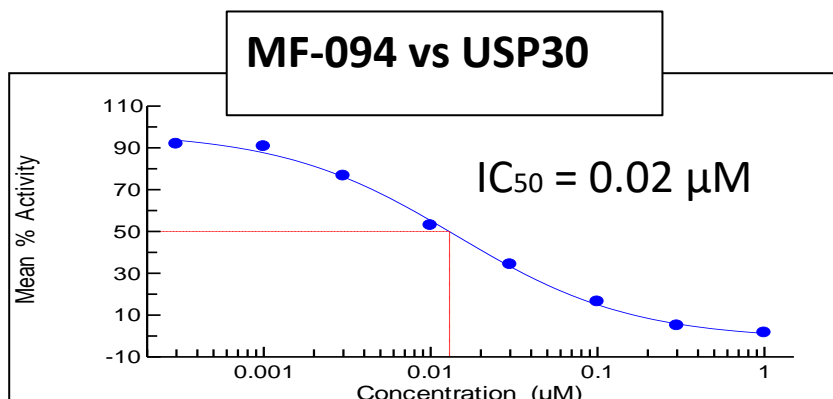
3.4. Investigating Potency And Specificity Of Known USP30 Inhibitors.

3.4.1. DUBprofiler™ Screening Of MF-094 Against A Panel Of DUBs.

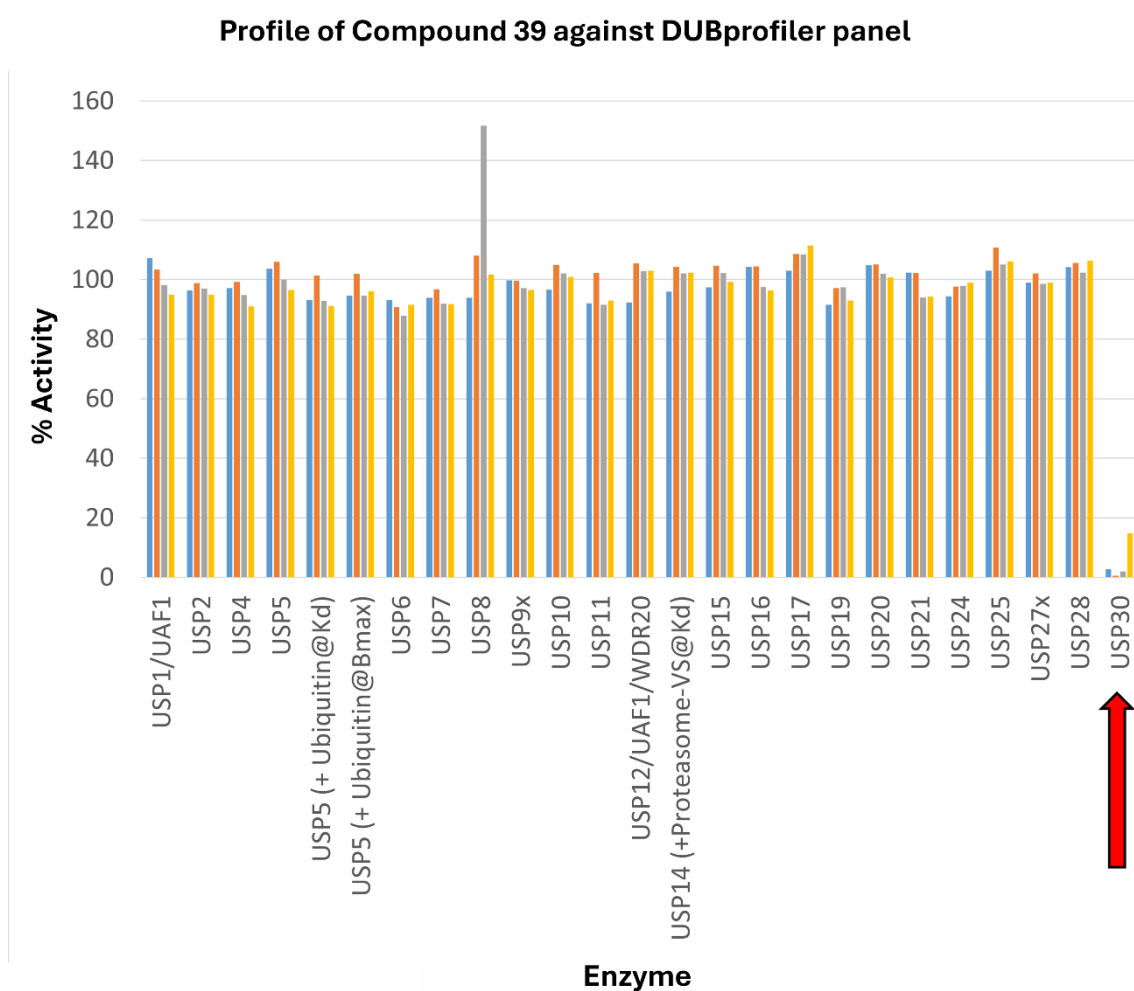
To measure the potency of an inhibitor and determine the concentration at which half of the enzyme is bound to the compound, the IC₅₀ value was calculated – i.e. the half-maximal inhibitory concentration of the inhibitor. The inhibitor was titrated at different concentrations and the IC₅₀ value of USP30 when bound to MF-094 was determined to be 0.02 μM (**Figure 18a**) which is six times lower than the reported IC₅₀ value of 0.12 μM reported in the literature (Kluge *et al.*, 2018).

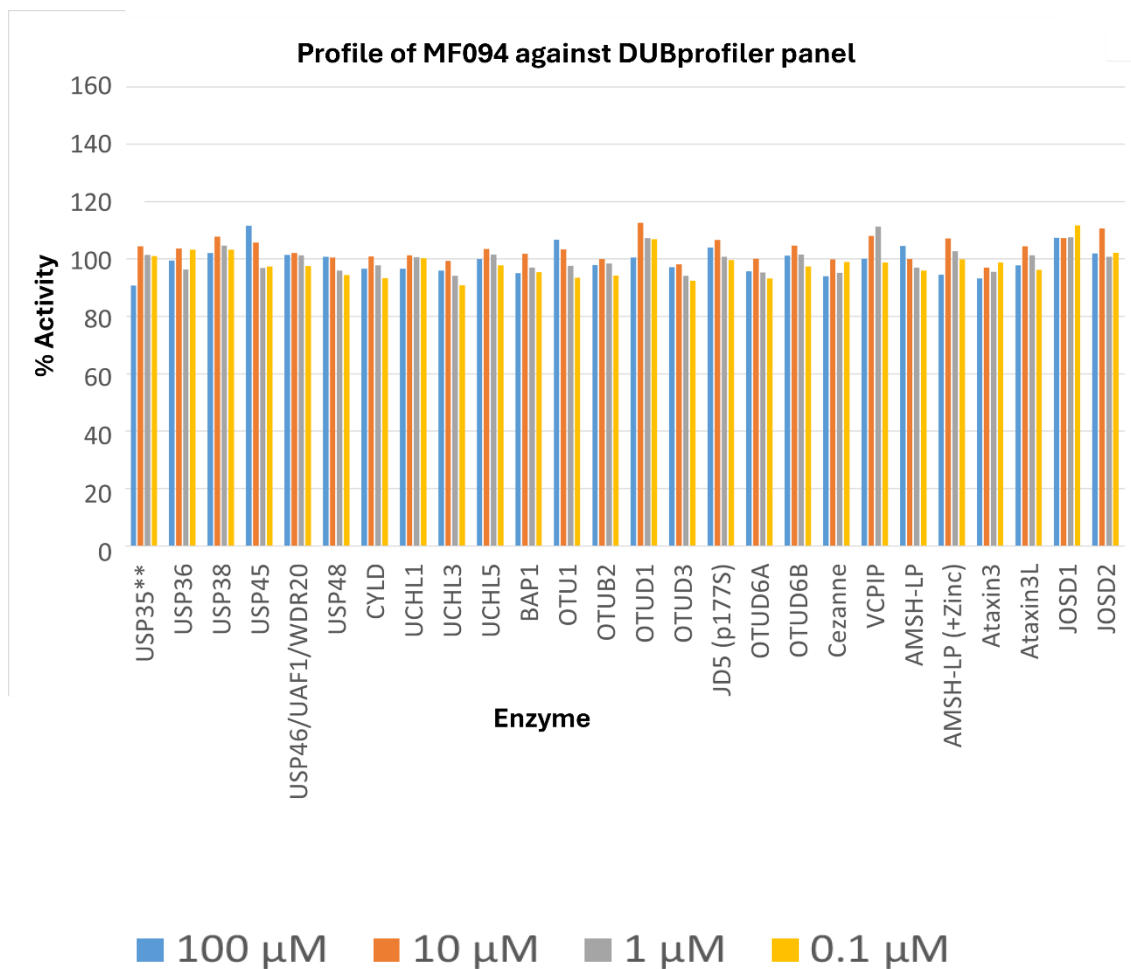
Once the IC₅₀ experiments confirmed that MF-094 is a potent inhibitor of USP30, the specificity for the DUB was measured using the Ubiquigent DUBprofiler™ assay (experiment performed by Steven Liness). DUBprofiler™ is an *in vitro* ubiquitin cleavage assay that uses ubiquitin bound to the fluorescent probe rhodamine (110)-glycine to produce a fluorescent signal after cleavage by a DUB. The inhibitor MF-094 was tested against the DUBprofiler™ panel of 48 DUBs in triplicate and the results are displayed in **Figure 18b**, which shows the inhibitor had a very strong selectivity for USP30, as it's the only DUB to show its activity drop below 90 % of its activity upon MF-094 incubation, regardless of the concentration. **Figure 18b** corroborates the strong potency of the MF-094 compound, as less than 20% of USP30 activity was left after the DUB was incubated with 0.1 μM of the MF-094 inhibitor – and this activity was nearly completely eliminated once higher concentrations (1, 10, and 100 μM) of the MF-094 inhibitor were used.

a.



b.





Experiment performed by Steven Liness (Ubiquigent).

Figure 18. MF-094 against a panel of DUBs including USP30.

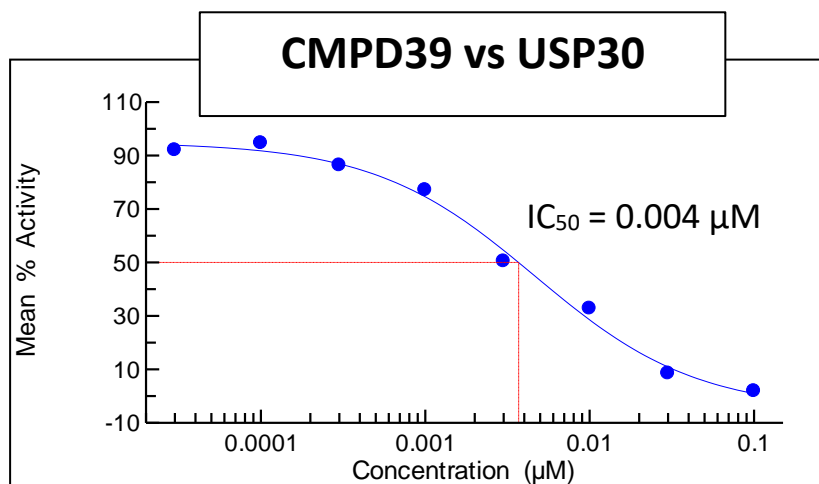
Figure 18a USP30 mean activity at increasing MF-094 inhibitor concentrations as calculated from the *DUBprofiler*[™] assay was plotted. The IC₅₀ value of MF-094 was thus determined to be 0.02 μM.

Figure 18b *DUBprofiler*[™] panel shows the effect of MF-094 as an inhibitor against a panel of 48 different DUBs. USP30 shows decreased activity at concentrations as low as 0.1 μM, indicating MF-094 potency. Additionally, even at inhibitor concentrations of 100 μM, USP30 (red arrow) is the only DUB to show a decrease in activity when treated with the inhibitor. The experiment was fully performed and by Steven Liness, who also processed the data to produce the graphs (Ubiquigent).

3.4.2. DUBprofiler™ Screening Of Compound 39 Against A Panel Of DUBS.

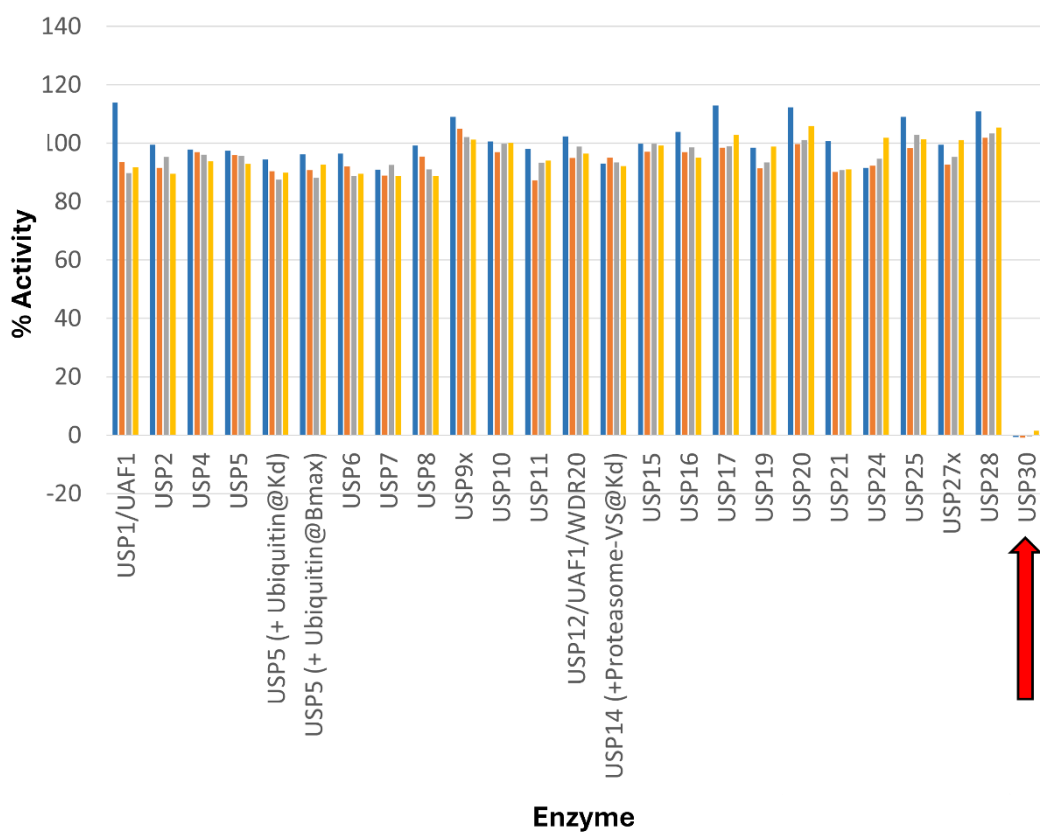
The IC₅₀ value of CMPD39 was calculated in the same way as with MF-094 and determined to be 0.004 μM (**Figure 19a**), therefore displaying five times higher potency than the reported literature IC₅₀ value of 0.02 μM (Rusilowicz-Jones *et al.*, 2020). Notably, CMPD39 also displays five times stronger inhibitory activity than MF-094 when comparing the IC₅₀ values, although both inhibitors show similar selectivity for USP30 compared to other DUBs; DUBprofiler™ evaluations of CMPD39 against the same panel of 48 DUBs (**Figure 19b**) showed USP30 was the only DUB to drop its activity below 90 % when CMPD39 was present. The strong potency of the compound was also corroborated by the DUBprofiler™ assay, as 0.1 μM of the inhibitor was able to nearly completely eradicate USP30 activity.

a.

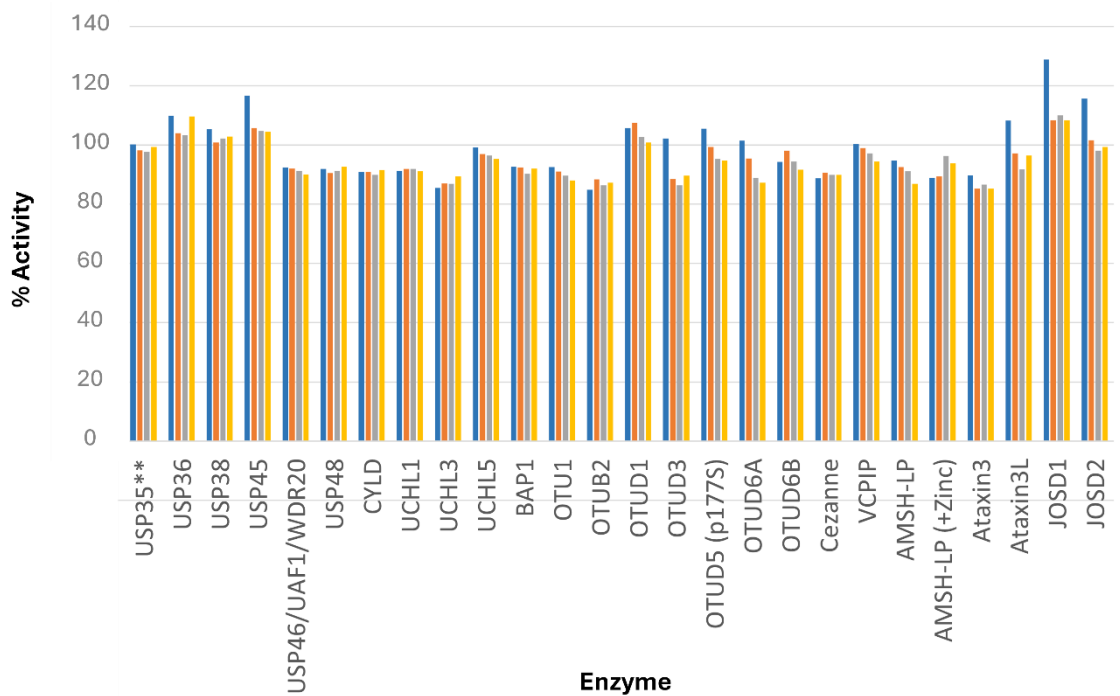


b.

Profile of Compound 39 against DUBprofiler panel



Profile of Compound 39 against DUBprofiler panel



■ 100 μM ■ 10 μM ■ 1 μM ■ 0.1 μM

Experiment performed by Steven Liness (Ubiquigent).

Figure 19. Compound 39 against a panel of DUBs including USP30.

Figure 19a USP30 mean activity at increasing CMPD39 inhibitor concentrations as calculated from the *DUBprofiler*[™] assay. The IC_{50} value of CMPD39 was thus determined to be of 0.004 μM .

Figure 19b *DUBprofiler*[™] panel shows the effect of CMPD39 as an inhibitor against a panel of 48 different DUBs. USP30 (red arrow) activity was remarkably reduced even in the presence of only 0.1 μM of CMPD 39. Additionally, USP30 was the only DUB to show a decrease in activity when treated with the inhibitor, even at 100 μM of CMPD39. The experiment was fully performed and by Steven Liness, who also processed the data to produce the graphs (Ubiquigent).

.....

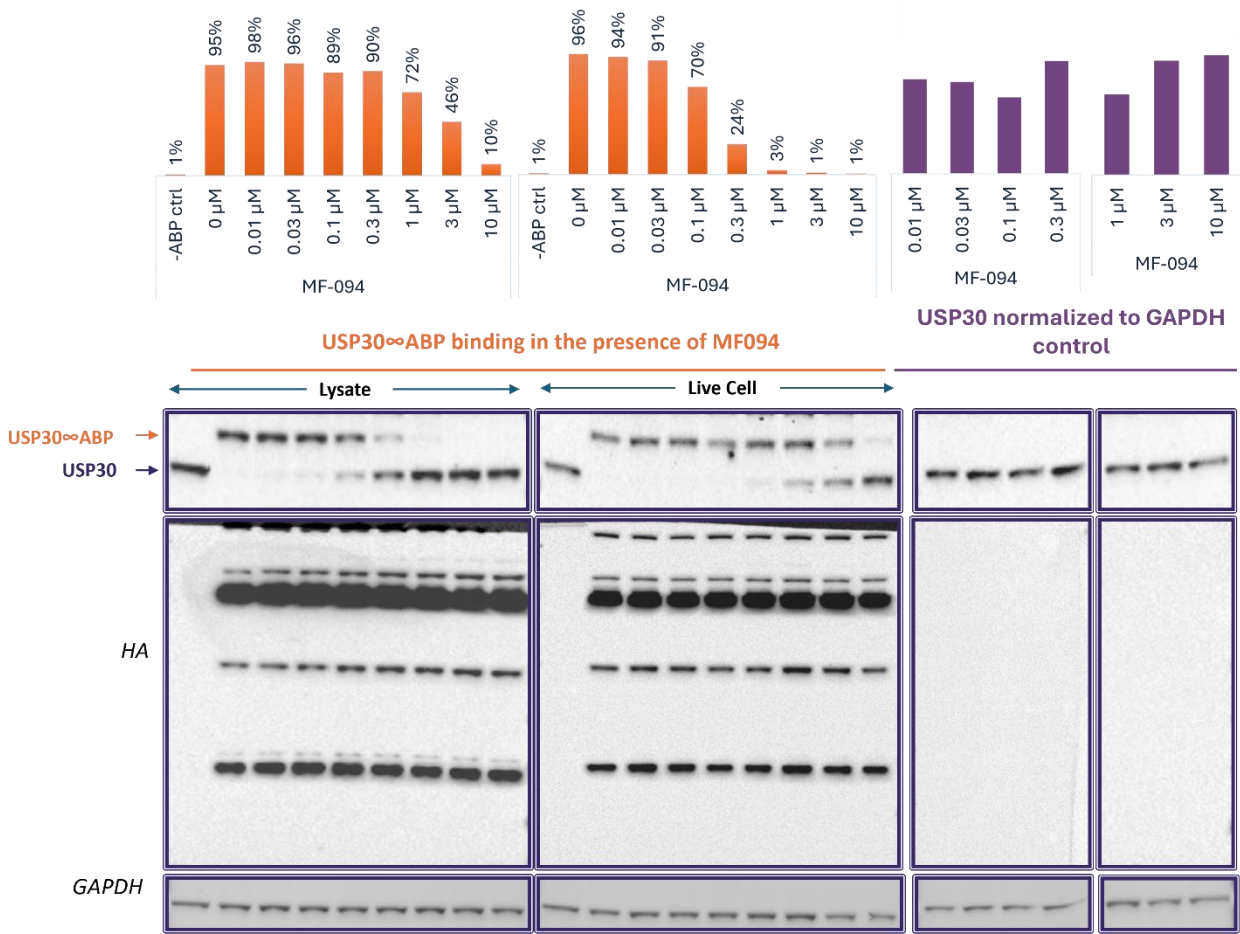
3.4.3. *DUBprofiler*-Cell[™] Of Endogenous USP30 UB-Probe Binding Inhibition Against MF-094.

DUBprofiler-Cell[™] uses a Ubiquigent proprietary activity-based probe (ABP) to bind active USP30 within the cell lysate and in live cells (experiment performed with the help of Kirsten Sinclair and João Oliveira). In cell lysates (**Figure 20a**), USP30 binding to the probe was observed to be similar to the no compound control for concentrations of MF-094 below 0.1 μM . At 0.1 μM MF-094 USP30 binding was inhibited by 26 % compared to USP30 probe-binding in the absence of the inhibitor. At 0.3 μM MF-094 USP30 probe engagement drops 72% further compared to the no inhibitor control, and at concentrations of 1 μM MF-094 and above, USP30 probe engagement was completely eradicated. The EC_{50} - similar to the IC_{50} value but performed to estimate its effective concentration for a half-maximal response– was determined to be 0.17 μM (**Figure 20b**).

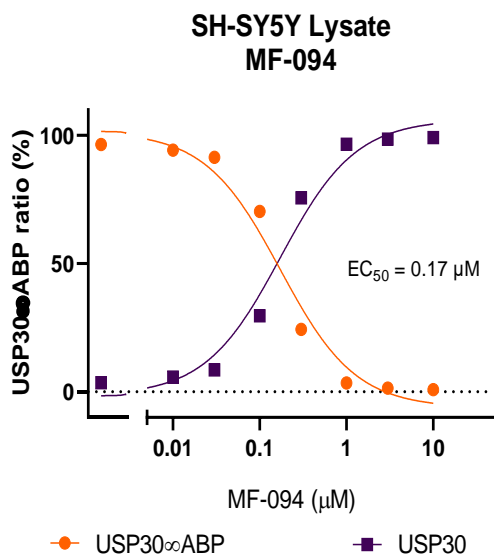
However, MF-094 was much less effective when evaluated in the live cell treatment. Probe binding was unaffected in concentrations below 1 μM MF-094, where the binding was reduced by 24 %. At 10 μM MF-094 probe engagement has a noteworthy decrease such that only 10% of the probe remains bound, with a calculated EC_{50} value of 4.3 μM (**Figure 20c**) – meaning the

EC₅₀ value derived from live cells was 25X lower than the EC₅₀ value from the lysate treatment. Additionally, an incubation with HA antibody was carried out to visualise other proteins bound to the probe. This confirmed the selectivity of MF-094 in lysates and live cells as no other HA-bands were impacted by the compound. Additionally, normalisation against the GAPDH of the live cell and lysate assay allows for quantification of the total levels of USP30 for later analysis, which confirmed the compound had no impact on the total USP30 levels.

a.



b.



c.

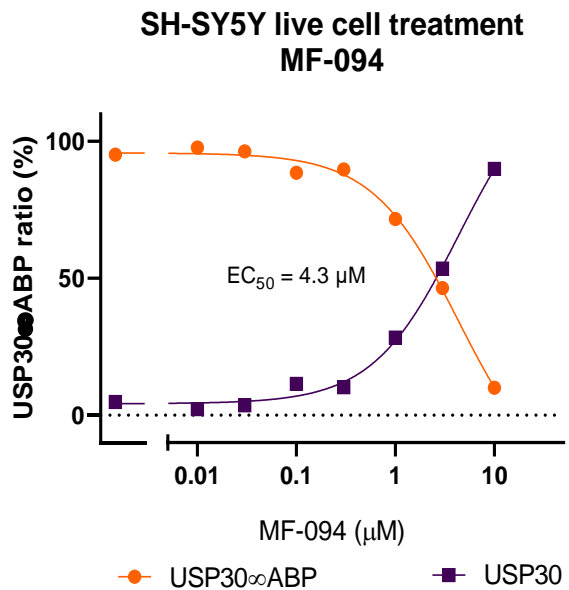


Figure 20. DUBprofiler-Cell™ of endogenous USP30 UB-probe binding inhibition by MF-094 in SH-SY5Y cells and cell lysate.

Figure 20a Western Blot of endogenous USP30 binding activity to the Ubiquigent proprietary Activity-Based ubiquitin Probe (ABP) in the presence or absence of increasing MF-094 concentrations. The left panel shows inhibition of probe binding to USP30 when the compound was incubated with the lysates. At MF-094 concentrations of 0.1 μM the effect of the inhibitor on probe binding starts being visible, and by 1 μM of inhibitor, USP30 was completely unable to bind the probe. This inhibition of probe binding was recapitulated in the live cell assay (right), but higher compound concentrations are required –USP30 binding was not completely abolished until 10 μM of compound was administered. A hemagglutinin antibody (HA) probe acts as a control to show the presence of other proteins bound by the probe. GAPDH acts as a loading control to ensure all the lanes have equivalent amounts of protein. Normalisation against the GAPDH of the live cell and lysate assay allows for quantification of USP30 to determine whether the compound impacts total USP30 levels. The cell work was performed by João Oliveira and Kirsten Sinclair (Ubiquigent), allowing me to lyse the cells, introduce the inhibitor and perform the SDS-PAGE and Western Blot. João Oliveira and Kirsten Sinclair (Ubiquigent) then processed the data to produce the EC_{50} graphs.

Figure 20b USP30 probe binding within the lysate assay was calculated by comparing the ratio of probe bound USP30 to free USP30. Values were then plotted against the different MF-094 concentrations and the EC_{50} was calculated to be 0.17 μM .

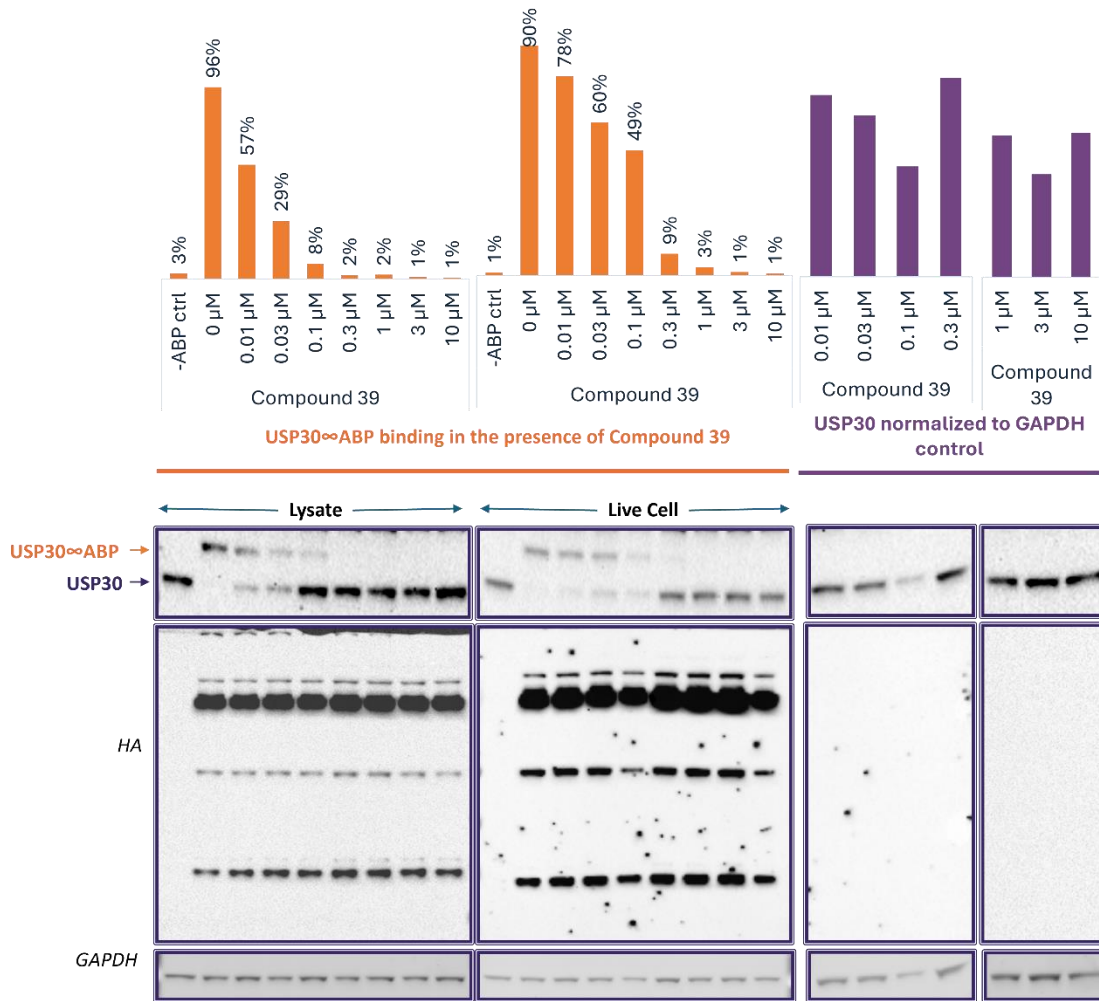
Figure 20c USP30 probe binding within the live cell assay was calculated by comparing the ratio of probe bound USP30 to free USP30. Values were then plotted against the different MF-094 concentrations and the EC_{50} was calculated to be 4.3 μM – more than 25 times less potent than the lysate value.

.....

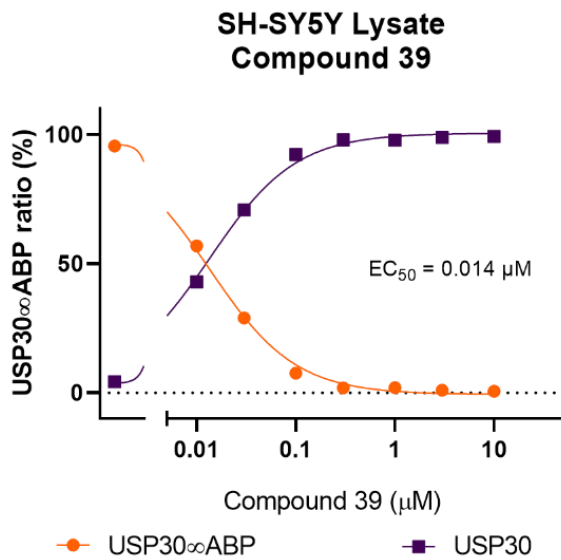
3.4.4. DUBprofiler-Cell™ Of Endogenous USP30 Ub-Probe Binding Inhibition Against Compound 39.

DUBprofiler-Cell™ showed CMPD39 cell lysate treatment caused USP30 probe engagement to decrease by 39 % relative to the no inhibitor control with only 0.01 μM (**Figure 21a**). By concentrations of 0.1 μM USP30 engagement was nearly completely abolished, making the EC_{50} of CMPD39 very potent (0.014 μM) (**Figure 21b**). Meanwhile, DUBprofiler-Cell™ data for CMPD39 treatment in live cells showed that probe engagement was not completely depleted until 0.3 μM (**Figure 21c**) of the inhibitor was used, whereupon the EC_{50} value of live cells was determined to have 6 times less potency than the counterpart lysate treatment. Thus, CMPD39 EC_{50} values showed 10X stronger potency than MF-094 for inhibiting USP30 in the lysate assay. Meanwhile in the live cell treatment DUBprofiler-Cell™ showed the EC_{50} of CMPD39 was 50X more potent than that of MF-094, concordant with the IC_{50} potency calculations from the DUBprofiler™ data.

a.



b.



c.

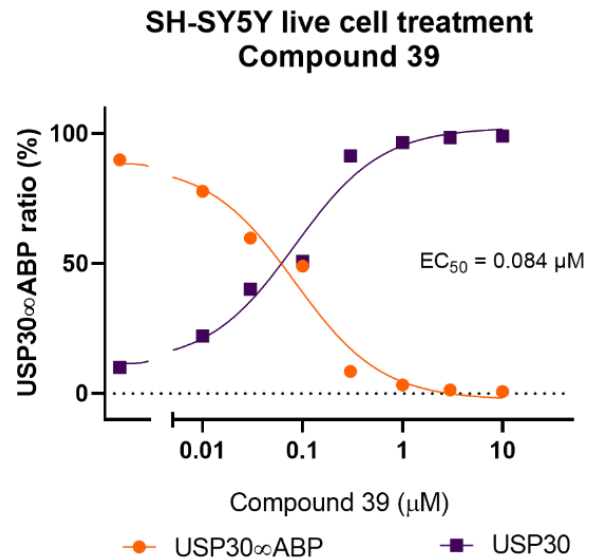


Figure 21. DUBprofiler-Cell™ of endogenous USP30 UB-probe binding inhibition against Compound 39.

Figure 21a Western Blot of endogenous USP30 binding activity against the Ubiquigent proprietary activity-based ubiquitin probe (ABP) in the presence of increasing CMPD39 concentrations. The left panel shows USP30 probe binding inhibition when the compound was administered to the lysates.

At 0.01 μM CMPD39, the effect of the inhibitor on probe binding starts being visible, and by 0.1 μM of inhibitor, USP30 was completely unable to bind the probe. This inhibition of probe binding was recapitulated in the live cell assay (right), but slightly higher inhibitor concentrations are required –USP30 binding was not completely abolished until 0.3 μM of inhibitor was administered.

A hemagglutinin antibody (HA) probe acts as a control to show the presence of other proteins bound to the probe within the reaction. GAPDH acts as a loading control to ensure all the lanes have been loaded equally. Normalisation against the GAPDH of the live cell and lysate assay allows for quantification of USP30 to determine whether the compound impacts total USP30 levels. The cell work was performed by João Oliveira and Kirsten Sinclair (Ubiquigent), allowing me to lyse the cells, introduce the inhibitor and perform the SDS-PAGE and Western Blot. João Oliveira and Kirsten Sinclair (Ubiquigent) then processed the data to produce the EC_{50} graphs.

Figure 21b USP30 probe binding within the lysate assay was calculated by comparing the ratio of probe bound USP30 to free USP30. Values were then plotted against increasing CMPD39 concentrations and the EC_{50} was calculated to be 0.014 μM .

Figure 21c USP30 probe binding within the live cell assay was calculated by comparing the ratio of probe bound USP30 to free USP30. Values were then plotted against the different CMPD39 concentrations and the EC_{50} was calculated to be 0.084 μM – only 6 times less potent than the EC_{50} of the lysate treatment.

.....

3.4.5. Investigating USP30 Inhibition Against MonoUB-MIRO1

The deubiquitinating activity of USP30 against monoUB-MIRO1 was investigated using the two model inhibitors MF-094 and CMPD39 (at 10 μ M) and the optimised USP30 concentration from the previous experiments (0.5 μ M USP30: 5 μ M MIRO1). To measure USP30 activity the levels of MIRO1 were quantified and normalised against the non-ubiquitinated MIRO1 using the LICOR, and two consecutive reactions were set-up. First, the MIRO1 was ubiquitinated to generate the substrate for USP30 as described in Section 3.2.1. The ubiquitination reaction was then stopped with the addition of apyrase to prevent competition between the forward and backward reaction and was followed by the substrate's deubiquitination by the DUB in the presence or absence of the selected inhibitor. This was then analysed via an SDS-PAGE gel as seen in **Figure 22**.

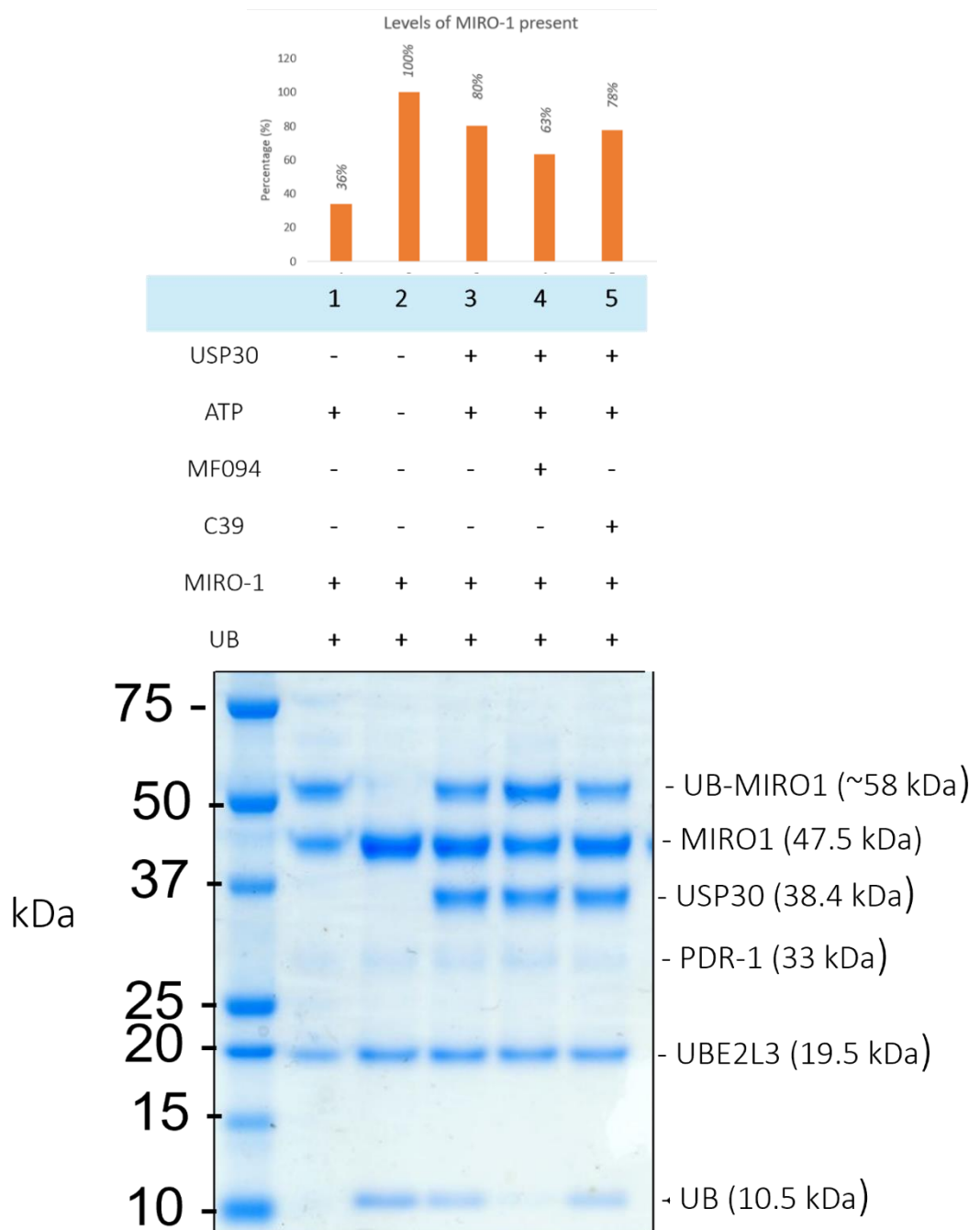


Figure 22. Investigating USP30 activity against monoubiquitinated-MIRO1 in the presence of inhibitors.

USP30 deubiquitinating activity against the generated monoubiquitinated-MIRO1 when treated with 10 μ M of MF-094 or 10 μ M of Compound 39 is shown here side by side (experiment conducted twice). Lane 2 is a negative control with no ATP that shows no MIRO1 ubiquitination while lane 3 shows a positive control where USP30 was active in the absence of inhibitors. Non-ubiquitinated MIRO1 levels were quantified using the

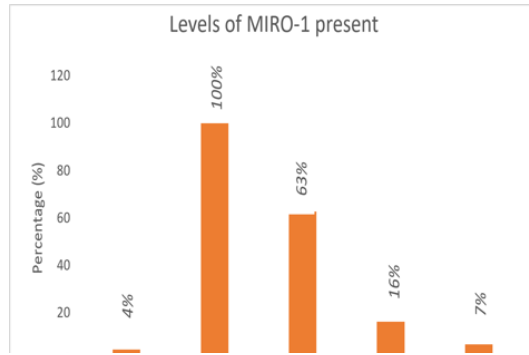
LICOR clx scanner and image Lite Software™ and normalised against the maximal signal lane i.e. the control with no USP30 or ATP present.

.....

In **Figure 22** the SDS-PAGE shows the first lane, where ATP is present but not USP30, acts as a negative control where the MIRO1 signal is reduced due to the successful production of UB-MIRO1. However, this doesn't occur in the second lane, which acts as a negative control without ATP, as this is essential for the ubiquitination mechanism to take place. Thus, this produces the strongest MIRO1 signal, later used for normalisation before quantification. Meanwhile, the third lane acts as a positive control for the deubiquitination reaction as no inhibitor is present. The fourth lane showed that MF-094 displayed a strong inhibition of USP30 – 63% of MIRO1 was generated, which is 37 % more cleavage compared to the maximal MIRO1 signal control (100%) in lane 2. Finally, lane 5 surprisingly showed that CMPD39 has a weaker inhibitory activity than MF-094, as 15 % more quantified MIRO1 was present in lane 4. However, despite MF-094 displaying a stronger inhibitory effect than CMPD39, the lanes for both inhibitors didn't show a strong difference from the control with no inhibitor present in lane 3.

3.4.6. Investigating USP30 Inhibition Against PolyUB-MIRO1

The same experiment described in 3.4.5 investigating USP30 deubiquitinating activity in the presence of both inhibitors was repeated using the polyUB-MIRO1 substrate (**Figure 23**). Here USP30 deubiquitinating activity against the substrate was more pronounced compared to the monoUB-MIRO1 cleavage by ~20 %, as the polyUB-MIRO1 displayed a 37 % decrease in the levels of quantified MIRO1. As for the inhibitors, CMPD39 showed stronger inhibition of USP30 activity compared to MF-094, but both inhibitors showed a remarkable decrease in USP30 activity when compared to the no inhibitor control (Lane 3), with deubiquitinating activity being nearly abolished with CMPD39.



	1	2	3	4	5
USP30	-	-	+	+	+
ATP	+	-	+	+	+
MF094	-	-	-	+	-
C39	-	-	-	-	+

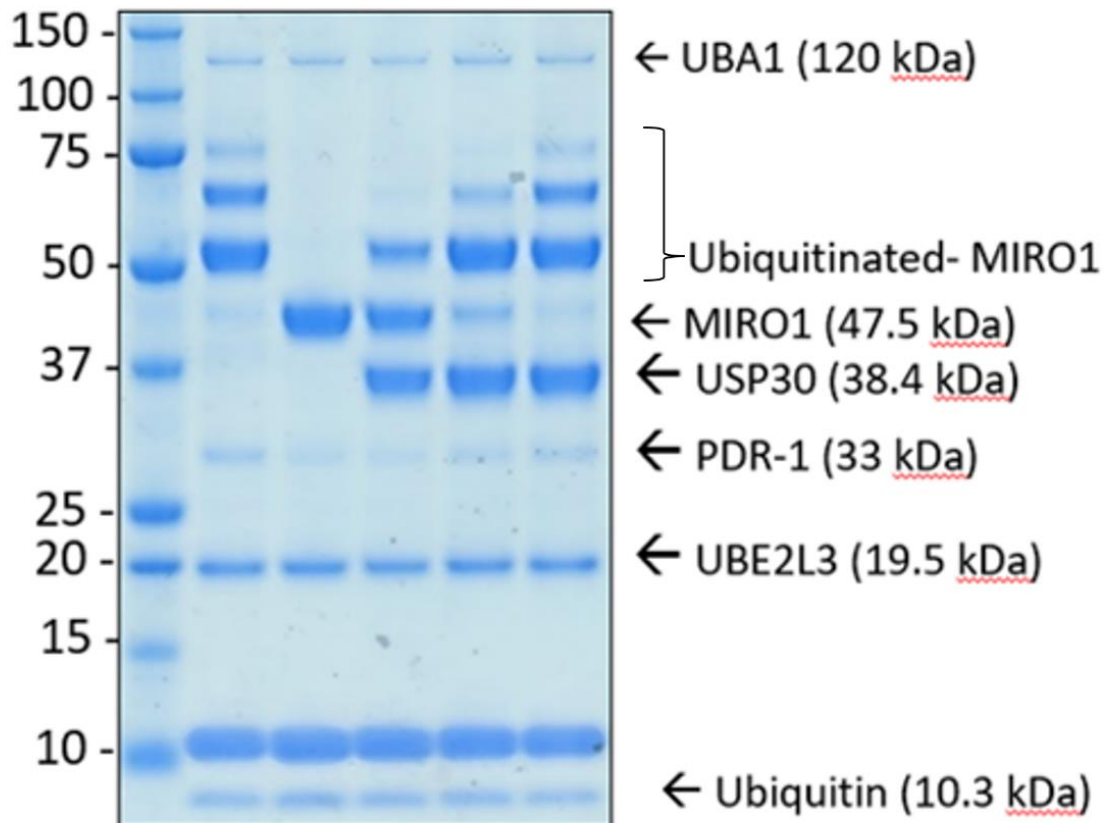


Figure 23. Investigating USP30 activity against polyubiquitinated-MIRO1 in the presence of inhibitors.

USP30 enzymatic activity against the generated polyubiquitinated-MIRO1 in the presence or absence of 10 μ M of MF-094 or Compound 39 (experiment conducted twice). A positive control showed USP30 was active in the absence of inhibitors. A negative control with no ATP was added to show no polyUB-MIRO1 substrate formation. MIRO1 levels were quantified using the LICOR clx scanner and image Lite Software™ and normalised against the maximal signal lane i.e. the control with no USP30 or ATP present.

.....

Chapter 4: Discussion

4.1 Previous biochemical characterisation of USP30

DUBs play a pivotal role in controlling cellular homeostasis, reversing ubiquitination and acting as an essential counterbalance within organisms. In recent years the development of inhibitors targeting DUBs has started to reach clinical trials for the treatment of several disorders, including Chronic Kidney Disease (CKD), neurodegenerative, autoimmune, and oncological diseases (Harrigan *et al.*, 2018). Of these, the DUB USP30 has started to gain momentum as an actionable drug target to treat mitochondrial dysfunction-related disorders, with particular interest in targeting loss-of-function mutations within the PINK1/Parkin ubiquitination pathway, which causes early-onset PD through dysregulation of mitophagy (Bingol *et al.*, 2014). Mitochondrial diseases characterised by dysfunction could also be potentially targeted, including other forms of PD, as well as certain types of Alzheimer's Disease or Amyotrophic Lateral Sclerosis (Rusilowucz *et al.*, 2020).

Understanding the substrate specificity of USP30 is fundamental to unraveling its physiological significance within mitochondrial maintenance. USP30 has been implicated in mitochondrial dynamics through its deubiquitinating interactions with mitochondrial proteins, including multiple substrates of Parkin (Bingol *et al.*, 2014; Cunningham, *et al.*, 2015; Gersch *et al.*, 2017). These common substrates identified through mass spectrometry approaches include several proteins hypothesised to be involved in mitophagy including MIRO1, MFN1 and TOM20 (Bingol *et al.*, 2014; Cunningham, *et al.*, 2015). This is purported to be due to K6 and K11 UB chain linkages regulating mitophagy – which fits the observed linkage preference of Parkin chain assembly and USP30 chain cleavage (Cunningham, *et al.*, 2015; Gersch *et al.*, 2017; Sato *et al.*, 2017).

In the original paper that reported USP30 action within the PINK1/Parkin pathway, TOM20 was the standard substrate used to characterise USP30 mitophagy (Bingol *et al.*, 2014).

Mitochondrial turnover after CCCP-induced depolarisation was measured by TOM20 immunostaining, which was blocked by USP30 action unless a catalytically dead mutant (USP30 C77S) was employed instead (Bingol *et al.*, 2014). Hence, TOM20 has become a well-known marker for mitophagy experiments (Liang, *et al.*, 2015; Palinkas *et al.*, 2016; Gersch, *et al.*, 2017; Phu, *et al.*, 2020). The 2014 Bingol *et al.*, paper that first identified USP30 substrates also prominently identified MIRO1, a mitochondrial GTPase involved in mitophagy, as one of the mitochondrial proteins that showed the strongest increase in ubiquitination upon USP30 KO.

However, it has not been as well characterized as a USP30 substrate as TOM20. Meanwhile, recent discoveries about the putative role of MIRO1 in the PINK1/Parkin pathway make it an increasingly more interesting substrate to examine (Safiulina *et al.*, 2018; López-Doménech *et al.*, 2021).

Thus, the use of MIRO1 could provide a useful alternative physiological tool against which to run orthogonal assays for USP30 action in the presence of a physiological substrate, particularly when testing the DUB against new potential inhibitors for therapeutic use once it has been tested in cells. As such, here a method to produce the physiological substrate ubiquitinated-MIRO1 is established with the objective to run *in vitro* enzyme assays to characterise USP30 substrate recognition and inhibition in the presence of these new highly potent and selective inhibitors to provide a springboard for future structural studies.

4.2. Producing the Physiological Substrate.

Here monoubiquitinated (**Figure 15,16**) and polyubiquitinated MIRO1 (**Figure 15, 17**) were produced using a standardised method to test USP30 deubiquitinating activity against alternative physiological substrates (**Figure 6c**) and thus characterise USP30 substrate recognition. However, before assembling the physiological substrate, all the proteins required for the ubiquitination and deubiquitination reactions were produced. Of these, **Figure 12** shows the purification of the C-terminal His-tagged ubiquitin at different stages. Curiously, in **Figure 12b** which displays the protein after gel filtration, you can see the formation of higher molecular weight bands forming in the 50-80 kDa range. While the presence of some impurities seems to be present in **Figure 12a** (strong band at approximately 80 kDa), the banding pattern seems to be distinct from that observed in **Figure 12b**. A likely reason for the formation of these higher molecular weight bands may be the formation of UB aggregates, however, changes in buffer composition and other potential factors should be considered as understanding the differences could be crucial for optimising the purification process for subsequent experiments. Alternatively, an extra purification step could be added such as ion exchange chromatography. Nonetheless, the successful ubiquitination of MIRO1 validates that all the proteins previously produced are fully functional, although further optimisation is still required for USP30 production. Namely, downscaling protein preparation volume would aid in preventing aggregation and increasing the amount of protease could reduce the amount of uncleaved-USP30 left behind in the affinity chromatography step (**Figure 14**).

A protein that was not made in this project was Parkin. Instead, PDR-1, the *C. elegans* homologue of Parkin was prepared previously in the lab and determined to have the same activity as Parkin. Since Parkin (and PDR-1) has been demonstrated to prefer K6 linkage formation (Michel *et al.*, 2017), when generating the polyUB-MIRO1 substrate it was assumed that the dominant chain being assembled would be K6-linkages, which is also the preferred linkage for USP30 cleavage (Gersch *et al.*, 2017; Sato *et al.*, 2017). This idea is supported by the strong deubiquitinating activity observed with the polyUB-MIRO1 (**Figure 23**), although further complementary experiments could be included to ensure that the polyubiquitinate chains being assembled are K6 linkages, including mass spectrometry of the ubiquitin linkages or Western blotting using antibodies specific to distinct ubiquitin linkages.

Concurrently, the assembly of pre-conjugated K6-diUB-MIRO1 substrate was also attempted, although too little yield was obtained to be able to carry out further experiments (**Supplementary Figure 4**). Despite the groundwork set for the production of K6-diUB-MIRO1 using the protocols established for the ubiquitination assays here, further optimisation will be required as the protocol described proved to be too inefficient for substantial substrate production. The efficiency of K6-diUB-MIRO1 production would benefit strongly by increasing the concentration of K6-di-ubiquitin, which was a limiting factor when designing the experiment, although the K6-diUB-MIRO1 production might also be improved by changing certain parameters of the methodology, such as by increasing the temperature and/or ubiquitination reaction time. Note that the K6-diUB-MIRO1 band has a ~64.5kDa compared to the polyUB-MIRO1 band at ~68.5 kDa due to the presence of the 6xHis tag (and linker) on the C-terminal of the ubiquitin used to produce the polyUB-MIRO1.

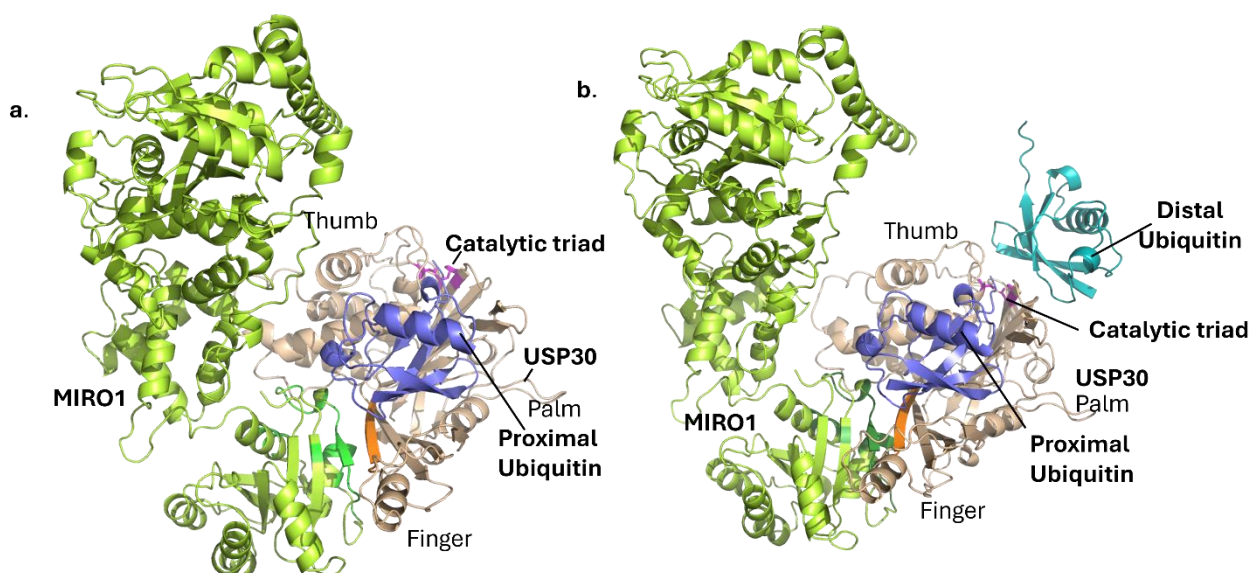
Additionally, while Parkin builds upon pre-conjugated ubiquitin chains on the mitochondrial surface, a potential limitation could be unforeseen issues arising from the interaction between PDR-1 (*C. elegans* Parkin) and the pre-assembled K6-diUB, such as subtle changes on how the E3 handle's the linkage geometry, positioning or flexibility, despite previous experiments conducted in the lab that show both forms of Parkin have the same activity. Hence another suggested future experiment would be to use human Parkin when profiling USP30 activity to ensure both E3 ligases behave the same way on the physiological substrate as was previously reported by the lab on alternative substrates/enzymes, where there were no other differences observed.

The successfully generated substrates, monoUB-MIRO1 and polyUB-MIRO1, were made by adjusting two key parameters, the ratio of UB to MIRO1 available and the time allowed for the ubiquitination reaction to run (**Figure 14**). However, a limitation that should be taken into account is the potential inconsistency in the rates of ubiquitination of the substrates as they were generated by running ubiquitination assays *in situ* instead of purifying ubiquitinated-MIRO1 batches to ensure the substrate was in its optimal state for the assay.

Once the substrates were generated, the ability of monoUB-MIRO1 and polyUB-MIRO1 to act as a substrate of USP30 was checked. To do this a simple gel-based assay using either monoUB-MIRO (**Figure 16**) or polyUB-MIRO1 (**Figure 17**) along with varied USP30 concentrations and deubiquitination reaction times was developed. From these gels the strongest deubiquitination effect was observed when a combination of maximal deubiquitination reaction time (30 minutes) and USP30 concentration (1 μ M) at a 1 USP30: 10 MIRO1 ratio was used. These gels also seem to indicate that USP30 preferentially cleaves polyUB-MIRO1 to monoUB-MIRO1 as the polyUB-MIRO1 bands (those above the 58 kDa monoUB-MIRO1 band) in **Figure 17** are clearly removed in a USP30 dependent fashion, compared to the monoUB-MIRO1 bands seen in **Figure 16-17**. This is further confirmed by the deubiquitination activity of USP30 not decreasing in the presence of inhibitors at 10 μ M when tested against the monoUB-MIRO1 substrate (**Figure 22**). Notably, however, the non-ubiquitinated MIRO1 levels increased in a USP30-dependent manner in **Figure 17**, with the lanes corresponding to higher USP30 concentration and reaction time reflecting stronger MIRO1 band signals. This would imply USP30 is cleaving the proximal UB from the substrate, as would be expected from an exoDUB. Since Parkin has been observed to be capable of monoubiquitinating MIRO1, the broader substrate recognition of USP30 would imply it has a further overlap antagonising Parkin activity, as well as suggesting it may play a more comprehensive regulatory role in mitochondrial dynamics and in the quality control pathways. Indeed, further understanding of the effects of mono-ubiquitination of MIRO1 in physiological function may be key to elucidating whether USP30 could be impacting other cellular processes. Notably, mono-ubiquitination of Mitofusin GTPase, another of the previously characterised substrates of Parkin, has been implicated in affecting its function, so the same may be true for other GTPases (Klosowiak *et al.*, 2016).

An AlphaFold 3.0 prediction of the USP30 interaction in the presence of mono ((**Figure 24a**) and poly- ubiquitinated MIRO1 (**Figure 24b**) was generated to see whether a direct interaction between USP30 and MIRO1 would be plausible, as would be required when cleaving the mono-ubiquitinated substrate. Residues within 5 Å between MIRO1 and USP30 were deemed to be

most likely to be involved in the interaction. While these residues (coloured dark green in MIRO1 and orange in USP30) are not close to the catalytic triad they could still be involved in a potential interaction between the two proteins, as the abundance of Lys, Arg, Glu and Asp residues found in the interaction site of USP30 suggest a potential electrostatic interaction. Additionally, residue clusters found in positions 111-115 and 121-150 of the USP30 5OHK sequence appear multiple times and likely are also involved in the interaction. From these clusters, residues Asp112, Arg114, Arg130, Asp115, Trp121, and Lys219 are within 5 Å of MIRO1 and are therefore the most likely residues to play a role in the interaction (**Figure 24c**). This makes further biochemical characterisation, and eventually future structural investigation, of USP30 in the presence of the physiological substrate MIRO1 an exciting avenue of future investigation.



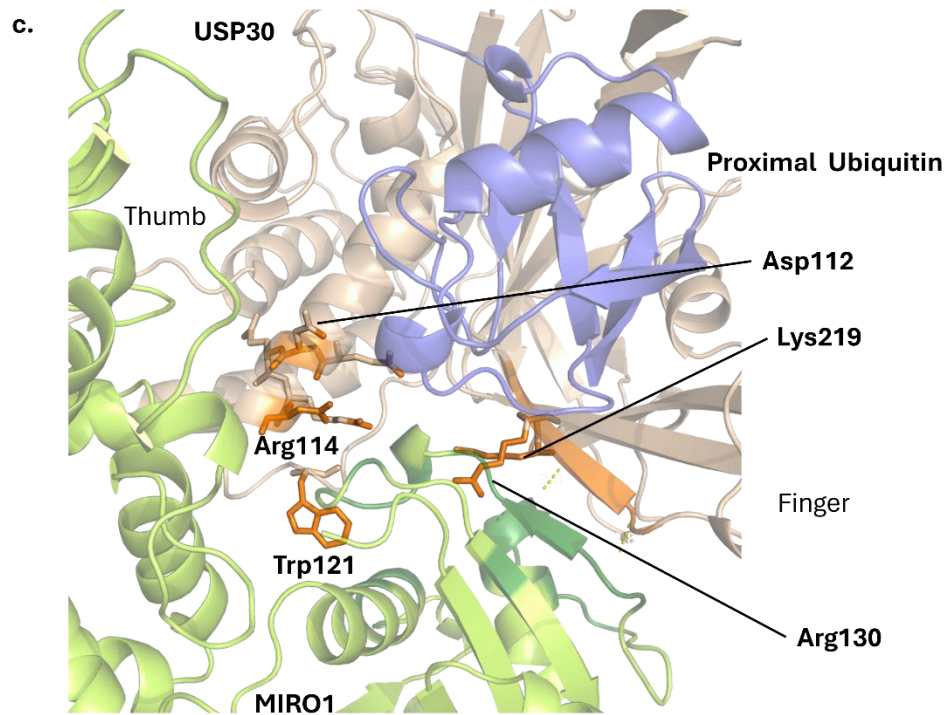


Figure 24. AlphaFold 3 prediction of USP30 bound to mono- and poly- ubiquitinated MIRO1.

Figure 24a. USP30 5OHK construct bound to monoUB-MIRO1 according to alphafold. Dark green residues in MIRO1 and orange residues in USP30 serve to highlight the residues within 5 Å of each other.

Figure 24b. USP30 5OHK construct bound to polyUB-MIRO1 according to alphafold.

Figure 24c. Close up of the residues (stick format) most likely to play a role within the MIRO1 and USP30 interaction.

.....

There are a few limitations on the experimental approach that need to be addressed. Firstly, and most importantly, the deubiquitination assays (**Figure 16 and 17**) are yet to be repeated to validate the results demonstrated there. This is of particular importance since **Figure 16** doesn't show the same USP30-dependent increase on MIRO1 levels seen in **Figure 17**, suggesting the need for more repeat experiments coupled with quantification of the bands to ensure statistical significance. Secondly, if USP30 is cleaving both the distal and proximal UB simultaneously, a gel showing a side-by-side comparison of USP30 activity against monoUB-MIRO1 and polyUB-MIRO1 should be run to provide a direct comparison of USP30 substrate recognition. Finally, in both **Figure 16 and 17**, there is an unknown band of approximately ~48 kDa in size. Repetition of the experiments is crucial to seeing if this band reappears, and if so, elucidating what is causing it. It could be speculated that the band is forming due to the

presence of contaminants or perhaps due to the degradation of one of the proteins employed. Regardless, if the band appears again in future repeat experiments, a MS analysis could also help shed light on what this ~48 kDa band is. Additionally, further experimentation using even higher USP30 concentration and longer reaction time may allow further optimisation of the reaction.

4.3 Re-evaluating USP30 inhibition using physiological substrate turnover.

Recently, two highly selective and potent inhibitors have been reported. Through the use of structure-activity relationships based on UB-rhodamine cleavage assays Kluge *et al.*, identified MF-094, with an IC₅₀ of 0.12 µM that showed less than 30% inhibition for other USPs when used at concentrations below 10 µM. At the same time, Rusilowicz-Jones *et al.*, characterised CMPD39 through *in vitro* enzyme activity assays and reported an IC₅₀ of ~20nM. Both values reported in the literature indicate a lower potency than the IC₅₀ values calculated here of 0.02 µM and 4 nM respectively. However, the use of different assay conditions and different batches of the compounds can lead to variations within this scale.

To further probe the potency, along with the selectivity of the compounds, the effect of the inhibitors on the activity of a panel of DUBs was measured by using DUBprofiler™, an enzymatic assay based on a UB-Rho substrate cleavage. The DUBprofiler screen showed that both inhibitors (**Figure 21 and 22**) have strong potency and specificity for USP30. This confirms previous CMPD39 screens and MF-094 reports by recapitulating its selectivity and potency (Kluge *et al.*, 2018; Schauer *et al.*, 2020; Rusilowicz-Jones, *et al.*, 2022; O'Brien *et al.*, 2023; Li *et al.*, 2022). These sulphonamide derivative inhibitors thus present an interesting new avenue for targeting USP30, with DUBprofiler™ showing that CMPD39 is capable of retaining selectivity even at concentrations as high as 100 µM.

The next step was to investigate whether the potency of the inhibitors was retained in cells. DUBprofiler-Cell™ measures the ability of endogenous USP30 to bind a Ubiquitin-proprietary UB-probe in the presence of increasing concentrations of inhibitor. Here the inhibition of USP30 probe engagement was measured with either MF-094 or CMPD39, with the inhibitor treatment performed either on cell lysate or on the living cells. For CMPD39 the EC₅₀ values as measured by lysate and living cell treatment were 0.014 µM and 0.084 µM respectively, indicating only a 6-fold decrease. In the case of MF-094, the EC₅₀ values measured by lysate and living cell treatment were 0.17 µM and 4.3 µM respectively, indicating a 25-fold decrease. The DUBprofiler-Cell™ results described here make up the first side-by-side comparison of the

two USP30-targeting drug candidates and the two EC₅₀ values calculated here from the lysate and live cell assays. The results suggest CMPD39 is a more potent inhibitor compared to MF-094, as well as possibly providing better cell penetration based on the difference between the lysate and live cell EC₅₀ values, which is particularly important for a drug to be able to advance through the clinical drug development pipeline.

The inhibition of USP30 with both compounds was then tested using the physiological substrates produced. Inhibition of USP30 activity against monoUB-MIRO1, as measured by SDS-PAGE, showed a stronger inhibitory effect in the presence of MF-094. However, the MIRO1 quantification in the presence of CMPD39 (**Figure 22**) showed levels similar to those when no inhibitor is present, implying a potential error in the CMPD39 lane. Hence repetition of the experiment using different conditions to optimise the reaction, such as increased USP30 concentration or increased reaction time, would provide a better understanding of USP30 deubiquitinating action on the monoubiquitinated substrate. This would also clarify whether MF-094 or CMPD39 is a stronger inhibitor, as the results observed in **Figure 22** contradict the expected potency ranking as measured in DUBprofiler™ (**Figure 18 and 19**) and DUBprofiler-Cell™ (**Figure 20 and 21**) as well as what was observed in **Figure 23** for the inhibition of USP30 in the presence of polyUB-MIRO1. Additionally, the quantification of USP30 cleavage of polyUB-MIRO1 showed similar MIRO1 levels to the control where no USP30 is present for both inhibitors, with MIRO1 levels decreasing to 16% with the MF-094 treatment and to 7% with CMPD39 treatment at the same concentration, indicating complete inhibition of USP30 at those concentrations. This data suggests that polyUB-MIRO1 substrate acts as a good biomarker of USP30 inhibition and therefore supports the hypothesis of the project, as the generated substrates can be employed for *in vitro* experiments characterising USP30 substrate recognition and inhibition in the presence of MF-094 and CMPD39.

4.4 Future Prospects using the physiological substrate.

Two structures of USP30 bound to inhibitors have been recently deposited in the PDB bank (8D0A and 8D1T) but the structure of USP30 in complex with one of the new inhibitors, MF-094 or CMPD39, would provide further information for the development and optimisation of inhibitors for therapeutic purposes. This would be informative, as we currently don't have structural validation of how these new, more specific, and potent inhibitors bind, although preliminary data from HDX-MS experiments indicates CMPD39 binds to the thumb-palm cleft of USP30 in a slow and tight manner reminiscent of a covalent bond taking place (O'Brien *et*

al., 2023). More information is required on how MF-094 binds, although biochemical experiments seem to indicate the inhibitor could be binding to the USP30 active site rather than restricting entrance of the ubiquitin tail to the thumb-palm binding pocket (Kluge *et al.*, 2018). Further understanding of how MF-094 engages, and elucidating the differences between the two inhibitors could provide further insight into the development and refinement of future USP30 inhibitors. As such, biochemical characterisation could be initially carried out to understand whether USP30 binds to these inhibitors and the substrate simultaneously or competitively. Among others, some biochemical experiments that could be used to study this include thermal shift assays or surface plasmon resonance experiments where a cooperative effect would be observed in case of simultaneous binding.

Additionally, aside from the insight that could be gained by the structural information of USP30 bound to the inhibitors, here a method to produce mono-ubiquitinated-MIRO1 and poly-ubiquitinated MIRO1 has been established, thus allowing for two new separate complexes to be visualised to gain further structural understanding of how USP30 binds its substrates. The complex containing USP30 bound to polyUB-MIRO1 could aid in the understanding physiological USP30 substrate recognition, whilst the complex containing monoUB-MIRO1 bound to USP30 could help understand the structural arrangement of USP30 bound with the end product of the deubiquitination reaction if USP30 leaves a monoubiquitin tag behind on MIRO1 or provide the minimal substrate for structural experiments if USP30 is capable of cleaving it. Negative staining could be employed for an initial quick and efficient nanometer resolution visualisation of the complexes, which could later be visualised via Cryo-Electron Microscopy (Cryo-EM). While the size of USP30 by itself (~38 kDa) may hinder cryo-EM structural efforts, the size of the enzymatic complex when the generated substrate is added would allow the circumvention of this drawback. These same complexes could then be utilised to run crystallisation trials if protein expression yields proved adequate. Structural information from Cryo-EM and X-ray crystallisation would validate previously published information aiming to understand whether USP30 undergoes conformational rearrangements upon substrate and/or inhibitor binding and confirming the regions where both, the substrates and compounds bind (O'Brien *et al.*, 2023). This would thus allow a more comprehensive understanding of the underlying USP30 molecular mechanisms for structure-based drug discovery.

Chapter 5: References

1. Belin, A. C. and Westerlund, M. (2008) 'Parkinson's disease: A genetic perspective', *FEBS Journal*, 275(7), pp. 1377–1383. doi: 10.1111/j.1742-4658.2008.06301.x.
2. Bingol, B. *et al.* (2014) 'The mitochondrial deubiquitinase USP30 opposes parkin-mediated mitophagy', *Nature*, 510(7505), pp. 370–375. doi: 10.1038/nature13418.
3. Bingol, B. and Sheng, M. (2016) 'Mechanisms of mitophagy: PINK1, Parkin, USP30 and beyond', *Free Radical Biology and Medicine*, 100, pp. 210–222. doi: 10.1016/j.freeradbiomed.2016.04.015.
4. Bonifati, V. (2012) 'Autosomal recessive parkinsonism', *Parkinsonism and Related Disorders*, 18(SUPPL. 1), pp. 4–6. doi: 10.1016/s1353-8020(11)70004-9.
5. Caba, C., Mohammadzadeh, A. and Tong, Y. (2022) 'On the Study of Deubiquitinases: Using the Right Tools for the Job', *Biomolecules*, 12(5). doi: 10.3390/biom12050703.
6. Chan, N. C. *et al.* (2011) 'Broad activation of the ubiquitin – proteasome system by Parkin is critical for mitophagy', *Human Molecular Genetics*, 20(9), pp. 1726–1737. doi: 10.1093/hmg/ddr048.
7. Chen, C., Turnbull, D. M. and Reeve, A. K. (2019) 'Mitochondrial dysfunction in Parkinson's disease—cause or consequence?', *Biology*, 8(2), pp. 1–26. doi: 10.3390/biology8020038.
8. Chen, S., Liu, Y. and Zhou, H. (2021) 'Advances in the Development of Ubiquitin-Specific Peptidase (USP) Inhibitors'.
9. Cornelissen, T. *et al.* (2014) 'The deubiquitinase USP15 antagonizes Parkin-mediated mitochondrial ubiquitination and mitophagy', *Human molecular genetics*, 23(19), pp. 5227–5242. doi: 10.1093/hmg/ddu244.
10. Cunningham, C. N. *et al.* (2015) 'USP30 and parkin homeostatically regulate atypical ubiquitin chains on mitochondria', *Nature Cell Biology*, 17(2), pp. 160–169. doi: 10.1038/ncb3097.
11. Dave, K. D. *et al.* (2014) 'Phenotypic characterization of recessive gene knockout rat models of Parkinson's disease', *Neurobiology of Disease*, 70, pp. 190–203. doi: 10.1016/j.nbd.2014.06.009.
12. Durcan, T. M. *et al.* (2014) ' USP8 regulates mitophagy by removing K6-linked ubiquitin conjugates from parkin ', *The EMBO Journal*, 33(21), pp. 2473–2491. doi: 10.15252/embj.201489729.

13. Elu, N. *et al.* (2022) 'Identification of substrates for human deubiquitinating enzymes (DUBs): An up-to-date review and a case study for neurodevelopmental disorders', *Seminars in Cell and Developmental Biology*, 132(November 2021), pp. 120–131. doi: 10.1016/j.semcdb.2022.01.001.
14. Faggiano, S., Alfano, C. and Pastore, A. (2016) 'The missing links to link ubiquitin: Methods for the enzymatic production of polyubiquitin chains', *Analytical Biochemistry*, 492, pp. 82–90. doi: 10.1016/j.ab.2015.09.013.
15. Ferrer, S., Muratore, M. E. and Buijnsters, P. (2022) 'The intriguing role of USP30 inhibitors as deubiquitinating enzymes from the patent literature since 2013', *Expert Opinion on Therapeutic Patents*, 32(5), pp. 523–559. doi: 10.1080/13543776.2022.2003780.
16. Gallagher, J. R. *et al.* (2019) 'Negative-Stain Transmission Electron Microscopy of Molecular Complexes for Image Analysis by 2D Class Averaging', *Current Protocols in Microbiology*, 54(1), pp. 1–29. doi: 10.1002/cpmc.90.
17. Gallego, R. A. *et al.* (2023) 'Design and Synthesis of Functionally Active 5-Amino-6-Aryl Pyrrolopyrimidine Inhibitors of Hematopoietic Progenitor Kinase 1', *Journal of Medicinal Chemistry*, 66(7), pp. 4888–4909. doi: 10.1021/acs.jmedchem.2c02038.
18. Gersch, M. *et al.* (2017) 'Mechanism and regulation of the Lys6-selective deubiquitinase USP30', *Nature Structural and Molecular Biology*, 24(11), pp. 920–930. doi: 10.1038/nsmb.3475.
19. Goldberg, M. S. *et al.* (2003) 'Parkin-deficient Mice Exhibit Nigrostriatal Deficits but not Loss of Dopaminergic Neurons', *Journal of Biological Chemistry*, 278(44), pp. 43628–43635. doi: 10.1074/jbc.M308947200.
20. Grossmann, D. *et al.* (2020) 'The Emerging Role of RHOT1/Miro1 in the Pathogenesis of Parkinson's Disease', *Frontiers in Neurology*, 11(September), pp. 1–20. doi: 10.3389/fneur.2020.00587.
21. Hospenthal, M. K., Freund, S. M. V. and Komander, D. (2013) 'Assembly, analysis and architecture of atypical ubiquitin chains', *Nature Structural and Molecular Biology*, 20(5), pp. 555–565. doi: 10.1038/nsmb.2547.
22. Hou, J., Eldeeb, M. and Wang, X. (2017) 'Beyond deubiquitylation: USP30-Mediated regulation of mitochondrial homeostasis', *Advances in Experimental Medicine and Biology*, 1038, pp. 133–148. doi: 10.1007/978-981-10-6674-0_10.
23. Jiang, H. K. *et al.* (2020) 'Probing the Active Site of Deubiquitinase USP30 with Noncanonical Tryptophan Analogues', *Biochemistry*, 59(24), pp. 2205–2209. doi: 10.1021/acs.biochem.0c00307.

24. Kluge, A. F. *et al.* (2018) 'Novel highly selective inhibitors of ubiquitin specific protease 30 (USP30) accelerate mitophagy', *Bioorganic and Medicinal Chemistry Letters*, 28(15), pp. 2655–2659. doi: 10.1016/j.bmcl.2018.05.013.
25. Ko TK, Tan DJY. Is Disrupted Mitophagy a Central Player to Parkinson's Disease Pathology? *Cureus*. 2023 Feb 25;15(2):e35458. doi: 10.7759/cureus.35458. PMID: 36860818; PMCID: PMC9969326.
26. Kubli DA, Gustafsson ÅB. (2012) 'Mitochondria and mitophagy: the yin and yang of cell death control'. *Circ Res*. 12;111(9):1208-21. doi: 10.1161/CIRCRESAHA.112.265819.
27. Kumar, A., Chaugule, V., Condos, T., Barber, K., Johnson, C., Toth, R., Sundaramoorthy, R., Knebel, A., Shaw, G., Walden, H. (2017). Parkin–phosphoubiquitin complex reveals cryptic ubiquitin-binding site required for RBR ligase activity. *Nat Struct Mol Biol* **24**, 475–483. Doi: <https://doi.org/10.1038/nsmb.3400>
28. Lange, S. M., Armstrong, L. A. and Kulathu, Y. (2022) 'Deubiquitinases: From mechanisms to their inhibition by small molecules', *Molecular Cell*, 82(1), pp. 15–29. doi: 10.1016/j.molcel.2021.10.027.
29. Lecker, S. H., Goldberg, A. L. and Mitch, W. E. (2006) 'Protein degradation by the ubiquitin-proteasome pathway in normal and disease states', *Journal of the American Society of Nephrology*, 17(7), pp. 1807–1819. doi: 10.1681/ASN.2006010083.
30. Li, X. *et al.* (2022) 'MF-094, a potent and selective USP30 inhibitor, accelerates diabetic wound healing by inhibiting the NLRP3 inflammasome', *Experimental Cell Research*, 410(2). doi: 10.1016/j.yexcr.2021.112967.
31. Liang, J. *et al.* (2015) 'USP30 deubiquitylates mitochondrial Parkin substrates and restricts apoptotic cell death', *EMBO reports*, 16(5), pp. 618-627. Doi: <https://doi.org/10.15252/embr.201439820>
32. Lihua Liu *et al.* (2019) 'UbiHub: a data hub for the explorers of ubiquitination pathways', *Bioinformatics*, 35 (16), pp. 2882–2884. doi: <https://doi.org/10.1093/bioinformatics/bty1067>
33. Liu, X. *et al.* (2019) 'Ubiquitin specific protease-13 independently regulates parkin ubiquitination and alpha-synuclein clearance in alpha-synucleinopathies', *Human Molecular Genetics*, 28(4), pp. 548–560. doi: 10.1093/hmg/ddy365.
34. López-Doménech, G. *et al.* (2021) 'Loss of neuronal Miro 1 disrupts mitophagy and induces hyperactivation of the integrated stress response', *EMBO Journal*, pp. 1–20. doi: 10.15252/embj.2018100715.
- 35.

36. Madeira, F. *et al.*, (2022) 'Search and sequence analysis tools services from EMBL-EBI in 2022', *Nucleic Acids Research*, 50 (W1), pp. W276–W279.
Doi: <https://doi.org/10.1093/nar/gkac240>
37. Mandal, S. *et al.* (2022) 'Novel Imidazole Phenoxyacetic Acids as Inhibitors of USP30 for Neuroprotection Implication via the Ubiquitin-Rho-110 Fluorometric Assay: Design, Synthesis, and In Silico and Biochemical Assays', *ACS Chemical Neuroscience*, 13(9), pp. 1433–1445. doi: 10.1021/acschemneuro.2c00076.
38. Marcassa, E. *et al.* (2018) 'Dual role of USP 30 in controlling basal pexophagy and mitophagy', *EMBO reports*, 19(7). doi: 10.15252/embr.201745595.
39. Mevissen, T. E. T. and Komander, D. (2017) 'Mechanisms of Deubiquitinase Specificity and Regulation'. *The Annual Review of Biochemistry*, 86, pp. 159 -192, doi: <https://doi.org/10.1146/annurev-biochem-061516-044916>.
40. Michel, M. A. *et al.* (2017) 'Ubiquitin Linkage-Specific Affimers Reveal Insights into K6-Linked Ubiquitin Signaling', *Molecular Cell*, 68(1), pp. 233-246.e5. doi: 10.1016/j.molcel.2017.08.020.
41. Miller, S. and Muqit, M. M. K. (2019) 'Therapeutic approaches to enhance PINK1/Parkin mediated mitophagy for the treatment of Parkinson's disease', *Neuroscience Letters*, 705(April), pp. 7–13. doi: 10.1016/j.neulet.2019.04.029.
42. Mission Therapeutics (2022), from: <https://missiontherapeutics.com/mission-therapeutics-authorized-to-initiate-first-clinical-trial-for-lead-dub-program-mtx652-in-kidney-disease/>
43. Morrow, M. E. *et al.* (2018) 'Active site alanine mutations convert deubiquitinases into high-affinity ubiquitin- binding proteins', pp. 1–9. doi: 10.15252/embr.201745680.
44. National Center for Biotechnology Information (2023). PubChem Compound Summary for CID 142474792, USP30 inhibitor 18. Retrieved August 2023 from <https://pubchem.ncbi.nlm.nih.gov/compound/USP30-inhibitor-18>.
45. Nijman, S. M. B. *et al.* (2005) 'Review A Genomic and Functional Inventory of Deubiquitinating Enzymes', pp. 773–786. doi: 10.1016/j.cell.2005.11.007.
46. Nguyen, T. N., Padman, B. S. and Lazarou, M. (2016) 'Deciphering the Molecular Signals of PINK1/Parkin Mitophagy', *Trends in Cell Biology*, 26(10), pp. 733–744. doi: 10.1016/j.tcb.2016.05.008.
47. O'Brien, D. P. *et al.* (2023) 'Structural Premise of Selective Deubiquitinase USP30 Inhibition by Small-Molecule Benzosulfonamides', *Molecular & Cellular Proteomics*, p. 100609. doi: 10.1016/j.mcpro.2023.100609.

48. Onishi, M. *et al.* (2021) 'Molecular mechanisms and physiological functions of mitophagy', *EMBO Journal*, pp. 1–27. doi: 10.15252/embj.2020104705.
49. Palinkas, L., Horwitz, S. and Green, C. (2016) 'Pharmacological Inhibition of USP30 activates Tissue-specific Mitophagy' *HHS Public Access, Physiology & behavior*, 176(1), pp. 139–148. doi: 10.1111/apha.13666.Pharmacological.
50. Parkinson, J. (1969) 'An essay on the Shaking Palsy', *Archives of Neurology*, 20(4), pp. 441–445. doi: 10.1001/archneur.1969.00480100117017.
51. Phu, L. *et al.* (2020) 'Dynamic Regulation of Mitochondrial Import by the Ubiquitin System', *Molecular Cell*, 77(5), pp. 1107–1123.e10. doi: 10.1016/j.molcel.2020.02.012.
52. Poewe, W. *et al.* (2017) 'Parkinson disease', *Nature Reviews Disease Primers*, 3, pp. 1–21. doi: 10.1038/nrdp.2017.13.
53. Qin, X. *et al.* (2022) 'Identification of an autoinhibitory, mitophagy-inducing peptide derived from the transmembrane domain of USP30', *Autophagy*, 18(9), pp. 2178–2197. doi: 10.1080/15548627.2021.2022360.
54. Rusilowicz-Jones, E. V. *et al.* (2022) 'Benchmarking a highly selective USP30 inhibitor for enhancement of mitophagy and pexophagy', *Life Science Alliance*, 5(2), pp. 1–9. doi: 10.26508/lsa.202101287.
55. Rusilowicz-Jones, E. V. *et al.* (2020) 'USP30 sets a trigger threshold for PINK1–PARKIN amplification of mitochondrial ubiquitylation', *Life Science Alliance*, 3(8), pp. 1–14. doi: 10.26508/LSA.202000768.
56. Rusilowicz-Jones, E. V. *et al.* (2020) 'A novel USP30 inhibitor recapitulates genetic loss of USP30 and sets the trigger for PINK1–PARKIN amplification of mitochondrial ubiquitylation', *Life Science Alliance*, 3(8), pp. 1–14. doi: 10.26508/LSA.202000768.
57. Sato, Y. *et al.* (2017) 'Structural basis for specific cleavage of Lys6-linked polyubiquitin chains by USP30', *Nature Structural and Molecular Biology*, 24(11), pp. 911–919. doi: 10.1038/nsmb.3469.
58. Safiulina, D. *et al.* (2019) 'Miro proteins prime mitochondria for Parkin translocation and mitophagy', *EMBO Journal*, pp. 1–18. doi: 10.15252/embj.201899384.
59. Sahtoe, D. D. and Sixma, T. K. (2015) 'Layers of DUB regulation', 11(52), pp. 1–12. Doi: <http://dx.doi.org/10.1016/j.tibs.2015.05.002>
60. Schauer, N. J. *et al.* (2020) 'Advances in Discovering Deubiquitinating Enzyme (DUB) Inhibitors', *Journal of Medicinal Chemistry*, 63(6), pp. 2731–2750. doi: 10.1021/acs.jmedchem.9b01138.

61. Silvan, L. F. (2022) 'PINK1/Parkin Pathway Activation for Mitochondrial Quality Control – Which Is the Best Molecular Target for Therapy?', *Frontiers in Aging Neuroscience*, 14(June), pp. 1–6. doi: 10.3389/fnagi.2022.890823.
62. Snyder NA, Silva GM. Deubiquitinating enzymes (DUBs): Regulation, homeostasis, and oxidative stress response. *J Biol Chem*. 2021 Sep;297(3):101077. doi: 10.1016/j.jbc.2021.101077.
63. Song, X., Butler, J., Li, C., Zhang, K., Zhang, D., Hao, Y., (2023) *PDB entry - 8DOA*, *wwPDB: 8DOA*. Available at: <http://doi.org/10.2210/pdb8d0a/pdb> (Accessed: 18 August 2023).
64. Song, X., Butler, J., Li, C., Zhang, K., Zhang, D., Hao, Y., (2023) *PDB entry - 8D1T*, *wwPDB: 8DOA*. Available at: <https://doi.org/10.2210/pdb8D1T/pdb> (Accessed: 18 August 2023).
65. Sterky, F. H. *et al.* (2011) 'Impaired mitochondrial transport and Parkin-independent degeneration of respiratory chain-deficient dopamine neurons in vivo', *Proceedings of the National Academy of Sciences of the United States of America*, 108(31), pp. 12937–12942. doi: 10.1073/pnas.1103295108.
66. Tsefou, E. *et al.* (2021) 'Investigation of USP30 inhibition to enhance Parkin-mediated mitophagy: tools and approaches', *Biochemical Journal*, 478(23), pp. 4099–4118. doi: 10.1042/BCJ20210508.
67. Tsefou, E. and Ketteler, R. (2022) 'Targeting Deubiquitinating Enzymes (DUBs) That Regulate Mitophagy via Direct or Indirect Interaction with Parkin', *International Journal of Molecular Sciences*, 23(20). doi: 10.3390/ijms232012105.
68. Varca, A. C. *et al.* (2021) 'Identification and validation of selective deubiquitinase inhibitors', *Cell Chemical Biology*, 28(12), pp. 1758–1771.e13. doi: 10.1016/j.chembiol.2021.05.012.
69. Wang, Y. *et al.* (2015) 'Deubiquitinating enzymes regulate PARK2-mediated mitophagy', *Autophagy*, 11(4), pp. 595–606. doi: 10.1080/15548627.2015.1034408.
70. Wang, F. *et al.* (2022) 'USP30: Structure, Emerging Physiological Role, and Target Inhibition', *Frontiers in Pharmacology*, 13(March), pp. 1–13. doi: 10.3389/fphar.2022.851654.
71. Wang, X. *et al.* (2011) 'PINK1 and Parkin Target Miro for Phosphorylation and Degradation to Arrest Mitochondrial Motility', *Cell*, 147(4), pp. 893–906. doi: 10.1016/j.cell.2011.10.018.
72. Yang, Y. *et al.* (2006) 'Mitochondrial pathology and muscle and dopaminergic neuron degeneration caused by inactivation of *Drosophila* Pink1 is rescued by Parkin',

Proceedings of the National Academy of Sciences of the United States of America,
103(28), pp. 10793–10798. doi: 10.1073/pnas.0602493103.

73. Yue, W. *et al.* (2014) 'A small natural molecule promotes mitochondrial fusion through inhibition of the deubiquitinase USP30', *Cell Research*, 24(4), pp. 482–496. doi: 10.1038/cr.2014.20.

74. Zhang, C. W. *et al.* (2016) 'Parkin regulation and neurodegenerative disorders', *Frontiers in Aging Neuroscience*, 7(JAN), pp. 1–15. doi: 10.3389/fnagi.2015.00248.

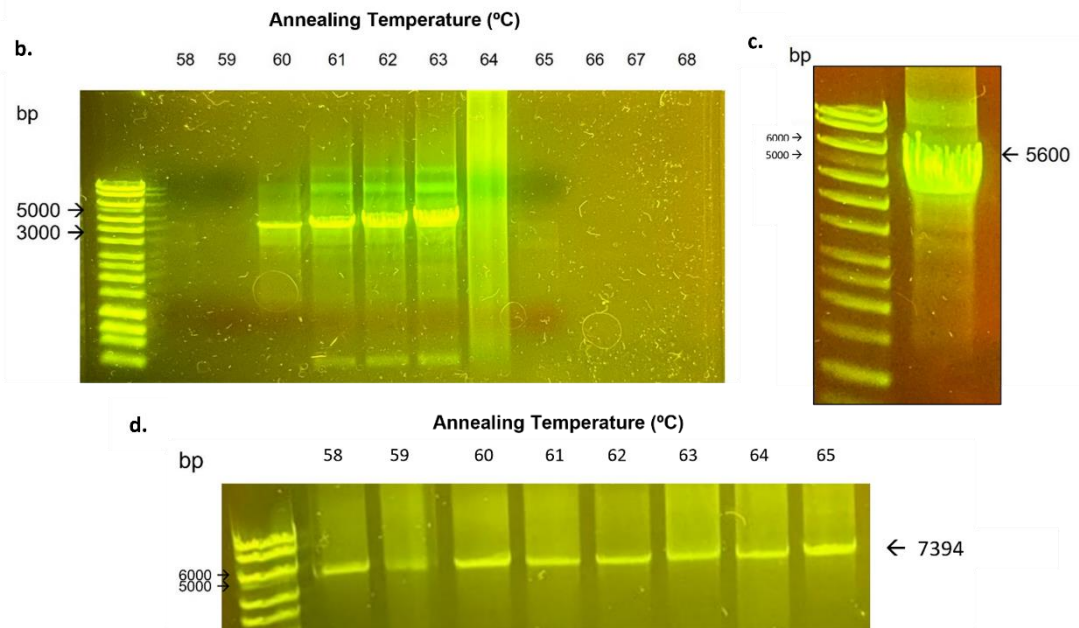
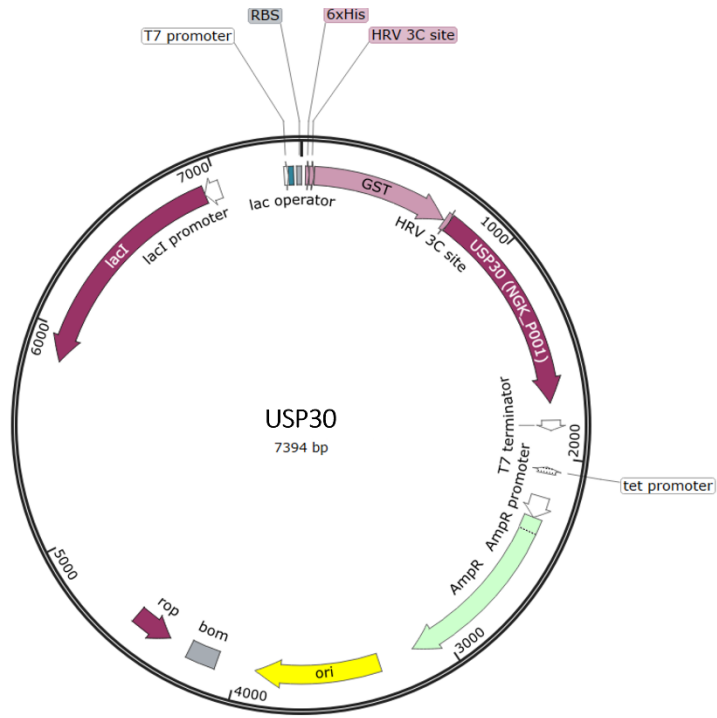
Chapter 6: Appendix

6.1 USP30 Plasmid Design and Cloning

To be able to construct the USP30 plasmid (**Supplementary Figure 1a**), the selected pET-15b-6b2 vector first had to be amplified and purified. **Supplementary Figure 1b** shows the agarose gel used to analyse the vector amplification, which was carried out using a temperature gradient ranging from 58 – 68 °C. A strong band corresponding to the expected vector size (5600 bp) can be observed in the lanes corresponding to the amplification carried out at 61 -63 °C when compared to the DNA hyperladder™ loaded on the first lane. At the amplification temperature corresponding to the 60 °C lane, a band corresponding to the vector molecular weight can also be observed. However, since the band was less intense than those observed for the 61 – 63 °C range, this sample was not utilised for the subsequent vector purification.

Thus, the lanes corresponding to the 61 – 63 °C amplification temperature were pooled together and purified as seen in **Supplementary Figure 1c**, where an intense band corresponding to the vector at the 5600 bp can be observed. This was then ligated to the designed hUSP30 insert and another temperature gradient ranging from 50 – 65 °C was carried out for the ligation annealing step. USP30 has a molecular weight of 1794 bp, therefore the total weight of a successful PCR product was expected to be 7394 bp after ligation. Since all lanes showed a clear distinct band at approximately the 6000 bp the molecular weight marker was assumed to have run faster than the PCR products. The ligated PCR product from the 65 °C annealing temperature was selected to be transformed and the resulting colonies were sent for sequencing via Eurofins to confirm the USP30 insert had been successfully cloned into pET-15b-6b2 vector (**Supplementary Figure 1d**).

a.



Supplementary Figure 1: Agarose gel analysis of the cloning of USP30 insert into pET-15b-6b2 vector.

Figure 1a. USP30 plasmid map in pET-15b-6b2 vector

Figure 1b Agarose gel image showing the result of the pET-15b-6b2 vector amplification PCR, where a gradient of annealing temperature was used. Lane 1 was loaded with the DNA molecular weight marker, whereas lanes 2-12 were loaded with the different PCR reactions where the annealing temperature varied from 58 to 68 degrees °C respectively. Note that the ladder ran faster than the sample, such that the 5600 bp sample appears to be at ~5000 bp.

Figure 1c Agarose gel image showing the result of the pET-15b-6b2 vector amplification PCR after purification. Lane 1 was loaded with the DNA molecular weight marker, whereas lane 2 was loaded with the PCR product.

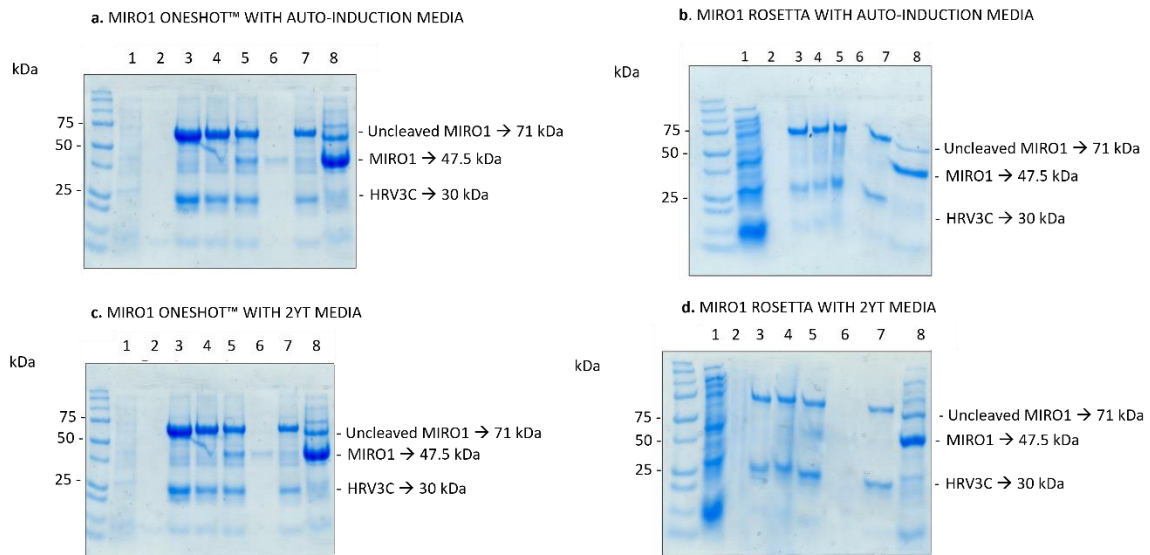
Figure 1d Agarose gel image showing the result of the reaction where the USP30 insert was ligated to pET-15b-6b2 vector.

.....

6.2 Protein Production Optimisation

6.2.1 MIRO1 Optimisation

MIRO1 and USP30 production was optimised to increase protein yield. To do this, two different parameters were changed: the cell type, with both BL21 One-Shot™ *E. coli* cells and Rosetta *E. coli* cells protein expression being examined, and the media, with 2YT and Auto-induction YT being employed (**Supplementary Figure 2**). However, the conditions used for Rosetta cells with the auto-induction media set differed from the rest as the protein was produced from 2L of media instead of the standard 3L used for the other optimisation experiments. Taking into account the expression difference caused by starting with less media, the Rosetta cells and auto-induction combination was determined to show the greatest yield and utilised for subsequent purifications of MIRO1.



Supplementary Figure 2. MIRO1 Optimisation

Affinity chromatography of MIRO1. The clear lysate was loaded into lane 1, and the flow through from the GSH column into lane 2. Lane 3 shows the resin after the washes while lane 4 shows the resin once the previously produced HRV3C protease was added and lane 5 shows the protein after overnight incubation was completed. Lane 6 shows MIRO1 after elution with the low salt buffer while Lane 7 shows the resin after the elution. MIRO1 was then spin-concentrated (Lane 8) before being further purified.

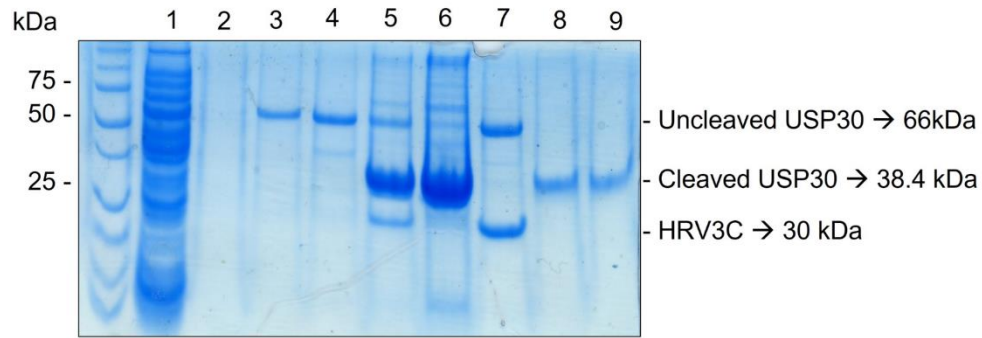
.....

6.2.2 USP30 Optimisation

For USP30 production the same parameters were varied as with MIRO1 and once again the same set of conditions – Rosetta Cells and Auto-induction media – was selected to maximise the yield after comparison of USP30 bands present for the sample after X3 dilution from

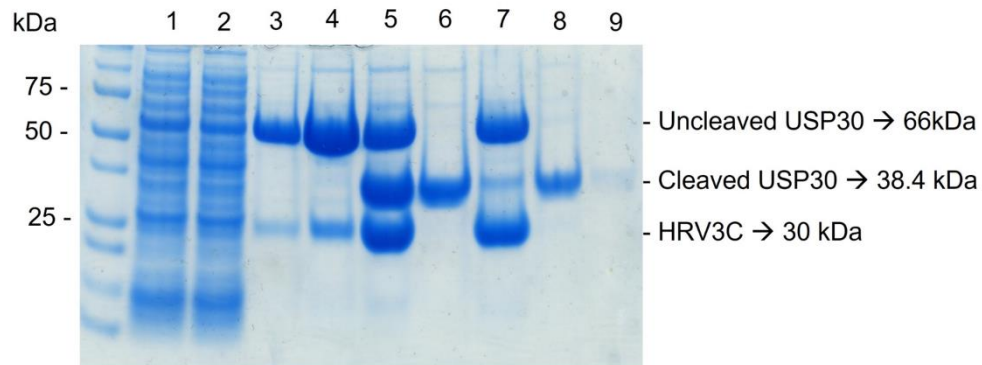
Supplementary Figure 3.

a. USP30 ONESHOT™ WITH AUTO-INDUCTION MEDIA



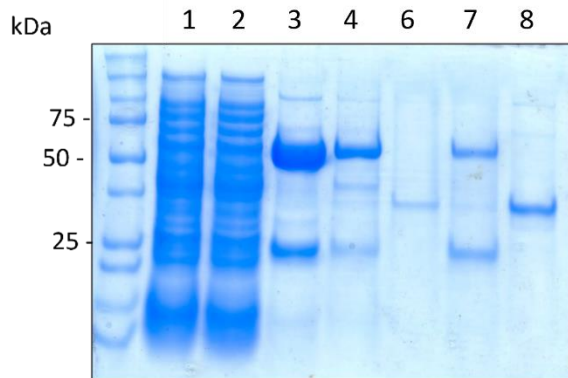
- 1 = Clear lysate
- 2 = GST lysate FT
- 3 = Resin 1
- 4 = Resin + HRV3C
- 5 = Resin + HRV3C after O/N cleavage
- 6 = Elution
- 7 = Resin after elution
- 8 = Sample after X3 dilution
- 9 = Sample after ResQ

b. USP30 ROSETTA™ WITH AUTO-INDUCTION MEDIA



- 1 = Clear lysate
- 2 = GST lysate FT
- 3 = Resin 1
- 4 = Resin + HRV3C
- 5 = Resin + HRV3C after O/N cleavage
- 6 = Elution
- 7 = Resin after elution
- 8 = Sample after X3 dilution
- 9 = Sample after ResQ

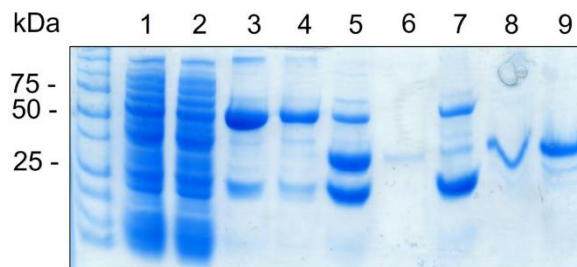
c. USP30 ONESHOT™ WITH 2YT MEDIA



- uncleaved USP30 → 66 kDa
- cleaved USP30 → 38.4 kDa
- HRV3C → 38 kDa

- 1 = Clear lysate
- 2 = GST lysate FT
- 3 = Resin 1
- 4 = Resin + HRV3C
- 6 = Elution
- 7 = Resin after elution
- 8 = Sample after X3 dilution

d. USP30 ROSETTA™ WITH 2YT MEDIA



- Uncleaved USP30 → 66kDa
- Cleaved USP30 → 38.4 kDa
- HRV3C → 30 kDa

- 1 = Clear lysate
- 2 = GST lysate FT
- 3 = Resin 1
- 4 = Resin + HRV3C
- 5 = Resin + HRV3C after O/N cleavage
- 6 = Elution
- 7 = Resin after elution
- 8 = Sample after X3 dilution
- 9 = Sample after ResQ

Supplementary Figure 3. USP30 Optimisation

Affinity chromatography of USP30. The clear lysate was loaded into Lane 1, and the flow through from the GSH column into Lane 2. Lane 3 shows the resin after the washes while Lane 4 shows the resin once the previously produced HRV3C protease was added. Lane 5 shows the protein after overnight incubation was completed (except in panel C, where this sample was

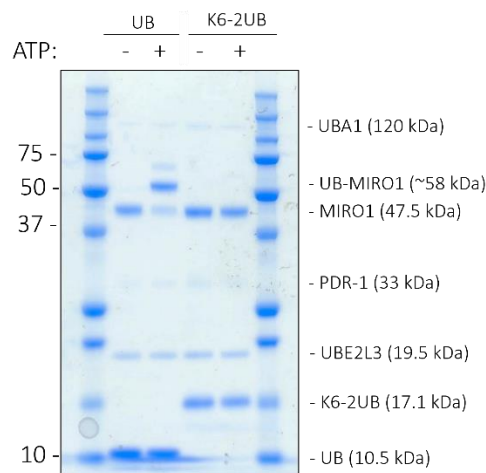
omitted and hence the numbering is non-sequential to allow the samples to match the other panels). Lane 6 shows USP30 after elution with the low salt buffer while Lane 7 shows the resin after the elution. USP30 was then spin-concentrated (Lane 8) before being further purified via ion exchange (Lane 9).

.....

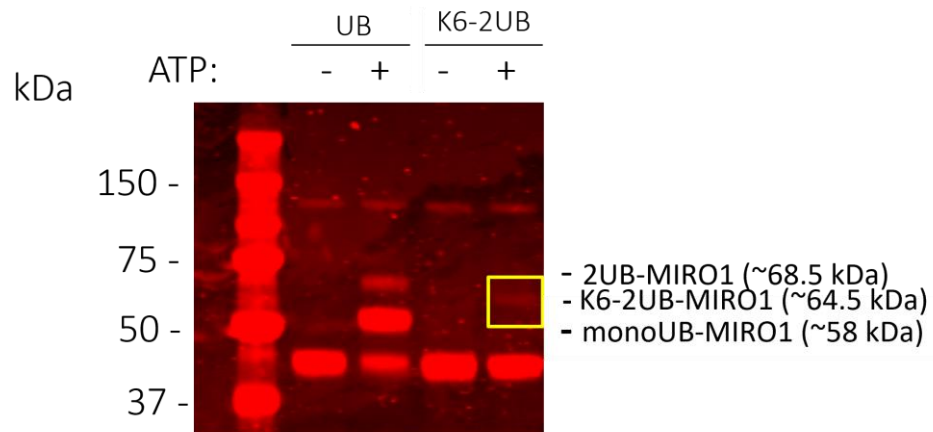
6.3 Production Of K6-Linked Diubiquitinated MIRO1 using pre-conjugated linkages.

MIRO1 ubiquitination using K6-linked di-Ubiquitin (supplied by Ubiquigent) as the only ubiquitin donor was carried out using the same components and concentrations as with the ubiquitination experiment outlined in Section 3.2.1. except for the concentrations of MIRO1 (7 μ M) and the K6-diubiquitin (3.50 μ M). The ubiquitination reaction was run for 15 minutes at room temperature before the reaction was stopped by the addition of LDS loading buffer. Note that the ratio used here of 2 MIRO1: 1 diUB and the time of the reaction were both selected from the optimal conditions used to produce monoUB-MIRO1.

a.



b.



Supplementary Figure 4. Production of K6-linked diubiquitin MIRO1

Figure 4a The K6-diubiquitination assay was performed using the conditions optimised in the previous mono-ubiquitination assay; 15-minute reaction using a 2:1 MIRO: UB ratio. The positive control shows a strong band at the expected molecular weight for monoubiquitinated-MIRO1 (monoUB-MIRO1) at ~58 kDa, while the negative controls with no ATP show no bands with higher molecular weight than the 47.5 kDa band corresponding to MIRO1.

Figure 4b The K6-diubiquitin (K6-diUB) band was very faintly visible on the SDS-PAGE, thus the gel was scanned with the LICOR Odyssey CLx and the contrast was increased using the Image Lite Software™ to clearly see the band.



Discrete ubiquitination of MIRO1 using K6-diubiquitin was also carried out to generate a substrate with the USP30 preferred linkage (**Figure 6c**). (Gersch *et al.*, 2017; Sato *et al.*, 2017).

Supplementary Figure 4a shows the SDS-PAGE gel used to analyse the site-specific ubiquitination of MIRO1 when the only donor available was K6-linked diubiquitin. To generate the substrate, Ubiquigent supplied the K6-diubiquitin at a concentration of 0.5 mg/ml. The optimal time (15 minutes) and 2 MIRO1: 1 diUB concentration ratio (15: 7.5 μM) established for the formation of monoUB- MIRO1 was used to perform this experiment. Two controls were also included: a positive control where the reaction was carried out using ubiquitin as per the previous ubiquitination assay and showed the clear formation of the monoUB-MIRO1 band; and negative controls where no ATP was supplied to either of the ubiquitination reactions and thus no ubiquitination bands were observed. The positive control using UB capable of binding to any site showed the formation of a strong band corresponding to monoUB-MIRO1 at ~58 kDa. Meanwhile, the negative control with no ATP showed no such high molecular weight

band, and instead only showed the bands confirming the presence of all the reaction components, including MIRO1 (47.5 kDa) and the corresponding unbound UB (10.5 kDa) or K6-diUB (17.1 kDa) moieties. Lane 5 initially appears to not have a high molecular weight band corresponding to K6-diUB-MIRO1 formation, but a high contrast LICOR scan of the gel (**Figure 16b**) confirmed the existence of a faint band at the expected molecular weight. The yield was too low to allow for further experimentation.